Three Essays on the Economic and Bioeconomic Dynamic Systems

By

XIUROU WU
DISSERTATION

Submitted in partial satisfaction of the requirements for the degree of

DOCTOR OF PHILOSOPHY

in

Agricultural and Resource Economics

in the

OFFICE OF GRADUATE STUDIES

of the

UNIVERSITY OF CALIFORNIA

DAVIS

Approved:

James E. Wilen, Co-chair

James N. Sanchirico, Co-chair

Bulat Gafarov

Michael R. Springborn

Committee in Charge

2022

i

Abstract

Environmental and resource issues usually involve complex, dynamic, interconnected systems with feedback across social and environmental dimensions. My dissertation is a three-essay thesis exploring economic and bioeconomic dynamic systems. It utilizes a range of tools useful for tackling problems about environmental and resource management, including: analytical modeling, dynamic optimization, mathematical programming, and econometrics. The topics of each essay are:

- modeling joint management of conflicting ecosystem services in the context of Lake Poyang
- commercial fishers' trip-level decision making about spatial location, fishing effort, and trip duration in the Gulf of Mexico longline fishery
- testing point identification of impulse response functions (IRF) using sign restrictions

Chapter 1 examines a coupled human-natural system characterizing the natural resource dynamics, human dynamics, and feedbacks between the two. The chapter develops a hydro-bio-economic model of ecosystem service management that illuminates the conflict between fishing operations and conservation of endangered and threatened waterfowl, specifically Siberian Cranes. The model is calibrated to fit the example of the China's largest freshwater lake, Lake Poyang, the wintering ground for the last surviving population of Siberian Cranes. It captures important features of the lake's hydrology, ecosystem, and economics to investigate the impact of uncoordinated and coordinated management of fishing and bird conservation. The coordinated (joint) management problem is a three-state non-smooth hybrid dynamic problem that is within-year continuous and between-year discrete. It is solved using the novel pseudo-spectral method from aerospace engineering. The current regulations do not account for the externality fishing imposes on the endangered cranes, which results in their population size decreasing over time. In general, we find that prolonging the fishing season extends the cranes' winter feeding and enhances survival but at a cost to the fishery. We characterize those trade-offs and then examine compensation schemes for fishery communities that induce crane conservation. With the decline in natural landscape quality, importance grows for utilizing working landscapes more effectively to provide ecosystem services.

Chapter 2 explores spatio-temporal human behavior using novel sources of high-resolution mobility data. With the advent of global positioning data in fisheries, now more than ever, we can empirically model fishers' decision-making at a detailed level. In the short-run, after choosing fishing gear, fishers decide where to fish, how much to fish in each location, and when to return to the port on a given trip. Most of the research investigating these decisions has focused on one aspect of the decision at a time (e.g., choosing a fishing location), treating other aspects exogenous or

separable. However, these decisions are arguably interconnected and also conditional on the underlying vessel capital stock (e.g., hold and fuel capacity).

This chapter constructs a novel spatial dynamic model of an individual fisher's trip-level decision-making that incorporates simultaneous decisions on location choice, fishing effort allocated at each location, and travel route. It is motivated by observations from a high-resolution data set on fishing trips from the Gulf of Mexico's bottom longline fishery. We demonstrate predictions from the model using numerical simulations of calibrated optimal trip decisions. Simulation results show that technology constraints endogenously influence the trip length. These constraints impose a shadow price that affects the individual fisher's sequence of choices of location and effort from the outset of a trip. We compare these optimal spatial patterns with those from a myopic fisher and a partially myopic fisher, where the former makes one-choice-ahead decisions and the latter undertakes different degrees of forward-looking choices (2, 3, and 6 decisions ahead). The myopic fisher does not optimize route planning or consider the technological constraints until it is time to return to port. Both factors result in large reductions in trip profit even though, for example, catches can be similar across the myopic and dynamic fisher. For the partially myopic fisher, the extent of route planning and consideration of technological constraints depends on the degree of forward-lookingness. Not surprisingly, the more forward looking the partially myopic fisher, the closer it approaches the fully spatial-dynamically optimal trip pattern. Building more refined models of trip-level spatial decision making is important for the design and assessment of spatial and aspatial fishery management instruments.

Chapter 3 focuses on identifying impulse response function (IRF), the dynamic effect of a shock in a given moment along a specified time horizon, using sign restrictions. Sign restrictions on impulse response functions (IRF) are used to put bounds on parameters in structural vector autoregressions (SVAR) models. In this chapter, we provide testable necessary and sufficient conditions under which these bounds collapse to single point. The main necessary condition is positive linear dependence of the vectors of sign restricted IRF coefficients. We provide a simple test for this condition with standard chi-squared critical values that remain valid in the presence of redundant sign-restrictions. The simulations suggest that the proposed test has high power against the alternative data generating process with partial-identification.

A constant presence of kind, interesting, and passionate individuals of every sort have nurtured me. I appreciate everyone that has and will enter my life because they have helped build me into who I am. Every year I am becoming a better me because of you. Antaeus was invincible, but only on the earth, his progenitor. All the connection I have is my earth.

Contents

List of Figures

List of Tables

CHAPTER 1

Modeling ecosystem service conflicts in China's Lake Poyang

1.1. Introduction

Lake Poyang is China's largest freshwater lake. It is a seasonal lake whereby a vast region floods under monsoon conditions and then recedes as the dry autumn-winter season unfolds. The lake provides important winter habitat for numerous endangered and threatened species of cranes and other waterfowl, including the last surviving population of Siberian Cranes. It also supports an ancient system of fishing that utilizes the seasonal patterns of water flooding and recession. This system is called ZQH (ZhanQiuHu) fishery[1]. Ever since the 12th century, local villages have constructed and maintained low dikes that trap water and fish in sub-lakes when the surrounding lake recedes. Local villages auction temporary user rights to individual contractors to extract fish from adjacent sub-lakes. Contractors execute a slow draining of the sub-lakes that allows low-cost harvesting of escaping fish, generating proceeds that are partly returned to the village.

Draining the lakes also exposes tubers, which are prime feed for critically endangered Siberian cranes and other species. The conflict emerges because the sub-lake drawdown that is dynamically optimal for within-season fishery production is not optimal for tuber foraging for the wintering wildfowl populations. As China's wealth has grown, the market value of tourism services associated with crane viewing and photography has grown, leading to conflicts within the various lake-side villages over how to trade-off multiple users of near-shore lake use. In addition, the central government is promoting the preservation of unique habitat and endangered species, actions that signal the growing recognition of non-market ecosystem values. Several private, state and NGO stakeholders have begun to monetize crane and wildfowl populations by developing infrastructure for viewing and photographing cranes during their winter feeding season at Lake Poyang. The state has also designated certain areas as refuges for cranes, encouraging modifications of traditional fisheries practices in ways that preserve some private values but that also enhance wildfowl habitat. This evolution of institutions reflects a changing economic reality for China, one where growing wealth is raising the value of natural nonmarket services from the ecosystem, precipitating changes in traditional institutions that favored marketed services.

---

[1]The literal translation of ZhangQiuHu is cut the lake in the autumn (by building dikes to catch fish).

The conflict between ZQH fishery and Siberian Crane habitat raises several interesting research questions. For example, how do the profit-maximizing motivations of the ZQH fishery impact the crane population over time? How would various modifications of ZQH fishery operations within a season increase the food available for cranes and the crane population? How might different policies incentivize local fishers to modify their current fishing practice? To answer these questions and understand the complicated interactions between local fishing practices, water level change, tuber exposure, and crane populations, this chapter constructs a novel structural model of the inter-annual hydrology of Lake Poyang coupled to a model of lake-bottom vegetation and intra-annual crane population biology. The within-year continuous population dynamics (consumes resource and dies continuously) and between-year discrete reproduction of the cranes add discrete and continuous components to the system.

Utilizing the hydrologic-bio-economic model and state-of-the-art pseudospectral numerical methods, we generate several dynamic simulation results from our baseline deterministic model to discuss the responses to the changing conflicts between local fisheries use and crane and wildfowl habitat use. Specifically, we determine optimal sub-lake drawdown for crane populations with various bio-economic conditions under coordinated and uncoordinated management, where the uncoordinated management stems solely from profit maximizing fishery decisions. We find that decisions that are dynamically optimized for the fisheries drain the sub-lake earlier than desirable for optimal crane population habitat provision. Simulation results show a 21% decrease in the crane population over 5 years of fishery operation. We also find extending the water draining to the end of the wintering season secures the cranes' winter feeding and enhances the crane population but at a cost of fishery revenue. The fishery revenue reduction, the opportunity cost for crane conservation, can be used for minimum compensation payments from the government to incentivize season extensions. The government could also subsidize post-season fish market or pay the fishers to maximize end-of-season crane population in the sub-lake.

The remainder of the chapter proceeds as follows. Section 1.2 describes the background of Lake Poyang, the Siberian crane, and the fishery. Section 1.3 introduces the deterministic hydrologic-bio-economic model for joint management. Section 1.5 talks about the results. Section 1.6 discusses about future extensions. Section 1.7 concludes.

1.2. Background

1.2.1. Lake Poyang. Lake Poyang in Jiangxi Province, is China's largest freshwater lake, and one of the largest freshwater wetlands in Asia (Figure 1.1). The lake is fed by five tributary rivers (Gan, Fu, Xin, Rao and Xiu) from the south, and connects to China's largest Yangtze River through a narrow outlet channel in the north. The lake basin is affected by subtropical monsoon weather. During part of summer, flooding from the five tributary rivers and a reverse flow from Yangtze River contribute to dramatic seasonal hydrological fluctuations in Lake Poyang. In summer, the

2

lake's area can exceed 4000 km^2 while in winter it reduces to less than 1000 km^2 (Shankman et al., 2006). In autumn receding water levels expose a maze of isolated sub-lakes. These sub-lakes are connected to the main lake body via rivers. The difference between summer high and winter low water levels can be as much as 11 meters (Harris, 2016).

The lake is a complex landscape that jointly provides ecosystem services like flood control, water purification, and fish supply, benefiting around 200 million people in the watershed. The unique hydrology also supports rich aquatic biodiversity and makes the basin the most important waterbirds wintering site in East Asia. Lake Poyang regularly hosts 400,000 waterbirds every winter, including 95% of the charismatic and Critically Endangered Siberian crane (*Grus leuceogeranus*)(Wu et al., 2009).

1.2.2. The Siberian Crane. The Siberian crane is also known as the Siberian white crane or snow crane. Adults are nearly all snowy white, with the black primary feathers visible only in flight. Adults have an average height of 5 ft and average weight of 13 lbs (International Crane Foundation, 2019). The Siberian crane holds the longevity record for all crane species. A Siberian crane living at the National Zoological Park of the Smithsonian Institute reached the age of 62 and another crane named Wolf is in the Guinness Book of World Records for the age of 83 (Birdorable Blog, 2019). The lifespan is unknown for wild Siberian cranes but predicted longevity is shorter than highest lifespans reached in captivity (Friedman, 1992). The average lifespan for Siberian cranes in captivity is about 36.2 years for males and 32.3 years for females (Flower, 1938).

The Siberian crane is the most aquatic member of its family, breeding and wintering in wetlands, and preferring wide expanses of shallow freshwater with good visibility. This species is mainly vegetarian but omnivorous in the breeding ground and the wintering ground (del Hoyo, 1997; Johnsgard, 1983)[2]. During the non-breeding season, it feeds mainly on roots, bulbs, tubers (especially of sedges), rhizomes, sprouts and stems of aquatic plants, and sometimes aquatic animals if these are readily available (del Hoyo, 1997). Therefore, the most important habitat component is the presence of aquatic plant roots, winter buds, and tubers[3]. (Burnham et al., 2017; Jia et al., 2013) show that *Vallisneria* tubers are critical food source for Siberian cranes. For efficient forage, soil conditions must allow digging to occur and water cannot be so high as to prevent access to the benthic zone[4]. The cranes feed in water within 25 to 68 centimeters depth (about as deep as their long legs allow them to wade). Most of the daylight hours during the wintering period are spent foraging.

---

[2]The Siberian crane is known to be omnivorous, feeding on both animal and plant matter, depending on the season, life stage and habitat. The diet is broader including both plants and animals during summer.

[3](Chiba, 2018) found that an immature Siberian Crane in Niigata, Japan mainly forage on water chestnut tubers during the 2016/2017 wintering season while other foods like rice grains, earthworms, grasshoppers and fishes are negligible.

[4]The benthic zone is the ecological region at the lowest level of a water body.
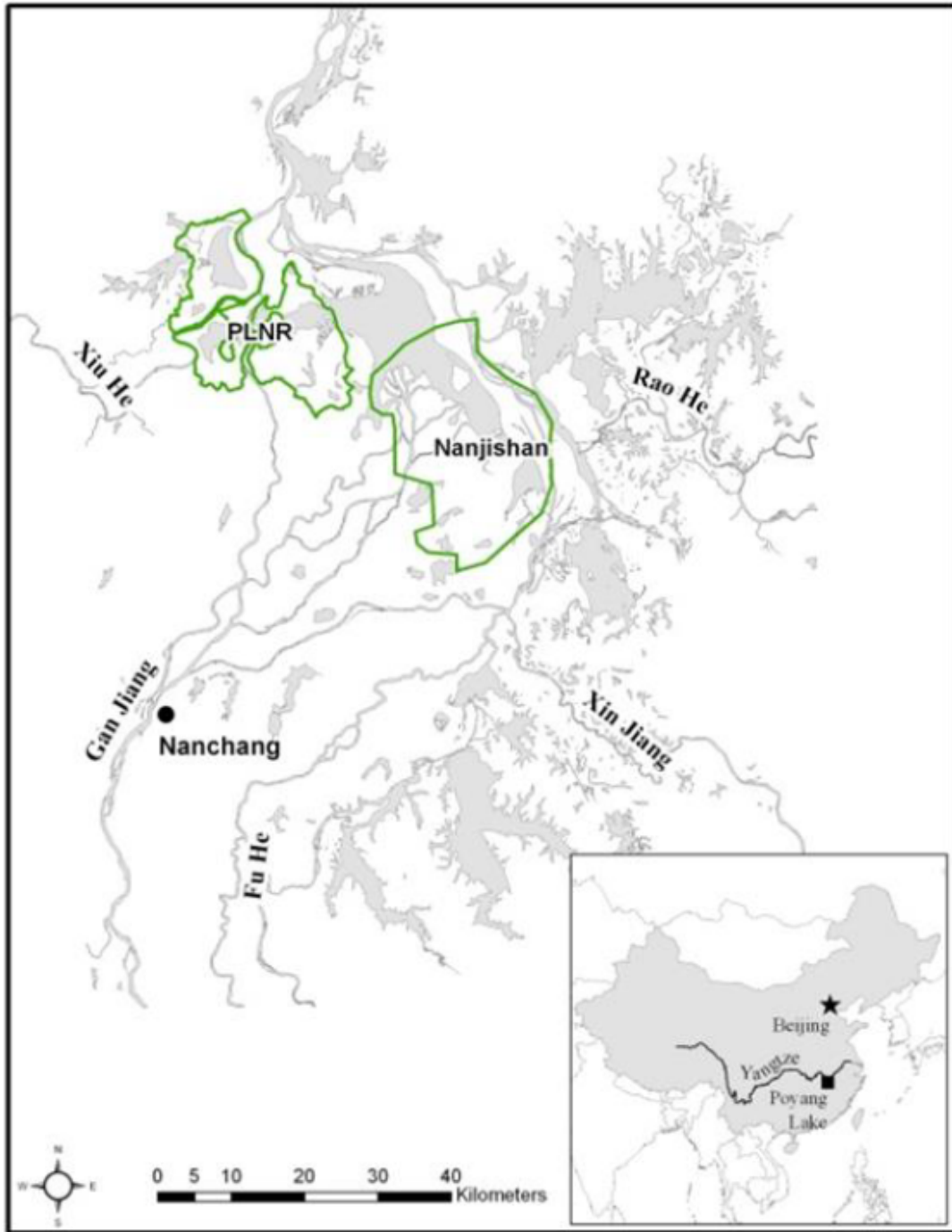
FIGURE 1.1. Map of Poyang Lake, with the Poyang Lake Nature Reserve (PLNR) and the Nanjishan Nature Reserve highlighted. Source: International Crane Foundation.

FIGURE 1.2. Migration routes, breeding and wintering sites. Source: Wikipedia.

Siberian cranes are migratory. They arrive on the northeastern Siberian breeding grounds in late May and eggs are generally laid in June. Incubation takes about 29 days. Two eggs hatch but only one chick typically survives and is raised. This chick fledges within 70 to 80 days and reaches sexual maturity in three years. The main autumn migration begins towards the end of September (Johnsgard, 1983). Scientists also report the recruitment rate of the Siberian crane based on observations in India to be around 10% or less (Johnsgard, 1983).

The population of the Siberian crane is thought to have decreased rapidly over the last three generations[5] (BirdLife International, 2018). There is only one remaining subpopulation of the Siberian crane. The current size of the eastern subpopulation, which breeds in northeastern Siberia and winters in Lake Poyang in China, is estimated to be 3500 to 3800 (Wetlands International, 2012), and makes up about 95% of the whole population of the Siberian crane (Wu et al., 2009). The western subpopulation was believed to be extirpated, but one individual was seen in Iran in 2010 (Wikipedia, 2019). A central subpopulation nested in western Siberia and wintered in India. There were 60-70 cranes seen in the mid-1970s, but the population then declined rapidly. The last sighting in India was documented in 2002 (Bove, 2019). See Figure 1.2 for the migrating routes, breeding, and wintering sites.

[5]The generation length of the Siberian crane is 13 years (BirdLife International, 2018).

5
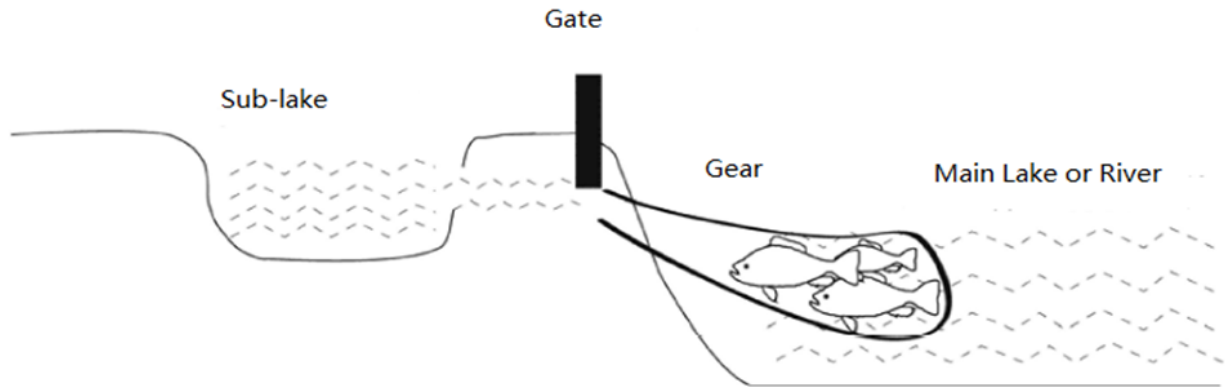
FIGURE 1.3. The ZQH fishing practice in Autumn-Winter. Source: Zeng (2014).

The greatest threats to the population now are habitat loss and degradation in China, highly affected by human activities such as fisheries, hydraulic engineering, and wetland reclamation for fisheries or agriculture. Construction of the Three Gorges Dam(TGD) has also changed the hydrologic pattern of the lower Yangtze River, resulting in lower water levels in winter[6]. Poyang Lake thus drains more rapidly into the Yangtze River during the low water period.

In summary, besides longevity, the Siberian crane has one of the longest and most arduous migratory routes, one of the lowest recruitment rates of all cranes, and highly specialized foraging requirements among all the cranes (Johnsgard, 1983). The population wintering in Lake Poyang is the last surviving group.

1.2.3. The ZQH fishing practice. Local communities around Lake Poyang depend primarily on fisheries and aquaculture. The autumn-winter fishing practice, called ZhanQiuHu(ZQH), has been applied to most of the sub-lakes in Lake Poyang for hundreds of years[7].

Local villages own the user rights of the sub-lakes. They generally allocate temporary user rights via auction to individual contractors on a 2 or 3-year lease contract. Historically, local fishers have constructed short dikes around the sub-lakes in the early spring which maintain the water depth after summer floods recede. Then the local fishers lift the water gates to discharge the sub-lake water into the main lake body. Fish naturally flow into the very fine-meshed fishing nets set at the gate (See Figure 1.3). More recently, fishers have continued draining the sub-lakes by electric pumps to collect as much fish as possible by early February to maximize short-run profits during the lucrative Chinese New Year period.

---

[6] TGD starts water storage on September 15th from 145 meter to meet the target water level of 175 meter. The water level is no higher than 158m by the end of September. By the end of October, the dam implements downstream water supplements while storing water to 175m. With insufficient inflow, TGD will continue water storage in November.

[7]Two stories mentioning the ZQH fishing practice suggest that it existed in Lake Poyang area as early as 1141 in *Record of the Listener* by Hong Mai(1123-1202)(Mai, 2018).The book spoke widely about incidents that are mythical, fantastic, and supernatural. More importantly, it provides rich material to understand every day life in Song Dynasty (960-1279) China.

1.2.4. The conflict. ZQH fishing practice is considered a key determinant of crane habitat. ZQH fishing practice in the sub-lakes slowly draws down the water and exposes tubers at a rate that optimizes fishery profits. Without ZQH fishing, the sub-lakes either remain full (if the gates remain closed) or experience quick water drawdown as the main lake recedes (if gates are left open). However, ZQH fishing starts early and ends early, which imposes negative externalities on Siberian cranes.

The timeline of ZQH fishing practice and the activity of the Siberian crane is shown in Figure 1.4 and Table 1.1. The Siberian crane winters in Lake Poyang from late October or early November to the end of March, mainly foraging on tubers of the submerged aquatic macrophyte *Vallisneria* in the shallow water and mud flats on the periphery of Lake Poyang (Wu and Ji, 2002). Tuber abundance and accessibility significantly affect foraging behavior. Vallisneria grows from April to October and forms tubers from July to October (Li et al., 2015). Photosynthesis and tuber formation can both be enhanced and constrained by light intensity, which varies with fluctuating water depth and clarity of the lake in summer time (Wu et al., 2009) [8]. In the winter, tuber accessibility by cranes is also determined by water levels and tuber location. Draining water in October and November exposes abundant subsurface food for wintering cranes. However, if the lake is drained dry by January or February, it will cause food shortages since the Siberian cranes stay until the end of March and can't forage in dry soils. Tuber consumption, influenced by water levels, determines fat accumulation by the cranes during the wintering period. Insufficient fat reserves may delay migration and subsequent breeding. Siberian Cranes experience such a short breeding season that late breeding might influence the fledging of the juvenile cranes in time to undertake migration (Meine and Archibald, 1996). This will reduce the recruitment of the Siberian crane population, which with a reproduction rate of less than 10%, is already low.
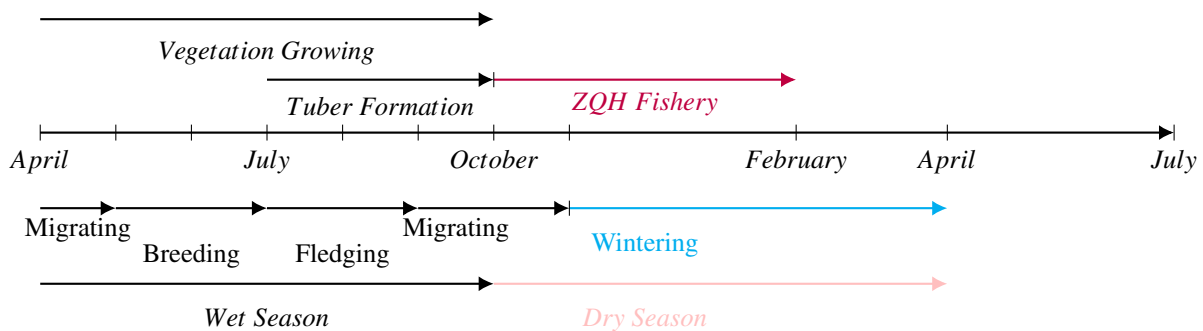
FIGURE 1.4. Timeline of the ZQH Fishery/Cranes/Tubers

---

[8]Yuan et al. (2012) argue that when the water level is too high or too low, tuber production is affected. At a low water level, water clarity decreases due to turbulence and turbidity. High turbidity at low water levels (below 13.5m) is attributed to wave-induced sediment resuspension at the lake periphery, common in shallow lakes (Scheffer, 1997). At a high water level, light attenuates with water depth. In both cases, tuber production decreases because of less photosynthesis.

Year	Birds Arrival	ZQH Fishery
2011-2012	October 26	November 4 - December 15 (Shahu and Dahuchi[†])
2012-2013	October 23	October 12 - December 9 (Shahu and Dahuchi)
2013-2014	October 23	October 20 - November 17 (Shahu and Dahuchi)
2018-2019	November 7	October 28 - February 1 (Xiabeijia Lake[‡])
2019-2020	November 4	Mid Oct. - (Sanni Lake[‡])

- †: Shahu and Dahuchi are rented to and controlled by the Nature Reserve.
- ‡: Xiabeijia Lake and Sanni Lake are controlled by ZQH contractors.

TABLE 1.1. Timing of Crane Arrival and ZQH Fishery Opertaion

There is thus a conflict between privatized ZQH fishing stakeholders and public goods stakeholders interested in the crane population or more generally, biodiversity. Two nature reserve bureaus have directly intervened to divert habitat from the ZQH fishery to crane conservation by renting the user-rights of five sub-lakes in Lake Poyang from 2000 to 2020. However, there are more than 100 sub-lakes and the nature reserve bureau cannot control the water discharge regimes of the remaining sub-lakes controlled by individual contractors. The current system thus does not account for the full system-wide spillover effects of the ZQH fishery on cranes.

1.3. Modeling the conflict

To understand the impact of ZQH fishery on the Siberian crane population under coordinated and uncoordinated management, we derive a hydrologic-bio-economic model of the ZQH fishery, the Siberian crane population, the *Vallisneria* tuber stock, and water discharge (see Figure 1.5). To start, we develop two separate models, one within-year continuous model for the ZQH fishery problem and one hybrid discrete-time/continuous-time model for the crane population problem.
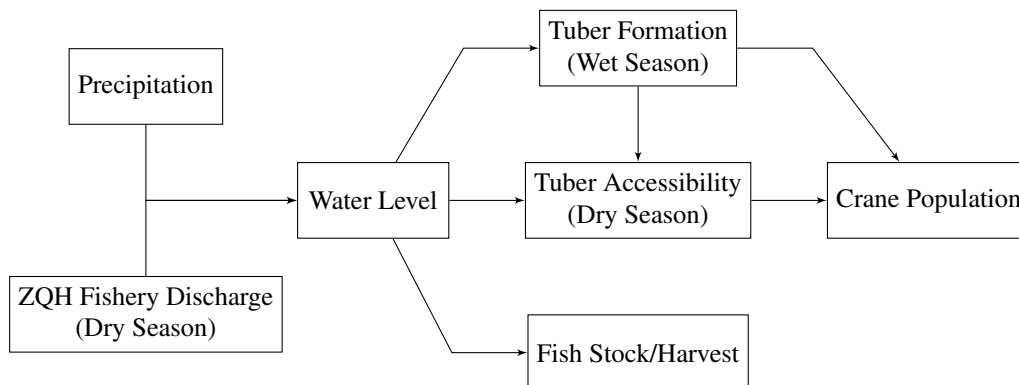
FIGURE 1.5. Ecological relationships between the ZQH Fishery and Siberian Cranes
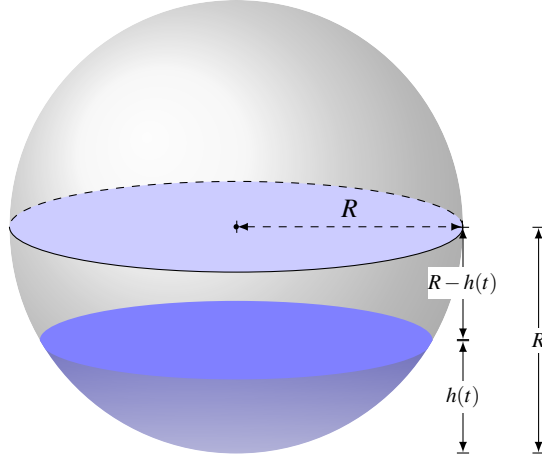
FIGURE 1.6. Lake as a half sphere

1.3.1. Modeling and assumptions. We focus on a representative sub-lake of the nine sub-lakes within Poyang Lake National Natural Reserve (PLNNR), which are among the most important crane and waterbirds wintering sites. We assume that all sub-lake is identical to and managed like the representative sub-lake [9].

1.3.1.1. *Modeling the lake as a half-sphere.* To capture the relationship among water level, the surface area of the lake (relevant to tuber exposure), and the volume of the lake (relevant to fish harvest), we model the lake as a half sphere with radius R (See Figure 1.6). The half sphere approximates the saucer-like lake.

If the lake is full, the initial water level $h(0)$ is R. The surface area and the volume of the half sphere are

$$(1.1a) \qquad S_{\frac{1}{2}\text{sphere}} = 2\pi R^2$$

$$(1.1b) \qquad W_{\frac{1}{2}\text{sphere}} = \frac{2}{3}\pi R^3$$

If the water level decreases to $h(t) < R$ or if the lake starts with an initial water level $h(0) < R$, the lake is a spherical cap with height $h(t)$. The surface area and the volume of the spherical cap are

$$(1.2a) \qquad S(t) = 2\pi R h(t)$$

$$(1.2b) \qquad W(t) = \frac{\pi}{3}(h(t))^2(3R - h(t))$$

---

[9]The cranes depend on all the sub-lakes and the management at the representative sublake is employed at every sub-lake.

1.3.1.2. *Draining the sub-lake.* Assume the ZQH fishery operator or the Nature Reserve staff chooses the aperture size $AP(t)$ of the discharge pipe. The outlet velocity $v(t)$ follows

(1.3a)
$$v(t) = C_v\sqrt{2gh(t)}$$

where $C_v = 0.97$ reflects the incompressibility of water. $g = 9.8\frac{m}{sec^2}$ refers to acceleration of gravity. The flow volume $V(t)$ is then

(1.3b)
$$V(t) = C_d AP(t)\sqrt{2gh(t)}$$

where $C_d = C_v \times C_c$. $C_c \in [0.42, 0.97]$ depending on the shape of the pipe. The aperture size may be restricted within $[\underline{AP}, \overline{AP}]$ [10].

1.3.1.3. *The decisions of the ZQH fishery.* We model the ZQH fishing practice as a sequence of independent within-year decisions. We begin with the following assumptions. See Table 2.1 for parameters and variables used in the model.

Harvest, revenues, costs and the objective functions The fish are uniformly distributed at the representative lake and are passive towards water flow (no behavior that draws them toward or away from outlet). So harvest $H(t)$ is proportional to flow volume $V(t)$, the proportion q is determined by the initial fish stock X_0 and initial volume of the sub-lake W_0:

(1.4a)
$$H(t) = qV(t), q = \frac{X_0}{W_0}$$

Profit $\pi(t)$ equals the revenue from harvest $H(t)$ minus water discharge costs. Fish price p is fixed. Marginal cost is assumed to increase with water flow because larger amount of water release may cause fish bruising, which can result in lower market prices. Larger flow may also destroy fishing nets and gates

(1.4b)
$$\pi(t) = pH(t) - \alpha V(t) - \beta V^2(t)$$

State variables There are two state variables: fish stock $X(t)$ and water volume $W(t)$. Both variables are functions of water level $h(t)$. There is no growth in the fish population $X(t)$ within the fishing season so that fish decreases by

---

[10]We are not including the restrictions in the optimizations. No fish flow out if the flow/aperture size is too small, therefore $AP(t) \geq \underline{AP}$. However, $\underline{AP}$ is a behavioral constraint rather than the technological constraint. It applies to the fishery optimization problem but not the crane optimization problem. There is a maximum outlet size due to a technology constraint, so $AP(t) \leq \overline{AP}$.

harvest $H(t)$:

(1.4c)
$$\dot{X}(t) = -H(t)$$

Water volume $W(t)$ decreases by released water flow $V(t)$:

(1.4d)
$$\dot{W}(t) = -V(t)$$

Endpoint conditions The initial water level $h(0) = R$, and the ending water level $h(T) = \varepsilon$. Initial fish stock X_0 is given. Initial water volume $W(0) = \frac{\pi}{3}(h(0))^2(3R - h(0)) = \frac{2\pi}{3}R^3$. The ending fish stock and water volume are free.

This is a finite-horizon problem with fixed start date and ending date. The ZQH contractor ends the fishing season by the Spring Festival. There are two main reasons for this assumption. First, the strong market and high prices of the fish disappear after the Spring Festival. Second, the rainfall after the Spring Festival increases the main lake water level so that water discharge and fish harvest may become impossible. To avoid the potential loss, the ZQH contractor will release water and reach the target water level at or before the festival. Therefore T^f is set to be the Spring Festival, February 1st [11]. Price after T^f is set to be 0.

The time variable representing days within a season is $t = t_0, \cdots, T^f$. The fishing season starts on a fixed day $t_0 = 0$, November 1st[12]. The season ends on February 1st, so the season length is $T^f = 93$ days.

The optimization problem. With the assumptions above, the economic problem of fish harvesting is that ZQH contractor chooses the size of aperture $AP(t)$ to maximize the present value of the total revenue $\pi(t)$.

(1.5)

$$\max_{AP(t)} \quad \int_0^{T^f} e^{-rt}\{pH(t) - \alpha V(t) - \beta V^2(t)\}dt$$

$$\text{s.t.} \quad \dot{X}(t) = -H(t) = -qV(t) \qquad \text{Fish Stock}$$

$$\dot{W}(t) = -V(t) \qquad \text{Water Volume}$$

$$W(t) = \frac{\pi}{3}(h(t))^2(3R - h(t))$$

$$V(t) = C_d AP(t)\sqrt{2gh(t)} \qquad \text{Water Flow}$$

$$t_0 = 0, T^f = 93, X_0, h_0, h_T \text{ given}$$

---

[11]The Spring Festival falls between January 21st and February 20th. In this analysis, Spring Festival is set to be February 1st.

[12]Table 1.1 reflects that the ZQH season start date differs across years and sub-lakes. The ZQH contractors usually start to release water when the water level difference between the sub-lake and main lake is sufficiently large (the main lake water level drops below a certain threshold which marks the beginning of the lake's dry season). The chapter starts with the simplified assumptions of a fixed start and end date. The choice of optimal start and end dates will be incorporated in future research.

The model can be reframed as a problem with one state variable water level $h(t)$ (see derivation in Appendix B.1)).

(1.6)

$$\max_{AP(t)} \int_0^{T^f} e^{-rt}[pqZAP(t)\sqrt{h(t)} - \alpha ZAP(t)\sqrt{h(t)} - \beta Z^2 AP^2(t)h(t)]dt$$

$$\text{s.t.} \quad \dot{h}(t) = \frac{-ZAP(t)\sqrt{h(t)}}{\pi(2Rh(t)-h^2(t))}$$

$$Z = C_d\sqrt{2g}$$

$$t_0 = 0, T^f = 93, X_0, h_0, h_T \text{ given}$$

1.3.1.4. *Optimal ZQH drawdown decisions: phase diagram analysis.* The model in Equation 1.6 can be used to examine optimal sub-lake drawdown decisions when control of sub-lakes rests with a contractor motivated by maximizing fishing profits. This setting, in fact, captures much of the implicit property rights sytem as it exists currently in Lake Poyang, in the sense that most sub-lakes are managed following centures old ZQH practices without regard to the impacts on cranes.

As a first step in characterizing how a ZQH contractor would be expected to manage sub-lake water levels, we construct a phase diagram of the system. The phase diagram allows us to see various optimal paths under different assumptions about various parameters. Some parameters of importance deal with the hydrological system (sub-lake size, initial depth, aperture characteristics), and others characterize economic factors (prices, costs, discount rate).

Phase diagrams Specifying the initial water level of the representative sub-lake as 5 meters and requiring the ending water level to be 0.3 meter, Figure 1.7 shows the numerical phase diagram with a few trajectories. There is a fairly rich variety of qualitative patterns to solution trajectories, ranging from those that start with a small aperture and decrease steadily with a extra long time horizon, to those that start with a wide aperture and increase till the end with a short time horizon. Note that with within-year horizons, the optimal path involves a wider aperture held over the short period until the ending volume hits the target. The shorter the time horizon, the more the optimal path is dictated by the simple need to drive the water level from an initial level to a targeted end level. As more time is allowed to optimize, economics begin to play a role in dictating the shape of the optimal trajectory. Two factors are at play: keeping the flow trajectory flat to keep costs low, and increasing benefits by having a larger aperture size and flow. Discounting also influences the trajectory, by tilting optimal flow paths to the present in order to capture fisheries benefits earlier [13] (Note: these points emerge more clearly when the phase diagram was computed using a higher discount rate in Figure 1.7c).

With this understanding of the qualitative nature of optimal decisions from the perspective of ZQH contractors, the next question is: how do these decisions impact the crane population? To understand this, we need to develop a crane population model. That model should characterize how various sub-lake drawdown decisions affect the tubers exposed

---

[13]Water level is higher at the beginning of the season and larger flow would yield more fish catch.

(a) discount rate $r = 0.0002$

(b) flow

(c) discount rate $r = 0.002$

(d) flow
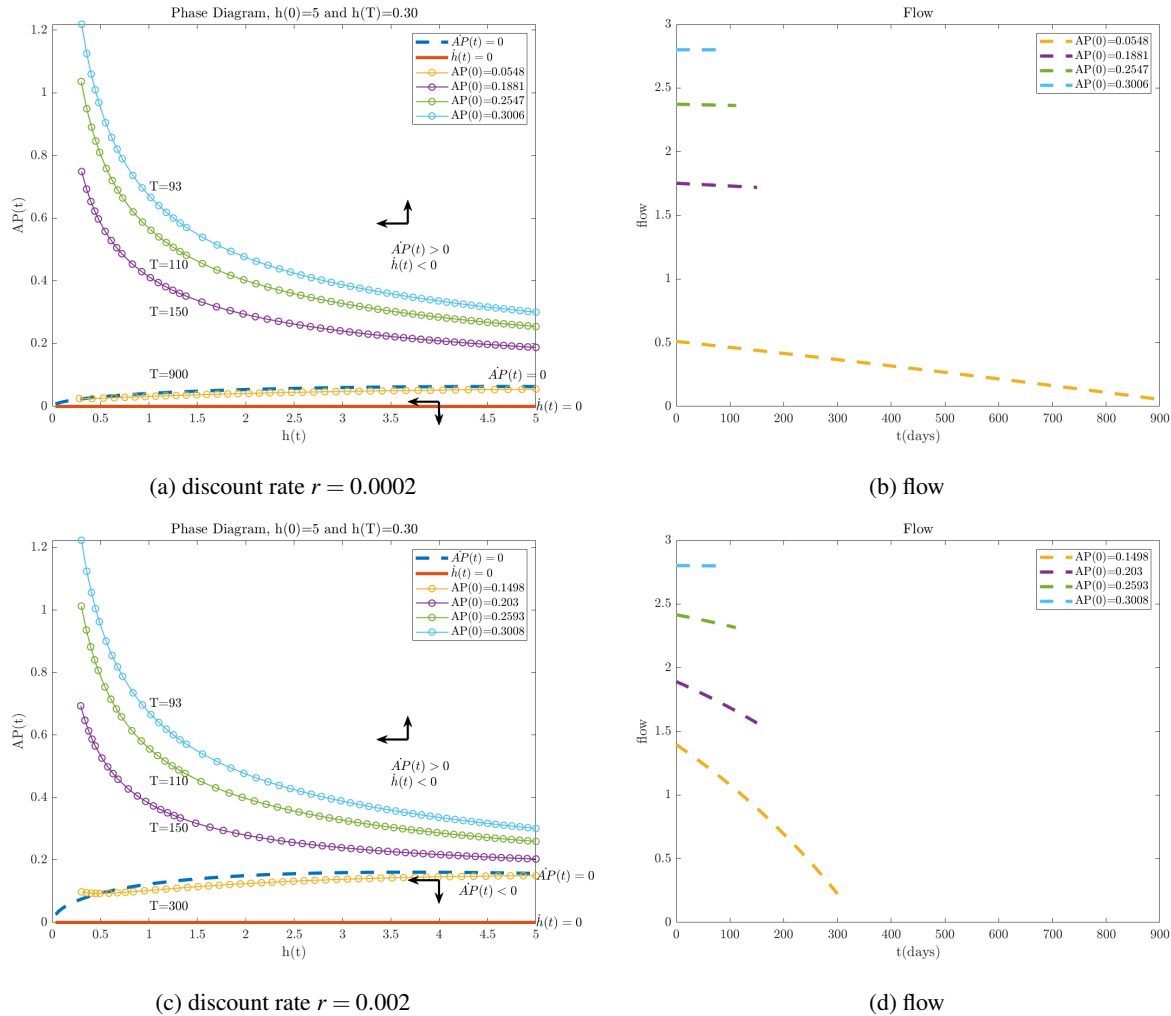
FIGURE 1.7. Numerical phase diagram

to cranes, how that tuber exposure affects the condition of the cranes, how crane condition (fat stored) affects crane survival during the wintering period, and how crane condition and population size affects subsequent reproduction during the summer breeding season in Siberia.

1.3.1.5. *The crane population model.* The high metabolic rate of birds implies continual energy consumption and the need for a constant supply of food (Biebach, 1996). Fat is a significant (but not exclusive) source of energy reserves when demand exceeds intake in situations such as migration (Blem, 1980; Bull et al., 1996). Fat reserves affect the fitness of the bird and its reproduction rate at the end of the season. The mortality rate increases if there is no sufficient intake and the fat level falls. For generalists such as the Siberian crane, habitat and diet shift (from shallow water to meadow, and from tubers to rice grains) under extremely adverse conditions for survival. However, significantly

different behavior patterns are observed in alternative habitats compared to optimal habitats. Jia et al. (2013) found that the Siberian cranes allocate significantly less time foraging and more time alerting in the wet meadow. The diet and habitat shift provide refugia for the cranes, but multi-year dependence on an alternative habitat can negatively harm the population level. Burnham et al. (2017) observed a lower juvenile to adult ratio of Siberian crane after the meadow foraging due to low *Vallisneria* tuber densities across sub-lakes because of the flood in Lake Poyang in 2010. Therefore, we model food shortage leading to lower wintering survival and lower reproduction success of the Siberian crane, which reduce the population.

For the bird problem, we begin with a simple model of the winter foraging and fattening strategy based on the dynamic state variable models of willow tits and juvenile salmon in Clark and Mangel (2000). To reduce model complexity, we ignore social interactions at wintering ground, migration, and breeding. This model also does not include predation risk and hoarding behavior because there is little evidence documented in the crane literature of either. The conceptual model is useful to describe and understand the within-season and between-season dynamics of the crane population.

The interaction between consumers (e.g., predators) and resources (e.g., prey) is a fundamental focus of ecology (Murdoch et al., 2003). There are two approaches to study such interactions: continuous-time models to capture population dynamics and discrete-time models for reproduction occurring in discrete pulses determined by season. Discrete-time models are a tradition for the host-parasitoid system (Nicholson-Bailey host parasitoid model) and plant-herbivore interactions (Edelstein-Keshet, 2005). Such an approach, however, ignores the within-season population dynamics due to different processes (Hastings and Gross, 2012). Therefore Singh and Nisbet (2007) and Murdoch et al. (2003) have used hybrid discrete/continuous-time models or semi-discrete models to represent within-season interactions with discrete between-season dynamics of host-parasitoid system. In the bird problem, the between-season discrete-time model is appropriate for the crane reproduction once per year. The processes of water discharging, foraging and mortality occur continuously during the dry season and are best represented by the continuous-time model. Therefore a hybrid approach is most appropriate to model the dynamics of various within-year processes in continuous time and reproduction as a discrete event.

For the initial model covering a 150-day wintering period (from November 1st to March 31st) at Lake Poyang, we begin with the following assumptions. There are three state variables: water level $h_j(t)$, crane population $B_j(t)$, and crane energy reserve $E_j(t)$. See Table 2.2 for parameters and variables used in the model.

Tuber growth and exposure Tubers are uniformly distributed at the bottom of the lake. Suppose we start with an initial water level $h_j(0)$ and initial tuber stock M_j. The surface area of the lake $S_j(0)$ is

(1.7a)
$$S_j(0) = 2\pi R h_j(0)$$

The area density of the tuber stock will be $\frac{M_j}{S_j(0)}$. The birds only forage on the newly exposed tubers by a fraction of $\rho \in (0,1]$. The exposed surface area will be the negative change rate of surface area. From Equation 1.2a and Equation B.5 , the change rate of surface area is

(1.7b)
$$
\begin{aligned}
S_j(t) &= 2\pi R h_j(t) \\
\Rightarrow \dot{S}_j(t) &= 2\pi R \dot{h}_j(t) \\
&= \frac{-2RC_d AP_j(t)\sqrt{2gh_j(t)}}{(2Rh_j(t)-h_j^2(t))} \\
&= \frac{-2RZAP_j(t)\sqrt{h_j(t)}}{(2Rh_j(t)-h_j^2(t))}
\end{aligned}
$$

Energy reserves dynamics The accessible tubers per crane at time t year j is the accessible tubers divided by bird population $B_j(t)$.

(1.7c) $\quad C_j(t) = \dfrac{-\dot{S}_j(t)M_j}{S_j(0)B_j(t)} = \dfrac{-\dot{h}_j(t)M_j}{h_j(0)B_j(t)} = \dfrac{2RZAP_j(t)\sqrt{h_j(t)}M_j}{(2Rh_j(t)-h_j^2(t))(2\pi Rh_j(0))B_j(t)} = \dfrac{ZAP_j(t)\sqrt{h_j(t)}M_j}{\pi h_j(0)B_j(t)(2Rh_j(t)-h_j^2(t))}$

Rate of fat accumulation increases while foraging. There is a fixed daily metabolic cost c for the cranes. There is no difference in the metabolic rate between foraging activity and rest. If a crane forages a fraction ρ of the exposed tubers, the energy reserve dynamics are given by:

(1.7d)
$$\dot{E}_j(t) = \rho C_j(t) - c$$

Within-season population dynamics The impact of accessible tubers per capita on crane population is asymmetric. The wintering mortality rate at t increases with the reduction in energy reserve because of insufficient tuber intake ($\dot{E}_j(t) < 0$). With a low density of the preferred *Vallisneria* tubers, some Siberian cranes will switch to other food such as rice and lotus root (Burnham et al., 2017; Jia et al., 2013). The cranes spend more time alerting and less time foraging with diet shift. We assume the risk of mortality is larger in the suboptimal wintering ground. If the tuber intake is sufficient to offset the metabolic cost, ($\dot{E}_j(t) > 0$), there is no mortality. Because reproduction takes place after the wintering period at the breeding grounds, there is no within-year increase in crane population.

(1.7e)
$$\dot{B}_j(t) = min[0, exp(\zeta \dot{E}_j(t)) - 1]B_j(t)$$

End-of-season conditions We use two time variables t, an index of the day in the winter season, and j, an index of the year. $t = 1, 2, \cdots, T^b$, and $j = 1, 2, \cdots, J$, where T^b is the length of the winter season (150 days from November 1st to March 31st) and J is the year horizon. The state variable $E_j(t)$ represents energy reserves of cranes at the end of day t of year j. On each day t of year j, the aperture size $AP_j(t)$ is chosen. The water level of the lake falls and tubers are exposed. Energy reserves increase while foraging. The crane population $B_j(t)$ of day t of year j stays stable or decreases during the wintering season and increases via reproduction at the end of the season.

We assume the initial water level $h_j(0) = R$ and ending water level $h_j(T) = \varepsilon$ for every year j. The initial energy reserve per crane $E_j(0)$ is fixed every year. The initial crane population $B_1(0)$ is set to be 3000. End of season crane population and energy reserve are free.

We also assume that the initial tuber stocks are the same across years, $M_j = M$, so that foraging in year j doesn't affect the initial tuber stock in year $j + 1$, M_{j+1}. Sponberg and Lodge (2005) finds no detectable carryover effects of waterfowl exclosure on *Vallisneria Americana* aboveground biomass in subsequent growing seasons despite a significant reduction of tubers during winter. The shifting habitat and diet behavior of Siberian cranes after an abnormal flood in 2010 in Jia et al. (2013) and Burnham et al. (2017) support this assumption[14].

Between-season population growth Insufficient energy reserves at the end of the wintering season T of year j may lead to low reproduction success. The cranes might stay longer at Lake Poyang or stop at extra migration sites to for energy necessary for migration. Both may delay the whole breeding process whereby the juveniles might not have enough time to fledge and therefore die in the cold winter of Siberia. The survival rate of the juvenile at year j f_j is a function of the end-of-season energy reserve $E_j(T)$.

(1.7f)
$$\begin{aligned} f_j &= 1 - exp(-pE_j(T)) \\ \frac{\partial f_j}{\partial E_j(T)} &= pexp(-pE_j(T)) > 0 \end{aligned}$$

The reproduction of the Siberian cranes happens after the winter season at the breeding grounds. With n as the reproduction rate and d as the natural death rate of the cranes, the crane population coming back to Lake Poyang in year $j + 1$ can be modeled as

(1.7g)
$$B_{j+1}(0) = (1 + nf_j - d)B_j(T)$$

The crane's fitness is characterized as the adult survival rate and reproductive success reflected by the juvenile survival rate.

---

[14]When the tuber density in a wintering ground drops below a threshold, the Siberian cranes will leave for new places or new food. The tuber stock won't be depleted and may recover next year.

1.4. Optimization numerical methods

The above model can be used for predictive exercises, such as exploring how various decisions by operators of the fishery system influence the cranes. The model can also be used for normative exercises. For example (and as a comparison with above), we might ask what draw-down policy is most beneficial to the crane population? Answering this requires postulating a benefit function for the crane population and an objective function.

There are various ways to set up the objective function for the bird's problem. One choice is to maximize the bird population at beginning of year $J+1$, $B_{J+1}(0)$ with a finite J, by choosing the aperture size of day t of year j. The second choice might maximize the discounted sum of crane conservation benefit minus water discharge cost $\Sigma_{j=1}^{J} \int_0^{T^b} e^{-rt}[g(B_j(t)) - \alpha ZAP_j(t)\sqrt{h_j(t)} - \beta ZAP_j^2(t)h_j(t)]dt$[15], by choosing the aperture size of day t of year j. The crane conservation benefit from bird watching and bird photography tourism is an increasing function of crane population at day t of year j, $g(B_j(t)) = \omega log(B_j(t))$, $\omega > 0$. This is an integrated goal to combine economic development with biodiversity conservation in the landscape. The crane conservation benefit is a flow of instantaneous return of the crane population.

(1.8)

$$\max_{AP_j(t)} \quad \Sigma_1^{J} \int_0^{T^b} e^{-rt}[\omega log(B_j(t)) - \alpha ZAP_j(t)\sqrt{h_j(t)} - \beta Z^2 AP_j^2(t)h_j(t)]dt$$

$$\text{s.t.} \quad \dot{h}_j(t) = \frac{-ZAP_j(t)\sqrt{h_j(t)}}{\pi(2Rh_j(t) - h_j^2(t))} \qquad \text{water level}$$

$$C_j(t) = \frac{-\dot{h}_j(t)M_j}{h_j(0)B_j(t)} \qquad \text{accessible tuber per capita}$$

$$\dot{E}_j(t) = \rho C_j(t) - c \qquad \text{energy reserve}$$

$$\dot{B}_j(t) = min[0, exp(\zeta \dot{E}_j(t)) - 1]B_j(t) \qquad \text{bird population}$$

$$f_j = 1 - exp[-pE_j(T)] \qquad \text{juvenile survival rate}$$

$$B_{j+1}(0) = (1 + nf_j - d)B_j(T) \qquad \text{crane reproduction}$$

$$Z = C_d\sqrt{2g}$$

$$B_1(0), \quad E_j(0), h_j(0), h_j(T), M_j, T^b \text{ given}$$

$$B_j(T), \quad E_j(T) \text{ Free}$$

A one-year version of the model is shown in Figure 1.8. We can relax various assumptions in a more complicated model to explore the importance of alternative mechanisms. For example, theoretical work shows that the size of the fat reserve depends on the trade-off between storage costs and anticipated needs (Lima, 1986; Witter and Cuthill, 1993). To account for this trade-off relationship, we could model daily metabolic costs that increase with the level of fat reserves instead of a fixed daily cost. Also, this model of reproduction doesn't consider Alee effects whereby the population goes extinct if it falls below a critical positive threshold level (Clark and Mangel, 2000).

---

[15]The water discharge cost is convex in released water flow because high flow may destroy the gate. The cost coefficients in the crane optimization problem can be smaller than the cost coefficients in the fishery optimization problem because the potential fishing nets damage is ignored.
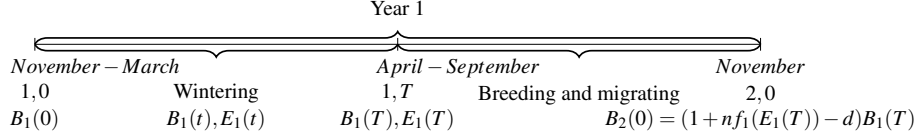
FIGURE 1.8. Timeline for the one-period birds problem

1.4.1. Joint management. Under the coordinated management system, the optimal policy chooses the size of the aperture within year to maximize the combined present value of total revenue from fishery and the crane conservation benefits minus the water discharge cost, subject to the state equation of water level and other constraints in the fishery system and bird-tuber system. The joint management time horizon within each year is from November 1st to March 31st, with $t_0 = 0$, $T^b = 150$.

(1.9)

$$\max_{AP_j(t)} \quad \sum_1^J [\int_0^{T^b} e^{-rt} \{pqV_j(t) + \omega log(B_j(t)) - \alpha V_j(t) - \beta V_j^2(t)\} dt]$$

$$\text{s.t.} \quad \dot{h}_j(t) = \frac{-ZAP_j(t)\sqrt{h_j(t)}}{\pi(2Rh_j(t) - h_j^2(t))}$$

$$V_j(t) = ZAP_j(t)\sqrt{h_j(t)} \qquad \text{water flow}$$

$$C_j(t) = \frac{-\dot{h}_j(t)M_j}{h_j(0)B_j(t)} \qquad \text{accessible tuber per capita}$$

$$\dot{E}_j(t) = \rho C_j(t) - c \qquad \text{energy reserve}$$

$$\dot{B}_j(t) = min[0, exp(\zeta\dot{E}_j(t)) - 1]B_j(t) \qquad \text{bird population}$$

$$f_j = 1 - exp[-pE_j(T)] \qquad \text{juvenile survival rate}$$

$$B_{j+1}(0) = (1 + nf_j - d)B_j(T) \qquad \text{crane reproduction}$$

$$Z = C_d\sqrt{2g}$$

$$X_0, h_0, h_T, E_0, B_1(0), M_j \text{ given}$$

$$t_j(0) = 0, T_j = T^b = 150$$

1.4.2. Numerical methods. The fishery problem is a single within-year optimal control problem with one state variable and one control variable. The Appendix Section B.3 solves the problem analytically using Pontryagin conditions. We also solve the problem numerically using using BVP4C in MATLAB.

The multiyear crane problem and the multiyear joint problem include three state variables and are within-year continuous and between-year discrete. The state variable crane population carries over years and experiences a between-year jump by the discrete reproduction event. This jump discontinuity in state makes the nonlinear problem nonsmooth. We use GPOPS-II, a MATLAB software to solve this nonsmooth and nonlinear optimal control

18

problems with three state variables (Patterson and Rao, 2014). GPOPS-II uses the Gauss pseudospectral method and sparse nonlinear programming.

Solving an optimal control problem using a direct method[16] requires the approximation of three types of mathematical objects: the integration in the objective function, the differential equation of the control system, and the state-control constraints. In a pseudospectral method, the continuous functions are approximated using polynomials at a set of carefully selected quadrature nodes (Gaussian quadrature collocation points in GPOPS-II)[17].

The optimal control problem may thus, be transcribed into a nonlinear programming problem and the NLP solved using solvers like SNOPT or IPOPT. Using the global polynomial with the Gaussian quadrature collocation points, the pseudospectral method converges exponentially if the solutions are smooth(Kang et al., 2008).

The discontinuities and switches in states, controls, cost functions and dynamic constraints in the hybrid optimal control problem[18] are allowed by the pseudospectral knotting method (Ross and D'Souza, 2005; Ross and Fahroo, 2004). Figure 1.9 shows a nonsmooth nonlinear problem with jump in state at t_1 and dynamics switch at t_2. The hybrid optimal control problem is treated as a three-phase problem where each phase is a continuous problem. The state jump and dynamics switch are pseudospectral knots, where the value of the function is allowed to be multivalued. Therefore the information is passed across phases in the form of discrete event conditions (boundary conditions) localized at the pseudospectral knots linking each phase.

In the crane problem and joint problem, each wintering season is treated as a phase. At the end of the wintering season, the crane population reproduces in Siberia and creates a jump in the state variable. The initial crane population of phase $i + 1$ as a function of the ending crane population and ending energy reserve of phase i is coded as discrete event constraints.

---

[16]An indirect method to optimization problems works by analytically constructing the necessary and sufficient conditions for optimality, which are then solved numerically. A direct method attempts a direct numerical solution by constructing a sequence of continually improving approximations to the optimal solution.

[17]The terms pseudospectral and orthogonal collocation have the same meaning. In a Gaussian quadrature (orthogonal) collocation method, the state is typically approximated using a Lagrange polynomial where the support points of the Lagrange polynomial are chosen to be points associated with a Gaussian quadrature(Eide et al., 2021). The most well developed Gaussian quadrature methods are those that employ either Legendre-Gauss (LG) points, Legendre-Gauss-Radau (LGR) points, or Legendre-Gauss-Lobatto (LGL) points. These three sets of points are obtained from the roots of a Legendre polynomial and/or linear combinations of a Legendres polymoial and its derivatives. All three sets of points are defined on the domain $[-1, 1]$, but differ significantly in that the LG points include niether of the endpoints, the LGR points include one of the endpoints, and the LGL points include both of the endpoints(Garg et al., 2011).

[18]A hybrid optimal control problem combines a continuous system with a discrete system.
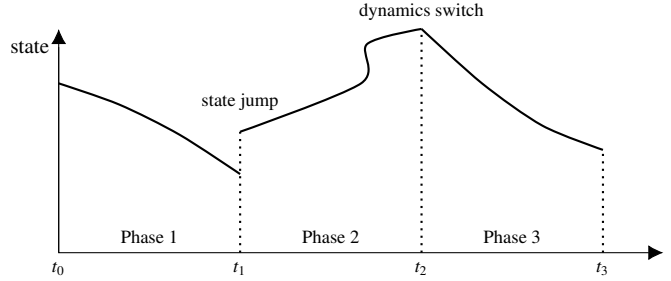
FIGURE 1.9. A (nonsmooth) multi-phase optimal control problem

1.5. Results: the integrated fishery, bird and tuber system

The integrated model can be utilized to examine the implications of various implicit property rights systems that generate alternative incentives that favour either the ZQH fishery system or the crane population. For example, we can assume that drawdown decisions are in the hands of the ZQH contractor, who is motivated to maximize fishery profits. The resulting profit maximizing drawdown paths can then be inserted into the crane and tuber system to simulate the impacts on the crane population. Alternatively, we can assume that a sub-lake is controlled by the Nature Reserve Bureau for the benefit of the cranes, and examine the impact (losses) to the ZQH fishery from pursuing crane conservation policies. Finally, we can examine the jointly optimal decision that seeks to maximize both fishry and crane benefits. Solutions to the joint problem would then be expected to look like the ZQH or Nature Reserve Bureau decisions depending upon the relative benefits placed on cranes vis-à-vis fishery benefits.

In this section, we solve several optimization problems to illustrate the implications of various control strategies. We build up intuition by first solving some simple (an incomplete) problems and then move to more general formulations. First, we solve two "one year" problems that assume some initial conditions and then optimize over a single within-season drawdown problem. There take the perspective of systems managed by the ZQH decision maker, and the Nature Bureau decision maker, respectively. Then we solve the same problems over a longer (5-year) horizon, and use the those solutions to discuss where the complete infinite horizon optimization problem is converging in the steady state. Finally, we solve the joint optimization problem that assumes the system is managed as n integrated system by managers that are interested in both fishery and crane conservation benefits simultaneously.

1.5.1. One-year solution.

1.5.1.1. *Fishery system.* Figure 1.10 shows the optimal path of aperture size and the water level with fixed season length of 93 days. Aperture size $AP(t)$ increases over time to maintain a relatively stable and unchanging water flow and minimize cost, because the cost is quadratic in water flow which depends on both the aperture size and water level ($V(t) = ZAP(t)\sqrt{h(t)}$). Harvest is proportional to water flow (Harvest(t) = $qV(t)$)). Therefore, same aperture size

releases more water and harvests more fish with a higher water level. Flow $V(t)$ is flat with a large quadratic cost coefficient $\beta = 0.05$ (Figure 1.10a), while it is downward sloping with a small quadratic cost coefficient $\beta = 0.005$ (Figure 1.10b). With discounting and small cost, it's optimal to harvest more fish with a larger flow at the beginning given the water level is higher, so that the discounted profit is higher. Without discounting, flow will be constant within season. There is no carryover effect from year to year. Therefore ZQH contractor will repeat the same path every year.

(a) Large quadratic cost $\beta = 0.05$, flat flow   (b) Small quadratic cost $\beta = 0.005$, earlier payoff with larger flow
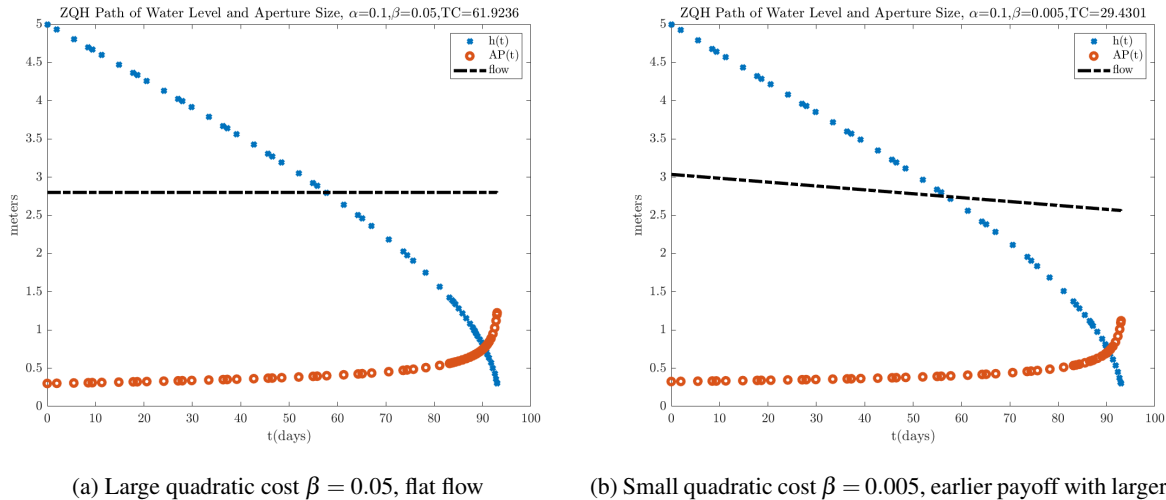
FIGURE 1.10. Fishery path

1.5.1.2. *Bird and tuber system.* We illustrate the multiyear crane and tuber system that is within-year continuous and between year discrete using the one-year version in this section. In a year with sufficient tubers for the crane population [19], the Nature Reserve chooses the aperture size $AP(t)$ that maximizes the conservation benefit minus the water discharge cost. The optimal path of aperture size and water level is shown in Figure 1.11a. Water is continuously released to expose tubers to the cranes. The aperture size increasing over time is to maintain the relative flat flow to minimize the cost. Within-season change in energy reserve and crane population is plotted in orange in Figure 1.11b. In a year with sufficient tubers, the Nature Reserve avoids crane mortality within the year and accumulates energy reserves. The initial crane population of year 1 is calibrated to be closer to the current population estimate of 3000, and the population coming back next year will be 3029 with an increase of around 1%.

1.5.1.3. *Impact of fishing practice on crane population.* Now we plug the fishery path into the crane population dynamics to see the impact of fishery on crane population. We get the within-season change of the Siberian crane

---

[19]In a year with sufficient tubers for the crane population, it is possible to avoid wintering mortality with continuous water draw-down, since the crane population is within the carrying capacity of the environment. In contrast, in a year with insufficient tubers, it is impossible to avoid the wintering mortality.

population and the individual energy reserve (blue paths in Figure 1.11b). The initial Siberian Crane population at Year 1 is 3000. From Figure 1.11b, the Siberian Crane at the end of Year 1 dropped by 5.5% to around 2834. The final energy reserve is also lower than that of the bird model, so that the juvenile survival rate will be lower. The fewer surviving adult cranes and the fewer surviving new born juveniles lead to a smaller crane population of 2861 coming back at Year 2 with a decrease of 4.6%.

The negative externality of the fishery on the crane population comes from the timing difference in operation (Figure 1.12). The fishing season ends early by the Spring Festival and leaves no tubers exposed to the cranes between the Spring Festival and the end of March. The wintering mortality rate increases for the cranes as they have to shift habitat to find food. This juvenile survival rate may fall because the breeding process will probably delay due to insufficient energy reserve. Both lead to a smaller population of the critically endangered Siberian crane.

(a) Path of Water Level and Aperture Size   (b) Path of Crane Population and Energy Reserve
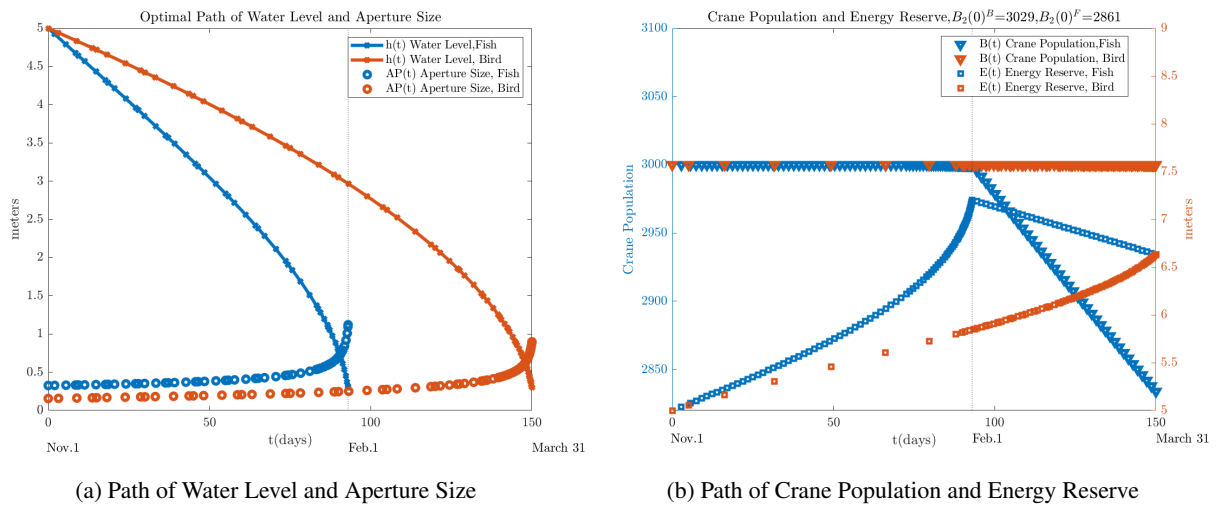
FIGURE 1.11. Impact of fishing practice on crane population

1.5.2. 5-Year simulation. The individual ZQH contractor repeats the optimal path of aperture size and water level of the fishery model year by year. The bird problem is a complicated multi-year optimal control problem that is within-year continuous and between-year discrete. Therefore, the joint management problem is also a multiyear hybrid problem. This section simulates the effect of three management regimes of fishery only, crane conservation only, and joint management with sufficient tubers over a five-year horizon[20].

1.5.2.1. *Fishery only.* To mimic the current system, Figure 1.13 shows a 5-year simulation with only fishery profit included in the objective function. Water release stops on February 1st every year, leaving the water level at the

---

[20]Results with insufficient tuber are in the Appendix Section D.
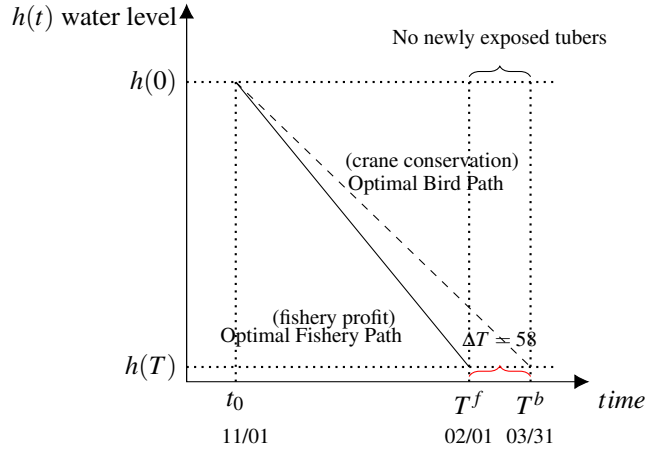
FIGURE 1.12. Comparison of fishery path and bird path of water level

target 0.3 meter from February 1st to March 31st. The crane population remains unchanged during the water release. But due to the early stoppage of fishery operation and no tuber exposure, the crane population drops by 21% from the initial 3000 to 2370 over the five years.
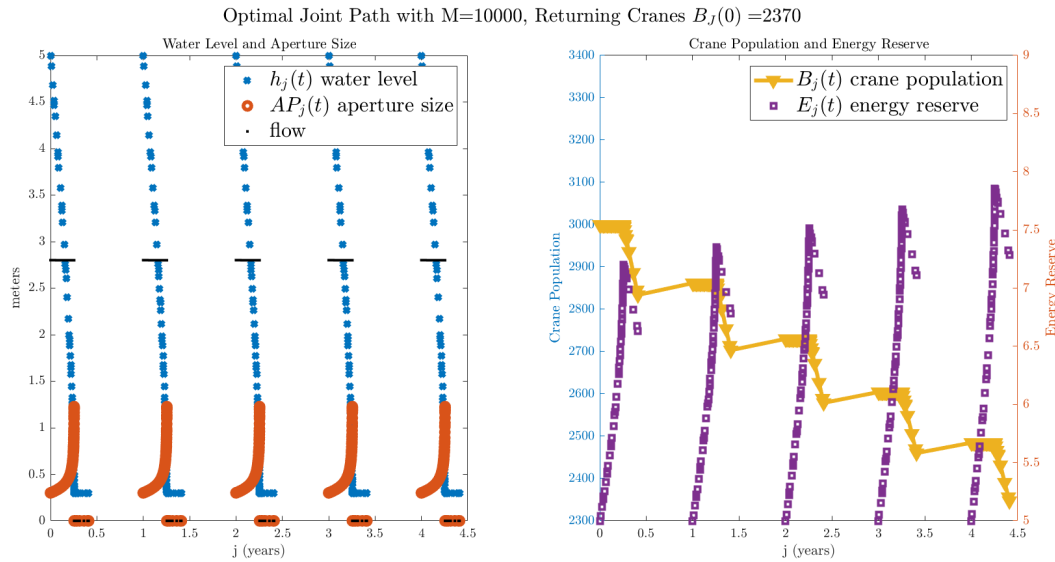
FIGURE 1.13. Fishery profit only, no water release after Feb 1st, cranes 3000 ↓ 2370 by 21%.

1.5.2.2. *Crane conservation only.* If we instead only focus on the crane conservation benefit in the objective function, Figure 1.14 shows the five-year simulation results. Water discharge extends to March 31st, the end of the wintering season for the Siberian cranes. There is no crane death within the wintering season and a steady increase via reproduction. The crane population increases by 5% from the initial 3000 to 3150 over the five-year. The water

23

flow is upward sloping because of cost minimization and discounting. Since every year has sufficient tubers, there is no within-year crane death with continuous water draw-down. Then the large flow is pushed to the end of the year to avoid high cost because of discounting.
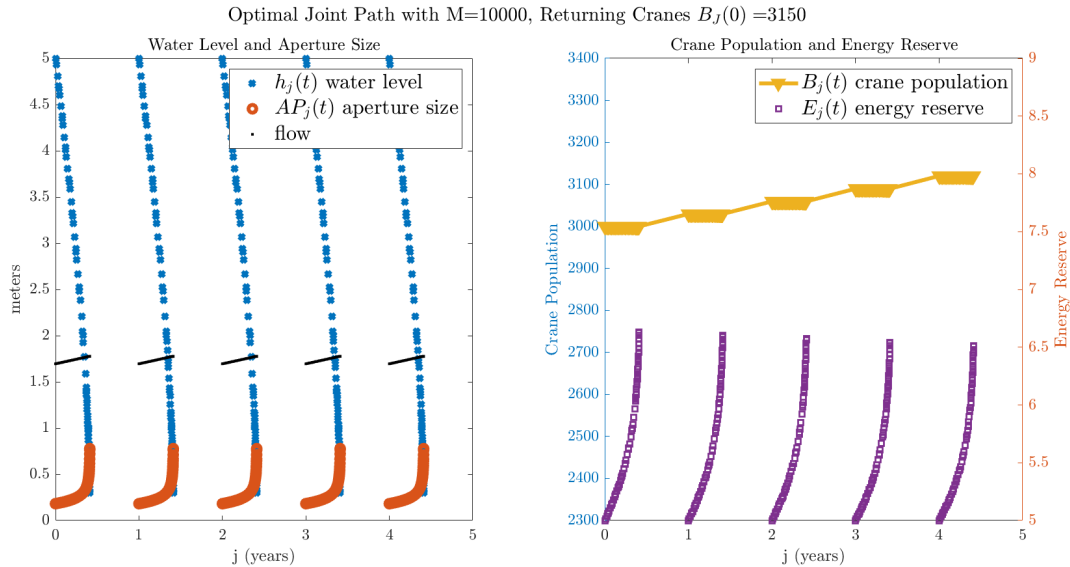
FIGURE 1.14. Crane conservation benefit only, water release till March 31st, cranes 3000 ↑ 3150 by 5%.

1.5.2.3. *Joint fishery and crane management.* Figure 1.15 shows the five-year simulation results considering both fishery revenue and the crane conservation benefit. Water release covers the whole wintering season from November 1st to March 31st. Yet there are two sets of aperture sizes/water flows. Because of sufficient tubers, there is no within-season crane death with continuous water draw-down. Fish price drops to zero after February 1st, therefore the social planner will catch as much fish as possible to maximize the fishery revenue via maximizing the water flow before February 1st. The social planner has to leave some water to prevent crane mortality from February 1st to March 31st. Thus, through the joint management, water releases continuously during the whole wintering season. The crane population increases by 5% from the initial 3000 to 3150 over the five year while most of the fishery revenue is reserved.

1.5.2.4. *Policy options.* In the joint fishery and crane management, the fishery revenue decreases by 25.5% because the lake is not drained and some fish are not harvested before the Spring Festival. The fishery revenue reduction measures the opportunity cost for crane conservation and can be used as the minimum compensation payments from the government to incentivize the fishery to extend the draining season. Alternatively, the government could pay the fishers a "bonus" for the end-of-season crane population or fitness conditions to incentivize the ZQH contractors to
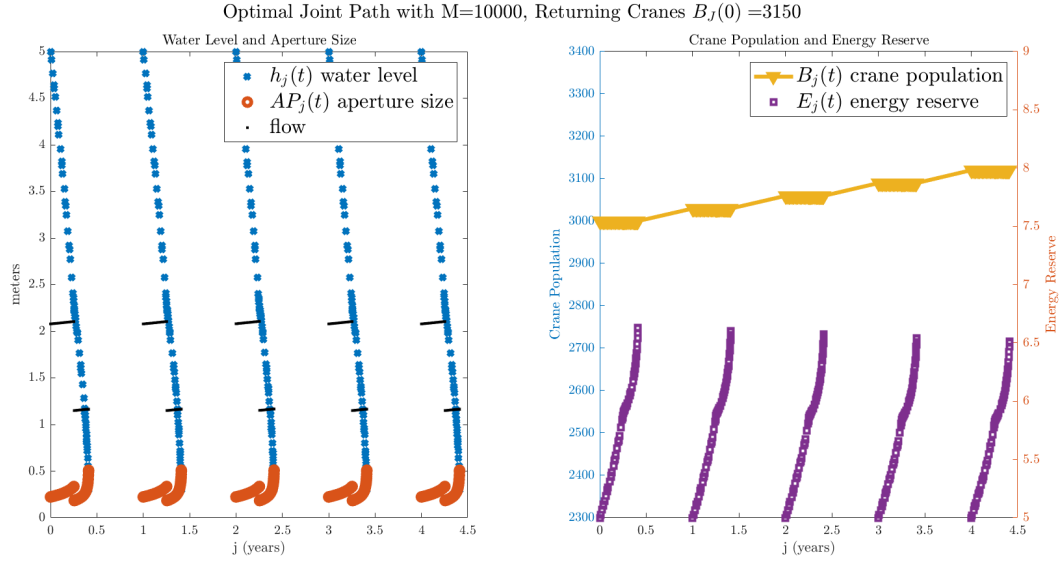
FIGURE 1.15. Joint Management, by extending water release season, cranes $3000 \uparrow 3150$ by 5% while preserving some fishery revenue.

adjust the fishing season. It may also work to develop or subsidize the post-Spring Festival fish market. This market-based approach offers economic rewards to offset the income loss of the contractors to extend the season.

The results also suggest the possibility of Coasian negotiations where the Nature Reserve controls the water draw-down and compensates the ZQH contractors for their losses. Since local villages own the user rights of the sub-lakes for centuries, the Nature Reserve can either permanently purchase or rent the sub-lake rights. There are currently four such sub-lakes. In those sub-lakes, the Nature Reserve rents the user rights to ZQH contractors at a lower price, requiring that the water draw-down to cater to waterfowls following the guidance.

1.6. Future extensions

1.6.1. Lake shape approximation. The current model approximates the sub-lake as a spherical cap. This approximation uses fewer parameters to construct the relationship between water level, surface bottom area, and water volume, than other approximations such as a cylinder or a cuboid. The more general relationship of area, capacity, and water depth without any shape assumption will be explored in the future.

1.6.2. Stochasticity. The deterministic model discussed above is a first step in understanding the complicated Lake Poyang system. In contrast to the simple deterministic model, weather variables vary randomly from year to year. We would also like to explore how this complicated system is likely to evolve under climate change, whose symptoms include sustained changes in temperature, precipitation patterns, and the frequency and intensity of droughts

and storms (Hurd et al., 2002). Climate change is projected to alter both inter-and intra-annual rainfall, the timing and length of monsoon and dry periods, and conditions in the Siberian landscape where birds breed after wintering in Lake Poyang. There are feedbacks associated with this system that are both detrimental and helpful to crane and wildfowl survival in the long term. For example, summer precipitation at the wintering grounds affects tuber growth in a nonlinear way. The stochastic simulation model could be used to identify critical mechanisms that influence crane and wildfowl survival in the Lake Poyang system and mitigation strategies that might counter adverse climate impacts on the cranes.

1.6.2.1. *Impact of precipitation and temperature on Siberian Cranes.* Precipitation in the wintering grounds during summer affects the water level and therefore tuber production. Tuber growth suffers under both too much rainfall and too little rainfall (Wu et al., 2009; Yuan et al., 2012), introducing important non-linear influences on post-wintering conditions and possible hysteresis impacts on interannual survival of crane and other wildfowl populations. In 1998, the greatest flood in a century occurred in the Yangtze River, threatening wintering waterfowl at Lake Poyang by causing tremendous reductions in food. Cui et al. (2000) found biomass and density of three dominant species including *Vallisneria spiralis* reduced significantly. The wintering population of Siberian Crane decreased by 65%, Hooded Crane decreased by 30%, White-naped Crane decreased by 74%, Common Crane by 79%, Great Bustard by 95%, Swan Goose by 65% and Swan by 74% (Zhao and Wu, 1999).

Besides precipitation at wintering grounds, the crane population can also be influenced by fluctuations in temperature at the breeding grounds. Germogenov et al. (2013) argued that the nesting success of Siberian cranes in the breeding grounds is positively correlated to the summer average temperature taken over two time periods, 21-31 May and 1-10 June. Burnham et al. (2017) therefore hypothesized an alternative explanation for the decline in juvenile to adult ratios in that conditions on the cranes' breeding grounds were anomalous relative to 2010 and 2012, although the temperatures on the nesting grounds between 2010 and 2012 were considered either "good" or "very good".

1.6.2.2. *Impact of precipitation on the ZQH fishery.* Heavy moosoon rains during the summer time at Lake Poyang area may bring floods and probably a higher initial fish stock. Lake Poyang is a main flood outlet for the Yangtze River and it has five tributary rivers. More fish may be trapped in the sub-lakes after flood water recedes when the sub-lakes are connected to the main lake for a long time.

Rainfall in the fishing season may shorten the season. With stochastic weather and climate events, there exists the risk of heavy rainfall that prevents the ZQH contractors to discharge water to the target level. Reed (1984) demonstrated that when fires, or other unpredictable catastrophes, occur in a time-dependent Poisson process and cause destruction, the policy effect of the risk of fire is equivalent to adding a premium to the discount rate that would be operative in a risk-free setting. Under climate change, the risk might be larger because of more extreme precipitation

events [21]. The uncertainty of heavy rainfall will further shorten the fishing season and escalate the conflict between the ZQH fishery and crane conserving.

1.6.2.3. *Model modification.* This chapter uses water level information at the beginning of the season as a measure of past precipitation and runoff. The initial conditions (dry season starting day, initial water level, tuber stock, fish stock,etc.) are constructed using statistical correlations from previous data. In the stochastic setting, the initial conditions may vary across years. Climate change may be incorporated with a trend of decreasing mean and increasing variability in water level.

The fisher-tuber-bird problem under stochasticity will require a different objective function, constraints, and optimization strategy. We may want to safely maintain the endangered species away from extinction. Therefore, we can set a quasi-extinction threshold (QET) to prevent the population from reaching small sizes at which viability is threatened by demographic stochasticity and Allee effects according to population viability analysis (Hastings and Gross, 2012). The QET is similar to the safe minimum standard in Margolis and Nævdal (2008). Recent work by Donovan et al. (2019) explores algorithms for finding policies that maintain the crane population above some viability threshold $\underline{B}$ over a rolling horizon with some confidence level $Pr(\cap_j^{j+J} B_{j+1}(0) > \underline{B})$.

1.7. Conclusions

With the loss of natural habitat due to human activities, working landscapes become important to preserve biodiversity and provide ecosystem services. Working landscapes include farmlands, ranches, forests, wetlands, and water bodies. They provide market goods such as crops, timber and fish as well as non-market goods such as clean water and wildlife habitat. Non-market ecosystem services are often ignored by landowners and governments, leading to underinvestment in the natural system and therefore a market failure. It is a fundamental premise of welfare economics that uncoordinated joint production of market and nonmarket goods is likely inefficient.

This chapter constructs a novel structural hydrological-bio-economic model to investigate the comparative impacts of uncoordinated and coordinated management of fishery and crane conservation in Lake Poyang. The model captures features of the ecosystem under current deterministic climate conditions. The joint management problem is a multiyear three-state hybrid optimal control problem which is continuous within-year and discrete between-year. From the results, the ZQH operators make a sequence of independent within-season decisions to drain the lake in a manner

---

[21] The climate is unequivocally warming while the changes in precipitation in a warming world are not uniform (Pachauri et al., 2014). (Pachauri et al., 2014) summarize that extreme precipitation events over most mid-latitude land masses and wet tropical regions will very likely become more intense and more frequent in the warming world. Projections also show that the area affected by monsoon systems will increase and monsoon precipitation is likely to intensify, while El Ni no-Southern Oscilla-tion (ENSO) related precipitation variability on regional scales will likely intensify (Pachauri et al., 2014). (Sheffield and Wood, 2008) and (Brown et al., 2011) argue that precipitation variability and extreme events will increase as a consequence of an acceleration of the hydrologic cycle.

that maximizes each identical season's profit. We find that the current fishing practice leads to a large and prompt reduction in the crane population due to the early stoppage of water release under uncoordinated management. Joint management accounting for both fishery revenue and crane conservation benefit results in a season extension that secures the crane winter feeding and enhances the crane survival, at a cost of fishery revenue.

In the future, we plan to generalize the model to explore management under stochastic weather conditions to understand the mechanisms and policy options when rainfall and other weather variables are expected to vary. The stochastic model can then be used to understand how future management might need to change as distributions of rainfall and temperature variables shifts. This provides insight into the conflicting ecosystem service management of wetlands under climate change, and may lead to more efficient and cost-effective natural resource management.

Fishery model parameters

TABLE A.1. Variable and parameter definitions with values and sources in fishery system

State and Choice Variable	Label	Range	
	Variables continuous within year		
$AP(t)$	size of aperture at t	$[\underline{AP}, \bar{AP}]$	
$h(t)$	water level at t	$[0, R]$	
$V(t)$	flow volume at t	$[0, C_d \bar{AP} \sqrt{2gR}]$	
$S(t)$	surface area under water at t	$[0, 2\pi R^2]$	
$W(t)$	water volume at t	$[0, \frac{2}{3}\pi R^3]$	
$H(t)$	harvest at t		
$X(t)$	fish stock at t	$[0, X_0]$	
$\pi(t)$	profit at t	$(-\infty, \frac{a^2}{2b}]$	
t	day	$[1, T]$	
Parameter	description	Value	Source
p	fish price	10	Guess
α	water discharge cost coefficient	0.1	Guess
β	water discharge cost coefficient	0.2	Guess
R	radius of the half sphere lake	5	Guess
q	proportion of fish harvest by discarging flow volume $V(t)$	$\frac{X_0}{W_0} = 0.0764$	
r	daily discount rate	0.0002	Guess
g	acceleration of gravity	$1.98\ m/sec^2$	
C_v	incompressibility of water	0.97	
C_c	contraction coefficient (sharp edge aperture 0.62, well rounded aperture 0.97)	0.97	
$C_d = C_c \times C_v$	flow discharge coefficients	0.9409	
X_0	initial fish stock	20	Varied
h_0	initial water level	R	Varied
h_T	final water level	0.3	Varied
t_0^f	fishing season start	November 1st	Data
T^f	fishing season length	93	Data

Derivations

B.1. Derivation of $\frac{dh}{dt}$

B.1.1. Method 1. Radius of slice h:

(B.1) $$radius(h) = \sqrt{2Rh - h^2}$$

Area of the circle of the slice with height h

(B.2) $$A(h) = \pi(radius)^2 = \pi(2Rh - h^2)$$

Water volume W up to h is

$$W(h) \quad = \int_0^h A(s)ds = \int_0^h \pi[2Rs - s^2]ds$$

(B.3) $$\Rightarrow \frac{dW}{dh} = \quad A(h)$$

$$\Rightarrow \frac{dW}{dt} = \quad \frac{dW}{dh}\frac{dh}{dt} = A(h)\frac{dh}{dt}$$

Because outlet flow volume is

$$\frac{dW}{dt} = \quad -V = -C_d AP(t)\sqrt{2gh(t)}$$

(B.4) $$\Rightarrow -C_d AP(t)\sqrt{2gh(t)} = \quad A(h)\frac{dh}{dt}$$

$$= \quad \pi[2Rh(t) - h^2(t)]\frac{dh}{dt}$$

$\frac{dh}{dt}$ becomes

(B.5) $$\frac{dh}{dt} = \frac{-C_d AP(t)\sqrt{2gh(t)}}{\pi(2Rh(t) - h^2(t))}$$

if $h(t) \neq 0$. $h(t) \neq 2R$ always holds because $h(t) \in [0, R]$.

B.1.2. Method 2. The alternative way to derive $\frac{dh}{dt}$ starts from the Equation 1.2b, which is an integration of

$W(h) = \int_0^h A(s)ds = \int_0^h \pi[2Rs - s^2]ds$

$$
\begin{aligned}
W(t) &= \tfrac{\pi}{3}(h(t))^2(3R - h(t)) \\
\Rightarrow \tfrac{dW(t)}{dt} &= 2\pi Rh(t)\tfrac{dh}{dt} - \pi h^2(t)\tfrac{dh}{dt} \\
\Rightarrow -V(t) &= (2\pi Rh(t) - \pi h^2(t))\tfrac{dh}{dt} \\
\Rightarrow \tfrac{dh}{dt} &= \tfrac{-V(t)}{2\pi Rh(t) - \pi h^2(t)} \\
&= \tfrac{-C_d AP(t)\sqrt{2gh(t)}}{\pi(2Rh(t) - h^2(t))}
\end{aligned}
$$

(B.6)

if $h(t) \neq 0$.

B.2. Fishery problem with fixed AP

B.2.1. Derivation of the relationship between T and AP. Assuming $AP(t) = AP$, the ordinary differential equation B.5 can be solved by separating variables.

(B.7)
$$
\begin{aligned}
\tfrac{2Rh - h^2}{\sqrt{h}}dh &= -\tfrac{C_d AP\sqrt{2g}}{\pi}dt \\
\int \tfrac{2Rh - h^2}{\sqrt{h}}dh &= -\int \tfrac{C_d AP\sqrt{2g}}{\pi}dt \\
\tfrac{4}{3}Rh^{\frac{3}{2}}(t) - \tfrac{2}{5}h^{\frac{5}{2}}(t) &= -\tfrac{C_d AP\sqrt{2g}}{\pi}t + \tfrac{4}{3}Rh(0)^{\frac{3}{2}} - \tfrac{2}{5}h(0)^{\frac{5}{2}} \\
\Rightarrow t &= \tfrac{\pi[(\tfrac{2}{5}h^{\frac{5}{2}}(t) - \tfrac{2}{5}h^{\frac{5}{2}}(0)) - (\tfrac{4}{3}Rh^{\frac{3}{2}}(t) - \tfrac{4}{3}Rh^{\frac{3}{2}}(0))]}{C_d AP\sqrt{2g}}
\end{aligned}
$$

or

(B.8)
$$
\begin{aligned}
\tfrac{2Rh - h^2}{\sqrt{h}}dh &= -\tfrac{C_d AP\sqrt{2g}}{\pi}dt \\
\int_{h(0)}^{h(t)} \tfrac{2Rh - h^2}{\sqrt{h}}dh &= -\int_{h(0)}^{h(t)} \tfrac{C_d AP\sqrt{2g}}{\pi}dt \\
\Rightarrow t &= \tfrac{\pi[(\tfrac{2}{5}h^{\frac{5}{2}}(t) - \tfrac{2}{5}h^{\frac{5}{2}}(0)) - (\tfrac{4}{3}Rh^{\frac{3}{2}}(t) - \tfrac{4}{3}Rh^{\frac{3}{2}}(0))]}{C_d AP\sqrt{2g}}
\end{aligned}
$$

If we set $h(0) = R$, and $h(T) = \varepsilon$, the time to drain the lake with given aperture size AP is

(B.9)
$$
T = \pi \frac{\tfrac{14}{15}R^{\frac{5}{2}} + \tfrac{2}{5}\varepsilon^{\frac{5}{2}} - \tfrac{4}{3}R\varepsilon^{\frac{3}{2}}}{C_d AP\sqrt{2g}}.
$$

Or the aperture size AP with given T is

(B.10)
$$
AP = \pi \frac{\tfrac{14}{15}R^{\frac{5}{2}} + \tfrac{2}{5}\varepsilon^{\frac{5}{2}} - \tfrac{4}{3}R\varepsilon^{\frac{3}{2}}}{C_d T\sqrt{2g}}.
$$

31

The present value of profit $\pi(t) = e^{-rt}\{p(t)qZAP\sqrt{h(t)} - \alpha ZAP\sqrt{h(t)} - \beta ZAP^2 h(t)\}$ could be calculated at each time point $t \in [0, T]$. The total profit over the horizon can be approximated by `trapz` function in MATLAB.

The numerical solution when $h(T) = \varepsilon = 0.3$, $T = 93$ is $AP^* = 0.4144$, $\pi = 16.8965$. Other parameters: $\alpha = 0.1, \beta = 0.2$, $p = 10$ (See Figure B.1).
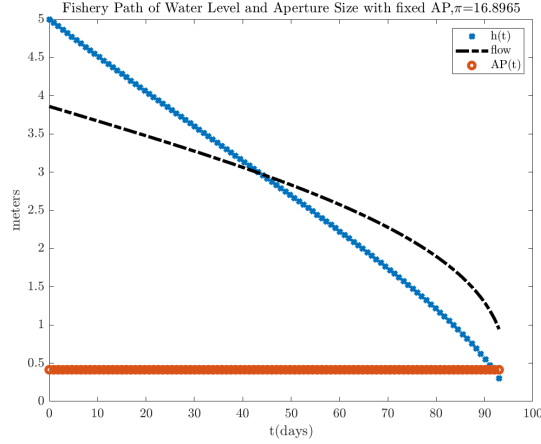
FIGURE B.1. Fixed aperture size

B.3. Fishery problem with $AP(t)$

B.3.1. Analytical Solution using Optimal Control Theory.

B.3.1.1. *Set up the Hamiltonian.*

$$(B.11) \qquad G^{CV}(t) = pqZAP(t)\sqrt{h(t)} - \alpha ZAP(t)\sqrt{h(t)} - \beta ZAP^2(t)h(t) + \lambda^{CV}(t)\frac{-ZAP(t)\sqrt{h(t)}}{\pi(2Rh(t) - h^2(t))}$$

B.3.1.2. *The Pontryagin conditions.*

$$(B.12a) \qquad \max_{AP(t)} G^{CV} \Rightarrow \frac{\partial G^{CV}(t)}{\partial AP(t)} = pqZ\sqrt{h(t)} - \alpha Z\sqrt{h(t)} - 2\beta Z^2 AP(t)h(t) - \lambda^{CV}(t)\frac{Z\sqrt{h(t)}}{\pi[2Rh(t) - h^2(t)]} = 0$$

(B.12b)
$$\begin{aligned}
\dot{\lambda}^{CV}(t) - r\lambda^{CV}(t) &= -\frac{\partial G^{CV}(t)}{\partial h(t)} \\
&= -pq\frac{ZAP(t)}{2\sqrt{h(t)}} + \frac{\alpha ZAP(t)}{2\sqrt{h(t)}} + \beta Z^2 AP^2(t) + \lambda^{CV}(t)\frac{ZAP(t)}{\pi}\left[\frac{1}{2\sqrt{h(t)}(2Rh(t) - h^2(t))} - \frac{2\sqrt{h(t)}(R - h(t))}{(2Rh(t) - h^2(t))^2}\right]
\end{aligned}$$

$$(B.12c) \qquad\qquad\qquad \dot{h}(t) = \frac{-ZAP(t)\sqrt{h(t)}}{\pi(2Rh(t) - h^2(t))}$$

32

From Equation B.12a, if $h(t) \neq 0$,

(B.12d) $$\lambda^{CV}(t) = [pq - \alpha - 2\beta ZAP(t)\sqrt{h(t)}]\pi[2Rh(t) - h^2(t)].$$

Therefore, we will have

(B.12e)
$$\begin{aligned}
\dot{\lambda}^{CV}(t) = \ & -2\beta ZA\dot{P}(t)\sqrt{h(t)}\pi[2Rh(t) - h^2(t)] - \frac{2\beta ZAP(t)}{2\sqrt{h(t)}}\dot{h}(t)\pi[2Rh(t) - h^2(t)] \\
& + [pq - \alpha - 2\beta ZAP(t)\sqrt{h(t)}]\pi[2R - 2h(t)]\dot{h}(t)
\end{aligned}$$

Plug $\dot{h}(t)$ Equation B.12c into $\dot{\lambda}(t)$ Equation B.12e,

(B.12f)
$$\begin{aligned}
\dot{\lambda}^{CV}(t) = \ & -2\beta ZA\dot{P}(t)\sqrt{h(t)}\pi[2Rh(t) - h^2(t)] - \frac{2\beta ZAP(t)}{2\sqrt{h(t)}}\frac{-ZAP(t)\sqrt{h(t)}}{\pi(2Rh(t) - h^2(t))}\pi[2Rh(t) - h^2(t)] \\
& + [pq - \alpha - 2\beta ZAP(t)\sqrt{h(t)}]\pi[2R - 2h(t)]\frac{-ZAP(t)\sqrt{h(t)}}{\pi(2Rh(t) - h^2(t))} \\
= \ & -2\beta ZA\dot{P}(t)\sqrt{h(t)}\pi[2Rh(t) - h^2(t)] + \beta Z^2 AP^2(t) \\
& - [pq - \alpha - 2\beta ZAP(t)\sqrt{h(t)}][2R - 2h(t)]\frac{ZAP(t)\sqrt{h(t)}}{2Rh(t) - h^2(t)}
\end{aligned}$$

Plug $\dot{\lambda}^{CV}(t)$ Equation B.12f and $\lambda^{CV}(t)$ Equation B.12d into Equation B.12b,

(B.12g)
$$\begin{aligned}
\dot{\lambda}^{CV}(t) - r\lambda^{CV}(t) = \ & -2\beta ZA\dot{P}(t)\sqrt{h(t)}\pi[2Rh(t) - h^2(t)] + \beta Z^2 AP^2(t) - [pq - \alpha - 2\beta ZAP(t)\sqrt{h(t)}][2R - 2h(t)]\frac{ZAP(t)\sqrt{h(t)}}{2Rh(t) - h^2(t)} \\
& - r[pq - \alpha - 2\beta ZAP(t)\sqrt{h(t)}]\pi[2Rh(t) - h^2(t)] \\
= \ & -pq\frac{ZAP(t)}{2\sqrt{h(t)}} + \frac{\alpha ZAP(t)}{2\sqrt{h(t)}} + \beta Z^2 AP^2(t) + [pq - \alpha - 2\beta ZAP(t)\sqrt{h(t)}]\pi[2Rh(t) - h^2(t)]\frac{ZAP(t)}{\pi}[\frac{1}{2\sqrt{h(t)}(2Rh(t) - h^2(t))} - \frac{2\sqrt{h(t)}(R - h(t))}{(2Rh(t) - h^2(t))^2}]
\end{aligned}$$

Rearrange Equation B.12g,

(B.12h)
$$\begin{aligned}
2\beta Z\sqrt{h(t)}\pi[2Rh(t) - h^2(t)]A\dot{P}(t) = \ & \beta Z^2 AP^2(t) - r[pq - \alpha - 2\beta ZAP(t)\sqrt{h(t)}]\pi[2Rh(t) - h^2(t)] \\
\Rightarrow A\dot{P}(t) = \ & \frac{ZAP^2(t)}{2\sqrt{h(t)}\pi[2Rh(t) - h^2(t)]} - \frac{r}{2\beta Z\sqrt{h(t)}}(pq - \alpha - 2\beta ZAP(t)\sqrt{h(t)})
\end{aligned}$$

if $h(t) \neq 0$.

Thus, given $h(t) \neq 0$, the Pontryagin conditions are

(B.13a) $$\dot{h}(t) = \frac{-ZAP(t)\sqrt{h(t)}}{\pi(2Rh(t) - h^2(t))}$$

(B.13b) $$A\dot{P}(t) = \frac{ZAP^2(t)}{2\sqrt{h(t)}\pi[2Rh(t) - h^2(t)]} - \frac{r}{2\beta Z\sqrt{h(t)}}(pq - \alpha - 2\beta ZAP(t)\sqrt{h(t)})$$

B.3.1.3. *Boundary conditions.* Boundary conditions are given T, given $h(0) = R$, $h(T) = \varepsilon$.

33

Birds and tubers system

TABLE C.1. Variable and parameter definitions with values and sources in birds and tubers system

State and Choice Variable	Label	Range	
	Variables continuous within year j		
$AP_j(t)$	size of aperture at t	$[\underline{AP}, \overline{AP}]$	
$h_j(t)$	water level at t	$[0, R]$	
$S_j(t)$	surface area under water at t	$[0, 2\pi R^2]$	
$C_j(t)$	accessible tubers per capita at t		
$E_j(t)$	energy reserve at t	$[0, \infty]$	
t	day	$[1, T]$	
	Variables continuous within year and discrete between year		
$B_j(t)$	number of cranes at time t year j		
	Variables discrete between year		
M_j	tuber stock at year j	10000	Guess
f_j	juvenile survival rate at year j	$[0,1]$	
Parameter	description	Value	Source
ρ	fraction of accessible tubers per capita that cranes forage	1	Guess
c	daily metabolic cost	0.1	Guess
ζ	wintering survival rate coefficient	0.1	Guess
p	juvenile survival rate coefficient	1	Guess
n	reproduction rate of the crane	10%	Johnsgard (1983)
d	death rate of the crane	0.09	Guess
g	acceleration of gravity	9.81 m/s^2	
C_v	velocity coefficient of water	0.97	
C_c	contraction coefficient (sharp edge aperture 0.62, well rounded aperture 0.97)	0.97	
$C_d = C_c \times C_v$	flow discharge coefficient	0.9409	
α	water discharge cost coefficient	0.1	Guess
β	water discharge cost coefficient	0.2	Guess
$E_j(0)$	initial energy reserve	5	Guess
$B_1(0)$	initial crane population	3000	Data
t_0^B	bird wintering season start	0(November 1st)	Data
T^B	bird wintering season length/end	150 (March 31st)	Data

Joint model with insufficient tubers

With insufficient tuber, the within-year crane death is inevitable.

- fishery only: we see water releases stops on February 1st and crane decreases over year from the initial 3000 to 1793 (Figure D.1).

- crane conservation only: water releases continuously from November 1st to March 31st. Yet, the crane population decreases from the initial 3000 to 1814 over five year (Figure D.2).

- joint management:water release covers the whole wintering season with two sets of water flow and aperture sizes. The crane population decreases from the initial 3000 to 1814 (Figure D.3).

Optimal Joint Path with M=1000, Returning Cranes $B_J(0) =1793$
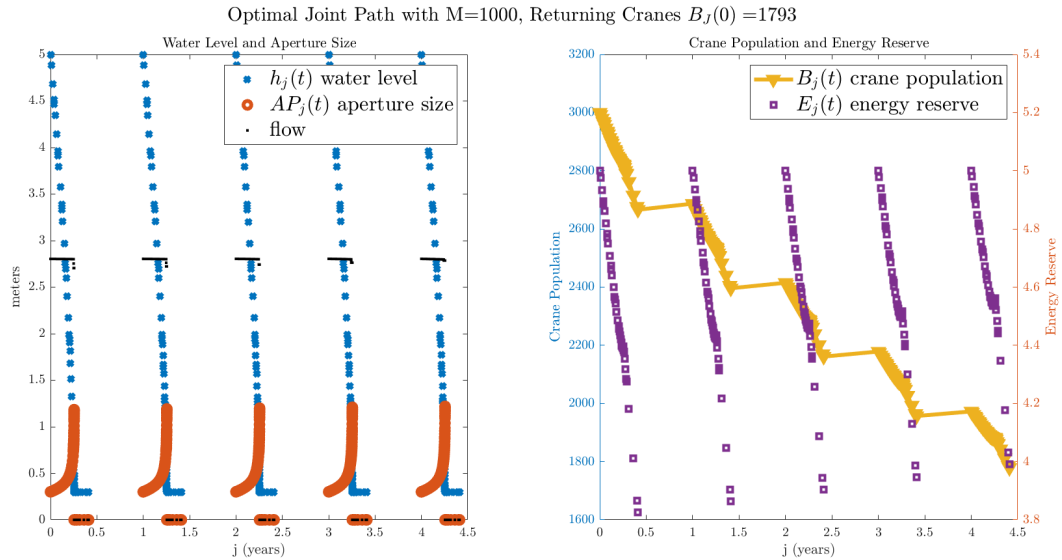
FIGURE D.1. Insufficient tuber, no water release after Feb 1st, cranes $3000 \downarrow 1793$.
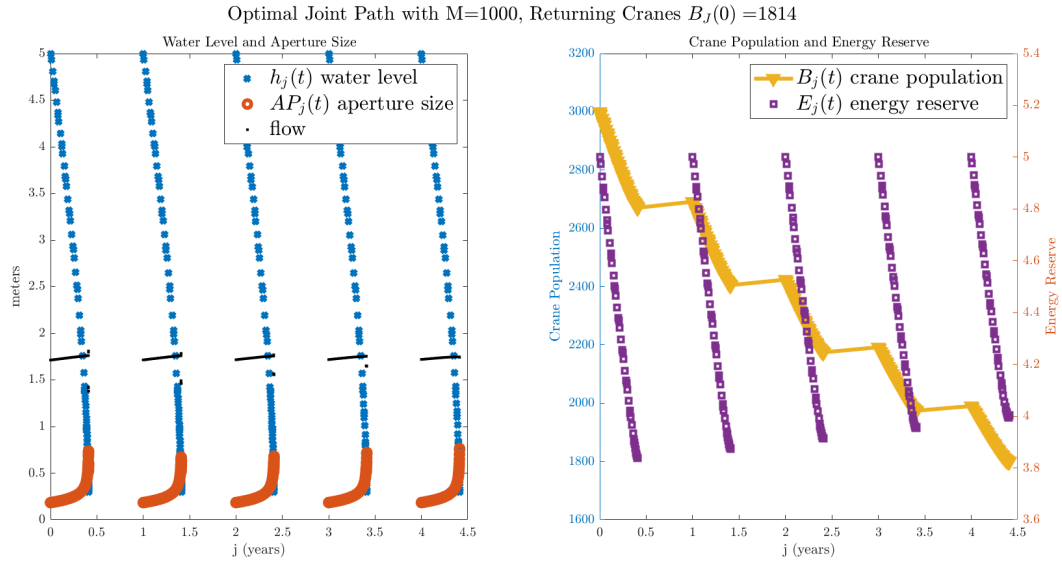
FIGURE D.2. Insufficient tuber, water release till March 31st, cranes $3000 \downarrow 1814 (> 1793)$.
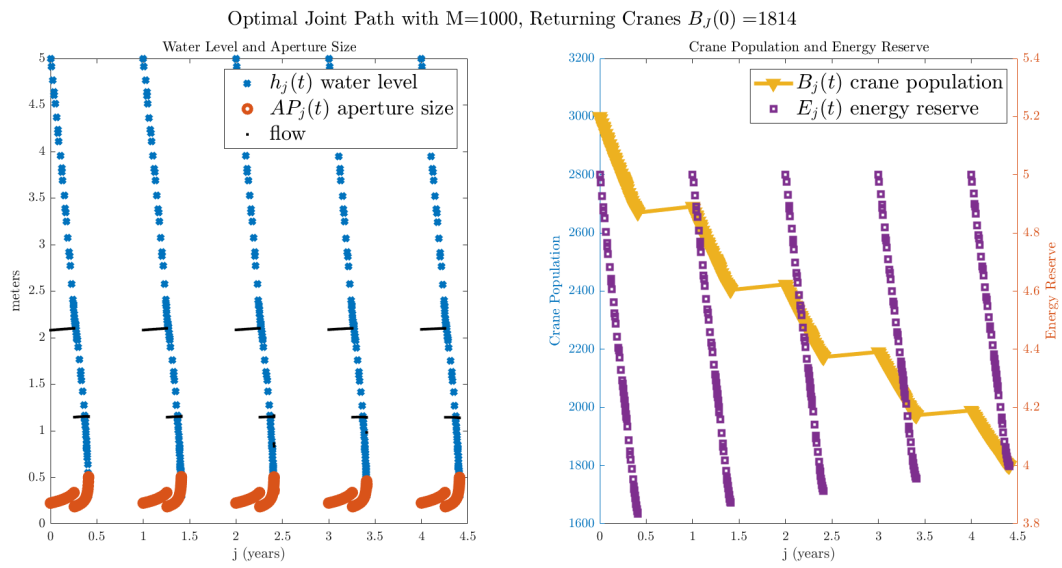
FIGURE D.3. Insufficient tuber, by extending water release season, cranes $3000 \downarrow 1814 (> 1793)$.

Sub-lake Information

There are 102 sublakes in Lake Poyang basin area including 9 sublakes in the Poyang Lake Nature Reserve and 33 sublakes in the Nanjishan Nature Reserve. The sublakes differ in shape, size, and elevation.

Sublakes	Lakeshore Elevation[†]				Lake Bottom Elevation	Drainage Gate Bottom Elevation	Water Area (km^2)	Volume ($10^8 m^3$)	Water Depth (m)
	Hills or Permanent Dikes		Short Dikes						
	Minimum	Maximum	Minimum	Maximum					
Dahuchi	19.02	22.31	14.37	17.59	11.82	10.36	29.45	0.679	15.0
Shahu	16.13	17.03	14.02	16.05	12.22	11.05	10.31	0.103	13.5
Banghu	19.64	21.1	12.12	18.09	10.82	9.77	43.66	0.309	12.0
Zhushihu	16.65	23.42	14.44	16.30	11.92	11.55	2.15	0.027	14.5
Changhuchi	17.45	21.84	12.38	15.94	12.12	11.41	2.91	0.038	13.5
Zhonghuchi	18.73	21.14	13.96	15.30	12.42	11.26	4.744	0.051	14.0
Meixihu	16.92	27.54	14.24	16.48	12.52	11.22	2.039	0.028	14.5
Xianghu	20.63	21.18	13.9	15.94	12.92	11.57	2.686	0.024	14.5
Dachahu[‡]	15.32	21.05	13.7	14.94	10.32	11.20	48.95	0.23	10.9

● †: Sublakes are generally connected to rivers. The dikes/levees between the sublake and the river are naturally formed and artificially enhanced. The remaining sections of the lake shore are generally hills or permanent dikes. In the photo of the dry Dahuchi in 2004 Figure E.1a, upper left is the hillside of Dingshan Hill while the upper right is the short dike next to Xiu River.
● ‡: Dachahu is a marsh. The drainage gate is the drainage ditch.

TABLE E.1. Geographic Information of 9 Sublakes in Poyang Lake Nature Reserve (Yellow Sea Elevation) (Source: Hu (2020))

(a) Dahuchi in 2004 (Source: Hu (2020)). Upper left is the hillside of Dingshan Hill while the upper right is the short dike next to Xiu River
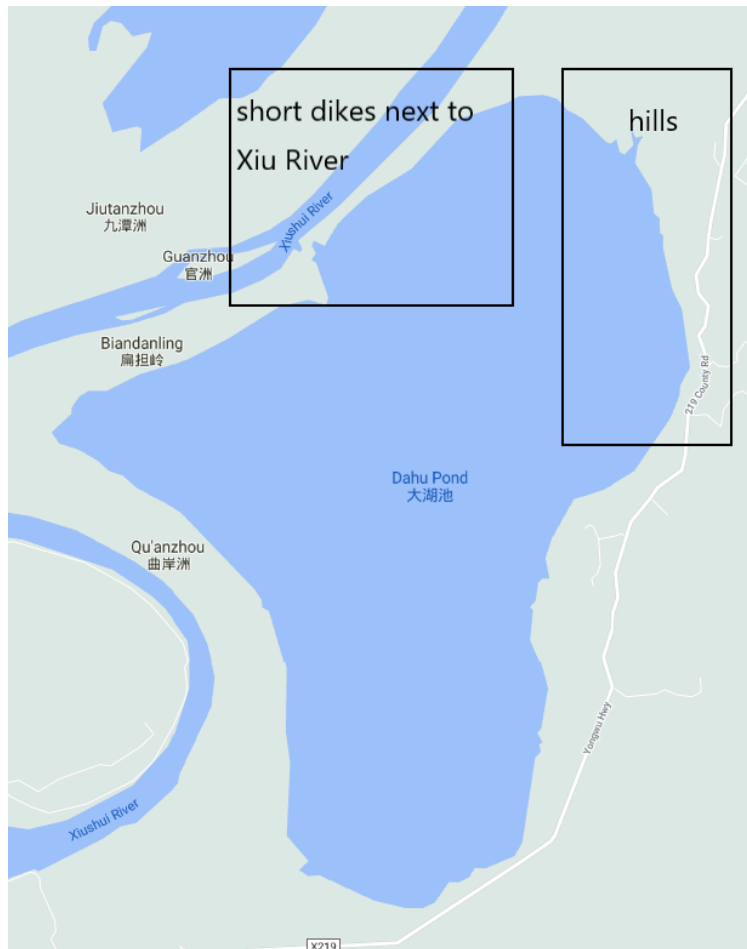
(b) Map of Dahuchi

FIGURE E.1. Sublake: Dahuchi

CHAPTER 2

Spatial-dynamic model of commercial fishing trip decision-making

2.1. Introduction

The existence of high frequency space-time data on human activities and movements is permitting the exploration and prediction of behavior in unprecedented ways. Cellphone data has been used to understand the differential abilities of income groups to respond to COVID-19 emergency declarations (Weill et al., 2020), to better predict traffic patterns (Wang et al., 2013), and to understand global mobility patterns (Kraemer et al., 2020). Economists are employing these data to measure/predict poverty and wealth (Blumenstock et al., 2015; Steele et al., 2017), measure consumer preferences (Athey et al., 2018), spatial concentration of urban economic activity and value of transportation infrastructure (Gupta et al., 2020; Kreindler and Miyauchi, 2021; Miyauchi et al., 2021), social networks and social connections (Athey et al., 2020; Björkegren, 2019; Büchel et al., 2020; Couture et al., 2021)

Satellite tracking data of vessels that report GPS coordinates throughout their voyage have been used to map patterns of fishing effort across the globe (Kroodsma et al., 2018), assess the effectiveness of the 200-nautical mile exclusive economic zone in limiting foreign vessels intruding into a coastal nations waters (Englander, 2019), investigate the explore-exploit tradeoff (OFarrell et al., 2019b), identify behavioral typologies of fishing vessels (OFarrell et al., 2019a) and the behavioral changes post the introduction of catch shares (Watson et al., 2018).

These data are also permitting researchers to revisit methodologies developed to explore space-time behavior to better understand their potential strengths and weaknesses. For example, Dépalle et al. (2021) use vessel monitoring system (VMS) data matched with logbook data on catches and effort to demonstrate potential biases in discrete choice random utility models of fishing location choices due to spatial aggregation. Figure 1 contrasts the traditional data used in modeling fishing choices (Figure 2.1a) with the vessel level tracking data that is available (Figure 2.1b and 2.1c). While the historical data had trip-level data on whether a vessel visited a site and catch, the VMS data includes finer spatial information on the vessel's path, site choice, and time spent in each location.

Motivated by the existence of this data, we develop a more refined trip level model of spatial-temporal decision-making of vessels to inform the design of spatial and aspatial management measures (Bockstael and Opaluch, 1983). On any trip, skippers decide where to fish, how to navigate to the sites, how much to fish, and when to return to the port

(a) Trip-level logbook data   (b) Fishing heatmap using hourly VMS data   (c) Simulated track plotted using VMS and Observer data
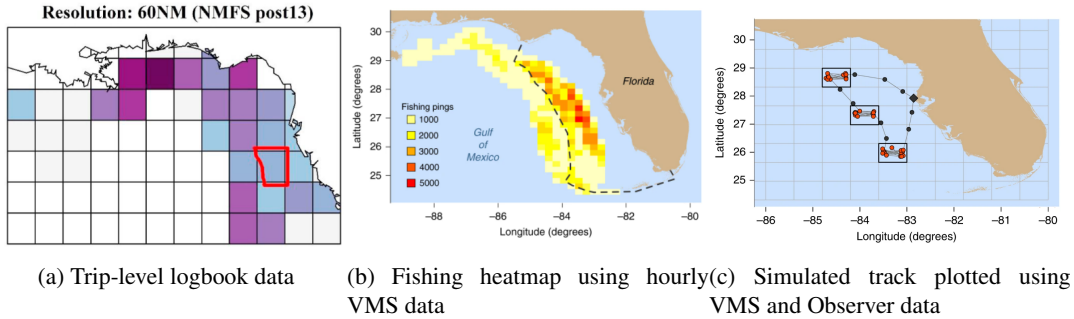
FIGURE 2.1. Data of longline fishing in the Gulf of Mexico. Figure 2.1a shows the 60NM-long statistical areas used by the U.S. National Marine Fisheries Service (NMFS) after 2013 for trip-level logbook reporting(Dépalle et al., 2021). Figure 2.1b is heatmap of fishing activity by longline vessels using the hourly Vessel Monitoring System (VMS) positions. Figure 2.1c is a simulated vessel track with VMS pings classified into fishing (red circles), transiting (black dots) or in port (black diamonds) using a supervised learning algorithm trained by onboard observer data. Figure 2.1b and 2.1b comes from OFarrell et al. (2019b).

conditional on vessel capital, labor, target species, and gear. The decisions are influenced by economic opportunities, technology (e.g., vessel hold and fuel capacity), and regulations (e.g., closed areas and seasons, gear restrictions).

On each trip, the short-run decision of location choice for commercial fishers is a dynamic spatial problem. Spatial patchiness of marine resources with different population levels and economic characteristics generates discontinuities in the spatial structure (Sanchirico and Wilen, 1999). Spatial decisions are therefore modelled as discrete choices among a finite set of fishing sites in commercial fisheries. Since the original Bockstael and Opaluch (1983) work, most of the empirical studies use a static random utility model (RUM) to investigate trip-level location choice under stock-induced uncertainty (see, e.g., Abbott and Wilen (2011); Eales and Wilen (1986)). For fisheries consisting of multiple day trips (e.g., tuna, groundfish), researches have incorporated dynamic behavior into the static RUM with state dependence, evolving information, and changing choice sets. While these advances capture some aspects of the decision-making calculus, they are still simplifications of the full dynamic choice problem. Mostly, as a means to maintain computational tractability, they fail to incorporate the interconnections between location choice, trip duration, and vessel characteristics. The studies that are more dynamic in fishers decision-making for multi-day trips[1], however, often assume an exogenous trip length for identification purpose (see, e.g., Hicks and Schnier (2006, 2008); Hutniczak and Münch (2018)). A notable exception is a recent paper by Abe and Anderson (2022) that models endogenous trip length resulting from freshness loss in a dynamic discrete choice model. However, the study does not include trip-level location choice analysis.

---

[1]Instead of maximizing current period utility in the static RUM, these studies consider the optimal trajectory of forward-looking fishing decisions and maximize the sum of expected utility from the multi-period cruise.

This research constructs a dynamic spatial model of an individual fisher's location choice (extensive margin), cruise trajectory, and effort allocation at each site (intensive margin) within a trip. The Gulf of Mexico's reef-fish bottom longline fishery provides the motivation and application of the method for numerical analysis. A key feature of the model is the explicit incorporation of route planning and trip-level production constraints on vessel hold capacity and/or fuel consumption. The binding technology constraints introduce a shadow price[2] into the decision-making of where to fish, how much to fish, and when to return to port. Route planning consists of finding the shortest path connecting the chosen locations. Both the shadow price and route planning are missing in the previous discrete choice modeling of fisher trip decisions. We illustrate the utility of modeling the spatial-dynamic decisions of fishers under binding technology constraints and route planning using numerical simulations.

At the same time that high frequency data are becoming available, advances in computational abilities and algorithms in operations research enable us to solve this complex spatial-dynamic problem. The fishing trip decision-making is very similar to the orienteering problem (OP), which is a routing problem with profits in the operation research literature (Gunawan et al., 2016; Vansteenwegen and Gunawan, 2019). Solving the OP corresponds to solving two well-known combinatorial optimization problems in an integrated way: the knapsack problem (KP) and the traveling salesman problem (TSP). The individual fisher's location choice problem modifies the OP to account for the effort allocated at each location and is formulated as a mixed integer quadratically constrained problem (MIQCP). It is solved by the off-the-shelf solver Gurobi using a branch-and-bound algorithm.

To understand how optimal spatial effort allocation decisions differ from the approaches often utilized in the literature, we also develop a myopic model where the individual fisher chooses a location at each decision point within a trip and the effort to allocate at each site. This stands in contrast to the dynamic optimal fisher that chooses a sequence of locations. The myopic model mimics the assumption in the discrete choice literature on fishing location decisions. We also consider cases of a partially myopic fisher that considers multiple forward decisions but is not optimizing the entire trip (e.g., 2 decisions ahead, 3 decisions, and 6 decisions).

Previous empirical studies find evidence that fishers are more likely to choose locations with high expected rewards, low travel distance and low risk. Our simulation results are consistent with the previous literature. Sites with high fish stock and low travel distance are visited. Simulation results also show that technology constraints such as fuel constraint and hold capacity constraint endogenously determine the trip length. The fuel constraint and the hold capacity constraint limit the number of fishing sites to go and the amount of fishing effort applied by constraining the total fuel usage and/or the total fish harvest. These technology constraints impose shadow prices that affect the decision of fishing effort and location choice from the outset of a trip. Comparing the results from the optimal trip

---

[2]The shadow price could be on fuel capacity or hold capacity depending on which constraint is binding.

decision-making with the myopic, we demonstrate how the prior research is subject to misspecification, as researchers have ignored the role of vessel capacity, fuel constraints and route planning in their estimations of fishers' location choice. We decompose the profit loss from ignoring route planning and technology constraint by modeling a partially myopic fisher who considers multiple choices at a time. The more sites the partially myopic fisher considers in the trip decision making, the higher the profit realized from better route planning and distribution of fishing effort.

The chapter is organized as follows. Section 2.2 reviews the literature in the short run location choice in commercial fishery. Section 2.3 presents the model of the short run decision on location choice and effort allocation by the dynamic fisher, the myopic fisher, and the partially myopic fisher. Section 2.4 describes the Gulf of Mexico demersal longline fishery and parameterization. Section 2.5 presents the simulation results. Section 2.6 concludes.

2.2. Literature Review

The short-run decision of location choice for commercial fishers at the trip level is a dynamic spatial problem. The individual fisher's problem is cast as choosing fishing sites to maximize the overall trip profits. Spatial patchiness of marine resources with different population levels and economic characteristics generate discontinuities in the spatial structure(Sanchirico and Wilen, 1999). Spatial decisions are therefore modelled as discrete choices among a finite set of fishing sites in commercial fisheries.

The discrete choice random utility model (noted as RUM) was first used in Bockstael and Opaluch (1983) to model the medium-run decision[3] of fishery choice in New England trawling fishery. Since then, the RUM has been utilized to model the short-run margin of the fishery production process, trip-level location choice in single and multispecies fisheries (Abbott and Wilen, 2011; Dupont, 1993; Eales and Wilen, 1986; Mistiaen and Strand, 2000; Smith, 2005; Sun et al., 2016), and trip-level fishery and location-choice in multi-species fisheries (Curtis and Hicks, 2000; Curtis and McConnell, 2004; Holland and Sutinen, 2000). Eales and Wilen (1986) and Sun et al. (2016) modeled the location choice of the first set, which is a very short-run decision.

The static RUM is usually formed as the following: fishers, conditional on taking a fishing trip, make a decision of where to fish to maximize the current period utility in time period t that is affected by travel costs and expected rewards linearly.

(2.1) $$U_{ijt} = \beta_{dist} \times \text{Dist}_{ijt} + \beta_{rewards} \times E[\text{Rewards}_{ijt}] + \varepsilon_{ijt}$$

---

[3]In the fishing production, medium run decisions include between fishing trip decisions such as switching ports, switching target species, and switching gear.

where i represents the vessel, j is the site and t is the decision point (usually in temporal dimension). ε_{ijt} is the random shock. $Dist_{ijt}$ denotes the distance to a given location. These studies show that fishers tend to visit a site with a high expected revenue and a short travel distance. Extensions of the static RUM include variables such as variance of the rewards (Dupont, 1993; Hutniczak and Münch, 2018; Mistiaen and Strand, 2000), preference heterogeneity (Smith, 2005), state dependence (your past experience affects future choice) (Holland and Sutinen, 2000; Smith, 2005), evolving information and information sharing (Abbott and Wilen, 2011; Curtis and McConnell, 2004; Dépalle et al., 2021), spatial correlation and learning (Hutniczak and Münch, 2018; Marcoul and Weninger, 2008), and bycatch avoidance (Abbott and Wilen, 2011; Haynie et al., 2009).

Applied studies of location choice spanned a diverse range of fisheries from sedentary species (Marcoul and Weninger, 2008; Smith, 2002, 2005) to pelagic species (Curtis and Hicks, 2000; Curtis and McConnell, 2004; Mistiaen and Strand, 2000). For sedentary species, most vessels fish single-day trips choosing 1-2 fishing grounds (Eales and Wilen, 1986; Marcoul and Weninger, 2008; Smith, 2005). For finfish species like groundfishes or tunas, vessels make multi-day trips (Abbott and Wilen, 2011; Curtis and Hicks, 2000; Curtis and McConnell, 2004; Hicks and Schnier, 2008; Hutniczak and Münch, 2018). This adds a layer of dynamic complexity to the problem. On a multiday cruise, spatial location choices may be made in a dynamic context instead of myopic day-to-day strategies. A set of papers incorporate skipper's forward-looking behavior in the RUM by adding expected future payoffs to the objective function (Curtis and Hicks, 2000; Curtis and McConnell, 2004; Hicks et al., 2004; Hicks and Schnier, 2008). The dynamic random utility model (DRUM), a static RUM entrenched in dynamic optimization developed and used in Hicks and Schnier (2006, 2008), is a middle ground approach[4] to include dynamic choices and remain computationally tractable.

Even in the pseudo-dynamic models, trip length for multi-day trips is usually assumed exogenous. For example, Curtis and Hicks (2000); Curtis and McConnell (2004); Hicks and Schnier (2006, 2008); Hutniczak and Münch (2018) assume the length of the trip is known before leaving port. Trip duration, as an input of the short-run fishery production process, is endogenously determined during a trip. (Curtis and Hicks, 2000) and (Curtis and McConnell, 2004) suggest that catch deterioration affects location choice through the impact on production horizon. A recent paper by Abe and Anderson (2022) models the dynamic choices of endogenous trip length due to freshness deterioration. However, the paper doesn't include the spatial margin of the trip level production process.

---

[4]It is a middle-ground approach as stated in (Hicks and Schnier, 2006) because the state space is deterministic, rather than stochastic and path dependent, to avoid the curse of dimentionality. The individual fisher formulates the expectation about the site conditions at the port and uses the deterministic information to calculate the value function for future periods. There is no information processing and expectation updating by vessels during the cruise.

Fuel and hold capacity are mainly discussed in the literature of capacity measures and capacity utilization[5]. Little attention has been paid to the role of fuel capacity and hold capacity in location and trip duration choice. One reason could be that few trips land a full load (Abe and Anderson, 2022; Smith and Hanna, 1990) or appear to use up all the fuel on a given trip. Although the ex-post constraints may not be binding, these constraints are likely to impact the ex-ante decision-making given that there is a risk violating them on any given trip[6]. Running out of fuel at sea also could have devastating consequences for the vessel capital and crew.

Up to now, the literature on trip-level location choice addresses portions of the full dynamic spatial problem faced by commercial fishers on a trip most likely due to model and computation complexity. As far as we are aware, no paper in the fishery economics literature on location choice captures the interlinked decision on location choice, fishing effort, travel route, and trip length with the technology constraints of fuel and hold capacity[7].

2.3. Methodology

To address the gap in the literature, we develop a structural model for the dynamic within-trip decision process of location choice, effort allocation and the path in a multi-day trip, while the trip duration is endogenously determined by fuel or hold capacity constraints. Although uncertainty is a key part of the problem, the chapter starts with a deterministic fish stock setting to disentangle the complex spatial dynamic problem. In ongoing work, we are incorporating uncertainty and passive learning over trip on the stock levels in each site.

The spatial dynamic fishing production problem of an individual vessel can be modeled as a single vehicle routing problem with profits (VRPP) or a traveling salesman problem with profits (TSPs with profits) in the operation research literature. In the routing problem with profits, all nodes of interest have a certain profit and not all of them need to be visited, but a selection has to be made. According to the way the two payoffs, profits and travel costs (mostly distance or time), are addressed, the single vehicle routing problem with profits could be categorized into three types of problems. In the profitable tour problem (PTP) (Dell'Amico et al., 1995), the objective function is to visit a subset of customers that maximizes the total collected profit minus travel cost. In the prize-collecting traveling salesman problem (PCTSP) (Balas, 1989), the objective is to minimize the total travel cost to collect a minimum amount of profit by visiting a subset of the customers. In the orienteering problem (OP) (Golden et al., 1987; Tsiligirides, 1984),

---

[5]Fishing capacity measures the capability of a vessel or fleet of vessels to catch fish (Gréboval, 2003; Smith and Hanna, 1990). Fuel consumption is an input measure to represent the effective effort applied to existing capital stock, usually not captured in the capacity analysis (Dupont et al., 2002; Felthoven and Morrison Paul, 2004; Kirkley et al., 2002). Hold capacity is the most widely used output-based physical measure of fishing capacity (Gréboval, 1999).

[6]An analogy could be range anxiety which is a well-known phenomena with the use of electrical vehicles (EV) (Li et al., 2017). EV owners worry about running out of electricity before reaching the destination given the limited driving range, even though many do not run out of a charge on any given trip.

[7]Haynie and Layton (2010) jointly estimated the expected catch value and location choice. However, the continuous catch is treated as a random variable instead of a choice variable after the location is chosen. There is no assumption about the fishers effort allocation rule.

the objective is to find a route that maximizes the total collected profit from the subset of nodes while not exceeding a given travel cost constraint (typically a time constraint).

The OP setting fits the spatial dynamic fishing production problem of an individual vessel the best. Because the individual vessel tries to maximize the total collected fishing profit from a subset of fishing locations and avoid violating two travel cost constraints: the hold capacity constraint and fuel capacity constraint. The OP actually integrates the difficulties of two complex combinatorial optimization problems: the knapsack problem (KP)[8] and the regular traveling salesman problem (TSP)[9]/the vehicle routing problem (VRP)[10] (Vansteenwegen and Gunawan, 2019).

The OP can be formulated as an integer programming model with the following binary decision variables: $y_i = 1$ if node i is visited, and $x_{ij} = 1$ if a visit to node i is followed by a visit to node j. We modify the OP for individual fisher's location choice problem by introducing a continuous decision variable, fishing effort, and rewriting the profit at each node as a function of fishing effort using a generalized Schaefer harvest function (Zhang and Smith, 2011). With the binary and continuous decision variables, this discrete-continuous problem is formulated as a mixed integer programming (MIP) problem. In the formulation of the routing problem, time is implicit and endogenous to the explicit spatial choice.

$$
\begin{aligned}
\text{profit}_i = & \quad p \times \text{harvest}_i - \text{cost}(\text{harvest}_i) \\
= & \quad p \times q \text{Effort}_i^\gamma \text{Stock}_i^\beta - \text{cost}(\text{Effort}_i)
\end{aligned}
$$

(2.2)

2.3.1. Model for the location choice problem.

2.3.1.1. *Assumptions.* The model features a vessel with a finite amount of fishing sites and a single port. The vessel starts and ends at the port (Node 1) in a fishing trip. Each fishing site $i \in N$ is associated with a non-negative fish stock, Stock_i. Fish stock is 0 at the port. In the deterministic case, the fisher has perfect information about the fish stock at each fishing site.

Since the distance from fishing site i to j is assumed to equal the distance from fishing j to i ($d_{ij} = d_{ji}$), we can model the problem as an undirected graph $G = (N, E)$, consisting of the set N of nodes and the set E of edges. In the undirected graph G, all the edges (i, j) are bidirectional, $x_{ij} = x_{ji}$. A brief explanation of the terms used in operation research is in Table 2.1.

The vessel is assumed to maximize profit. The profits from fishing at each site are aggregated into a trip-level return and each site can be visited at most once.

---

[8]In the KP, each item has a profit and requires some volume. The goal is to determine the combination of items that maximizes the total profit and that fits in a given volume. In the fishing production context, fish catch requires storage space.

[9]The objective of the TSP is to find the shortest single route visitng all customers.

[10]The objective of the VRP with a single vehicle is to minimize the total distance required to visit a fixed set of customers starting from a depot.

TABLE 2.1. Terms used in fishery operation research

Node	A fishing site or a port. Nodes in the problem are numbered 1 to N
Edge	A connection between any two nodes representing movement
Tour	A fishing trip. It involves departure from a port, a sequence of fishing site visits and the return to the port.

2.3.1.2. *Formulation.* The goal of the individual vessel is to find a route that visits a subset of N fishing sites and to choose the fishing effort at each site to maximize the total profit subject to technology constraints imposed by fuel and hold capacity constraints. The problem of the individual vessel is

(2.3)

$$
\begin{aligned}
\max_{x_{ij},y_i,A_i} \quad & \sum_{i \in N}(p_i q A_i^{\gamma} Stock_i y_i - afc_{fuel}A_i) - \sum_{(i,j) \in E} d_{ij}x_{ij}bfc_{fuel} \\
\text{s.t.} \quad & \sum_{(i,j) \in E} d_{ij}x_{ij}bf + \sum_{i \in N} A_i af \leq F_{max} && \text{Fuel constraint} \\
& \sum_{i \in N} q A_i^{\gamma} Stock_i y_i \leq C_{max} && \text{Hold capacity constraint} \\
& \sum_{j=2}^{N} x_{1j} = 2y_1 && \text{Entering and Leaving 1} \\
& \sum_{i=1}^{N-1} x_{ik} = 2y_k, x_{ik} = x_{ki} \text{ if } i > k, i \neq k, k = 2, \cdots, |N|^{[11]} && \text{Entering and Leaving } k \\
& y_1 = 1 && \text{Visit Node 1} \\
& \sum_{i \in S}\sum_{j \in S} x_{ij} \leq \sum_{i \in S \setminus \{k\}} y_i, \forall S \subset N \setminus \{1\}, |S| \geq 3, k \in S && \text{Subtour elimination} \\
& x_{ij}, y_i \in \{0,1\}
\end{aligned}
$$

Table 2.2 summarizes the model variables and parameters that will appear repeatedly in the chapter. Each constraint in (2.3) is explained in turn below.

Objective function The vessel chooses the fishing site y_i, path x_{ij} and fishing effort A_i at each fishing site to maximize the total trip profit. Fishing profit equals to harvest revenue minus fishing cost and traveling cost.

(2.4)
$$
\max_{x_{ij},y_i,A_i} \quad \text{Profit} = \sum_{i \in N}(p_i \text{harvest}_i y_i - afc_{fuel}A_i) - \sum_{(i,j) \in E} d_{ij}x_{ij}bfc_{fuel}
$$

The price per node is allowed to be different across fishing sites and we assume that the harvest function is a Cobb-Douglas production function.

(2.5)
$$
\text{harvest}_i = q\text{Stock}_i^{\beta} A_i^{\gamma}
$$

where q is catchability coefficient, defined as the fraction of the population fished by an effort unit (Gulland, 1983). The Schaefer harvest function is a special case when $\gamma = 1, \beta = 1$ (Schaefer, 1954) .

Constraints The individual fisher faces the following constraints.

---

[11]Edge $x_{ik} = x_{ki}$ in the undirected graph.

TABLE 2.2. Variable and parameter definitions

Decision Variables	Label	Range
x_{ij}	$= 1$ if the edge ij is visited, 0 otherwise. $x_{ij} = x_{ji}$ in the undirected case.	(0,1)
y_i	$= 1$ if the node i is visited, 0 otherwise	(0,1)
A_i	fishing effort (hook number × fishing hour) at node i	continuous
Parameters	description	Value
N	the set of nodes in the network (the port and fishing sites)	15
E	the set of edges in the network	
S	the set of subtours	
k	an index representing the node	
d_{ij}	travel distance in nm between node i and j. $d_{ij} = d_{ji}$ in the undirected case	
$Stock_i$	fish stock at node i	
p_i	price of harvest at node i	300
q	catchability coefficient	$9.4 \times 10^{-6\dagger}$
f	fuel usage, gallon per hour	5
c_{fuel}	$ per gallon, unit cost of fuel usage	2
a	fishing effort fuel consumption coefficient	0.002
speed	traveling speed, knots (nautical mile per hour)	5
b	traveling fuel consumption coefficient, 1/speed,	0.2
F_{max}	fuel capacity	
C_{max}	hold capacity	
γ	output elasticity of fishing effort	0.7
β	output elasticity of fish stock	1

- †: See derivation in Appendix Section H.2

Fuel constraint limits the total fuel usage of fishing $(\sum_{i \in N} A_i a f)$ and traveling between sites $(\sum_{(i,j) \in E} d_{ij} x_{ij} b f)$ given the fuel capacity of the vessel F_{max}. :

$$(2.6) \qquad \sum_{(i,j) \in E} d_{ij} x_{ij} b f + \sum_{i \in N} A_i a f \leq F_{max}.$$

The total trip harvest must be less than or eqaul to the available hold capacity C_{max}:

$$(2.7) \qquad \sum_{i \in N} q Stock_i A_i^{\gamma} y_i \leq C_{max}.$$

The set of port constraints ensure the vessel starts from and ends at the port (Node 1).

$$(2.8) \qquad \sum_{k=2}^{N} x_{1k} = 2 y_1.$$

$$(2.9) \qquad y_1 = 1.$$

The connectivity constraint ensures connectivity at node k in terms of entering and exiting the location. The vessel arrives at Node k via edge (i,k) and leaves Node k via edge (k,j). Edge $x_{kj} = x_{jk}$ because edges are bidirectional.

(2.10)
$$\sum_{i=1}^{N-1} x_{ik} = 2y_k, x_{ik} = x_{ki} \text{ if } i > k, i \neq k, k = 2, \cdots, |N|.$$

Suppose $N = 3$, we can rewrite the connectivity constraint as the following. If the vessel visits Node 3 ($y_3 = 1$), then the travel path is either 1-3-2 ($x_{13} = x_{32} = 1$) or 2-3-1 ($x_{23} = x_{31} = 1$). Because the edge is bidirectional, edge $x_{13} = x_{31}$, $x_{12} = x_{21}$. Then the equation $x_{12} + x_{13} = 2y_2$ describes the two possible paths that the individual vessel visits Node 3.

(2.11)
$$\begin{aligned}
x_{12} + x_{13} &= 2y_1 \\
x_{12} + x_{23} &= 2y_2 \\
x_{13} + x_{23} &= 2y_3
\end{aligned}$$

Subtour elimination constraints eliminate possible subtours[12]. For every subset of nodes (port excluded), the number of visited edges inside the subset (x_{ij}-values equal to 1) should be strictly smaller than the number of nodes in the subset. Dantzig et al. (1954) proposed the following subtour elimination constraints for the travelling salesman problem (Equation 2.12). It is the strongest known linear relaxation for the travelling salesman problem but the exponential number of constraints makes the implementation impractical (Palomo-Martínez et al., 2017). The set of subtours is $|S| = \sum_{i \in S} y_i$.

(2.12)
$$\sum_{i,j \in S} x_{ij} \leq |S| - 1; \forall S \subset N \setminus \{1\}, S \neq \varnothing.$$

Since not all nodes are visited in the solution of the orienteering problem, Feillet et al. (2005) defined a stronger formulation[13] (see Equation 2.13) (Palomo-Martínez et al., 2017). The bidirection setting of x_{ij} naturally deleted subtours with only two nodes[14].

(2.13)
$$\sum_{i,j \in S: i \neq j} x_{ij} \leq \sum_{i \in S \setminus \{k\}} y_i; \forall S \subset N \setminus \{1\}, |S| \geq 3, k \in S.$$

The edge choice variable x_{ij} and node choice variable y_i are both binary variables: $x_{ij} \in (0,1)$ and $y_i \in (0,1)$. Fishing effort (fishing hour $\times$ hook number), A_i, is continuous.

---

[12]Subtours: The optimal solution found doesn't give one continuous path through all the points, but instead has several disconnected loops (subtours). Appendix Section G includes an example of TSP solution with subtours.

[13]The formulation is stronger for the orienteering problem where only a subset of nodes is visited. In the traveling salesmen problem, the formulation is different because all nodes are visited.

[14]A subtour of two nodes i and j requires both $x_{ij} = 1$ and $x_{ji} = 1$. But the bidirectional edge $x_{ij} = 1$ represents either the edge from i to j is taken or the edge of j to i is taken but not both. Therefore there are no subtours of two nodes with the bidirectional edge x_{ij}.

Solution We solve for an open-loop solution that does not account for the strategic interaction between players through the evolution of state variables over time and the associated control adjustments (aka feedback rule). The player chooses the plan for the whole trip at the beginning and commits to it (Cellini and Lambertini, 2004).

2.3.2. 1-site ahead myopic fisher.

2.3.2.1. *Assumptions and setup.* Period-by-period static random utility model for location decisions depicts a myopic fisher. Using the similar formulation of the dynamic fisher, the individual fisher does a rolling maximization by choosing only one site at each decision point.

Because time is implicit and endogenous to spatial location in this framework, the decision point is in the spatial dimension. At the initial decision point one, the fisher is at the port (Node 1) and chooses to go to site k. Then the fisher is at site k, the decision point two where the second site is chosen. The time between two decision points (chosen locations) equals to the fishing time at the previous decision point (location) plus travelling time from the previous decision point (location) to the current decision point (location). It is endogenously determined by the location choice and effort allocation. The temporal dimension can be constructed using the model solution of location choice, effort allocation and path.

If the available storage is used up, the fisher has to return to the port. Moreover, if the fuel cannot support the trip from the current site to any next site and then back to the port, the fisher will return to the port immediately[15]. Otherwise, the vessel will be adrift at sea after fishing at the next site due to insufficient fuel.

In this setting, we modify the fuel constraint as Equation 2.14 since the fisher considers the distance between the next site and the port in addition to the distance between current site and the next site. The bidirectional edge x_{ij} used in the dynamic fisher's problem (Equation 2.3) doesn't capture the difference between travel distance back to the port of edge (i, j) and that of edge (j, i). The distance from site i to site j to the port (Node 1) is not equal to the distance from site j to site i to the port because the distance from the site to port depends on the current site ($d_{ij} + d_{j1} \neq d_{ji} + d_{i1}$ because $d_{i1} \neq d_{j1}$ given $i \neq j$).

The myopic 1-step ahead fisher problem is a directed graph with directional edges.

$$(2.14) \qquad \sum_{(i,j) \in E} (\mathrm{d}_{ij} + d_{j,1}) x_{ij} bf + \sum_{(i) \in N} aA_i f \leq F_{max}^t$$

---

[15]Going back to the port results in negative profit because there is no fish stock at the port. Negative profit is allowed in the rolling maximization to make this happen.

2.3.2.2. *Formulation.* The myopic problem at each decision point t can be formulated as

$$\max_{x_{ij}, y_i, A_i} \quad \sum_{i \in N}(p_i q A_i^\gamma Stock_i y_i - afc_{fuel}A_i) - \sum_{(i,j) \in E} d_{ij}x_{ij}fc_{fuel}$$

$$
\begin{array}{lll}
\text{s.t.} \quad \sum_{(i,j)\in E}(d_{ij}+d_{j,1})x_{ij}bf + \sum_{(i)\in N}A_i af \leq & F_{max}^t & \text{Fuel constraints}\\[4pt]
\sum_{i\in N} qStock_i A_i^\gamma y_i \leq & C_{max}^t & \text{Hold capacity constraints}\\[4pt]
\sum_i^N x_{ik} + \sum_i^N x_{ki} = & y_k, i \neq k & \text{Entering and Leaving k}\\[4pt]
y_k = & 1 & \text{Starting from Node k}\\[4pt]
\sum_i^N x_{ki} = & 1, i \neq k & \text{Starting from Node k}\\[4pt]
\sum_{i,j} x_{ij} = & 1 & \text{One edge is visited}\\[4pt]
\sum_{i=1}^N y_i = & 2 & \text{Two nodes are visited}\\[4pt]
A_k = & 0, k \in \text{visited nodes} & \text{No harvest at previously visited nodes}\\[4pt]
y_k = & 0, k \in \text{visited nodes} \setminus \text{starting node} & \text{Visited nodes in previous trip exclusion}\\[4pt]
x_{ij}, y_i \in & \{0,1\}
\end{array}
$$

(2.15)

F_{max}^t (C_{max}^t) is the available fuel capacity (hold capacity) at decision point t, equal to the available fuel capacity (hold capacity) subtracted by realized fuel consumption (harvest) at the previous decision point $t-1$.

$$
\begin{aligned}
F_{max}^t &= F_{max}^{t-1} - d_{ij}x_{ij}^{t-1}bf - A_i^{t-1}af\\
C_{max}^t &= C_{max}^{t-1} - qStock_i(A_i^{t-1})^\gamma y_i^{t-1}
\end{aligned}
$$

(2.16)

2.3.3. M-site ahead partially myopic fisher.

2.3.3.1. *Assumption and setup.* Instead of site-by-site choice, the m-site ahead partially myopic fisher chooses a sequence of up to m sites before returning to the port at every decision point. The fisher follows the sequence to visit the chosen fishing sites. The degree of forward looking m is between 1 and $N-1$, while N denotes the total number of sites including the port[16]. At the first chosen site, the fisher re-optimizes the trip by choosing another sequence of up to m sites before returning to the port. The whole choice set includes no more than $m+1$ sites because at some decision point t, the remaining fuel constraint and/or capacity may not be sufficient to support travelling and fishing to another m sites and returning to the port. This process repeats until the fisher arrives at the port.

Specifically, the modeling for the m-site ahead partially myopic fisher is:

(1) At the port (the first decision point, $n_1^0 = 1$), the myopic fisher chooses the first set of $m+1 \leq N$ sites (n_1^1, n_2^1, $\cdots$, n_m^1, port) before going back to the port, subject to fuel constraint $F_{max}^1 = F_{max}$ and capacity constraint $C_{max}^1 = C_{max}$. The superscript 1 of choice n_m^1 and technology constraints F_{max}^1 and C_{max}^1 denotes the choice is made at the first decision point. The subscript m of choice n_m^1 denotes it is the mth chosen location in the choice set.

---

[16]When $m = 1$, the m-site ahead fisher is the pure myopic fisher described in the previous section. When $m = N$, the m-site ahead fisher is the pure dynamic fisher.

(2) After fishing at the chosen site n_1^1 (the second decision point), the fisher makes the second choice set of m sites before returning to the port (n_1^2, n_2^2, $\cdots$, n_m^2, port), subject to fuel constraint F_{max}^2 and hold capacity constraint C_{max}^2. F_{max}^2 equals to fuel constraint at the first decision point F_{max}^1 minus the fuel usage from the port (the first decision point) to site n_1^1 (the second decision point) and fishing fuel usage at site n_1^1. C_{max}^2 equals to hold capacity constraint at the first decision point C_{max}^1 minus the fish catch at the second decision point site n_1^1.

(3) After fishing at Site n_1^t (the $t+1$th decision point), the fisher chooses the $t+1$th sequence of sites (n_1^{t+1}, n_2^{t+1}, $\cdots$, n_m^{t+1}= port) subject to constraints of fuel F_{max}^{t+1} and hold capacity C_{max}^{t+1}.

(4) This repeats T times until the fisher chooses the port ($n_1^T = port$) at Site n_1^{T-1} (the Tth decision point). The travel path of the fisher is (port, n_1^1, n_1^2, ..., n_1^t,...,n_1^T =port). See Appendix Section I for the choice sets, fuel capacity constraints and hold capacity constraints at each decision point.

2.3.4. Formulation. At the tth decision point, Site n_1^{t-1}, the partially myopic fisher chooses a sequence of sites, travel routes and fishing efforts to maximize the profit. Decision point t ranges from 1 to T. The m-site ahead partially myopic fisher's problem is an undirected graph.

(2.17)

$$
\max_{x_{ij}, y_i, A_i} \quad \sum_{i \in N}(p_i q A_i^\gamma Stock_i y_i - afc_{fuel}A_i) - \sum_{(i,j) \in E} d_{ij}x_{ij}bfc_{fuel}
$$

s.t. $\sum_{(i,j) \in E} d_{ij}x_{ij}bf + \sum_{i \in N} A_i af \leq$	F_{max}^t	Fuel constraint
$\sum_{i \in N} qA_i^\gamma Stock_i y_i \leq$	C_{max}^t	Hold capacity constraint
$\sum_{j=2}^{N} x_{1j} =$	$y_1 + 1\{t=1\}y_1$ [17]	Entering and Leaving 1
$\sum_{j=2}^{N} x_{n_1^{t-1}j} =$	$y_{n_1^{t-1}}$, if $t \geq 2$ [18]	Entering and Leaving n_1^{t-1}
$\sum_{i=1}^{N-1} x_{ik} =$	$2y_k, x_{ik} = x_{ki}$ if $i > k, i \neq k, k = 2, \cdots, |N|$ [19]	Entering and Leaving k
$y_1 =$	1	Visit Node 1
$y_{n_1^{t-1}} =$	1 [20]	Visit Node n_1^{t-1}
$\sum_{i \in S}\sum_{j \in S} x_{ij} \leq$	$\sum_{i \in S\setminus\{k\}} y_i, \forall S \subset N \setminus \{1\}, |S| \geq 3, k \in S$	Subtour elimination
$\sum_{i \in N} y_i \leq$	$m + 1 + 1\{t \geq 2\}$ [21]	Node Visit constraint
$x_{ij}, y_i \in$	$\{0,1\}$	

---

[17]If the fisher is at the port (the first decision point), $\sum_{j=2}^{N} x_{1j} = 2y_1$ because the fisher leaves and returns to the port. If the fisher is at another site other than port, $\sum_{j=2}^{N} x_{1j} = y_1$ because the fisher has to return to the port.

[18]If the fisher is at another site n_1^{t-1} other than the port (the tth choice set , $t \geq 2$), this constraint denotes that fisher departures from Site n_1^{t-1}.

[19]Edge $x_{ik} = x_{ki}$ in the undirected graph.

[20]When the fisher is at the port,$n_1^{t-1} = 1$, this constraint duplicates $y_1 = 1$ and becomes redundant. When the fisher is at Site n_1^{t-1} other than the port, the constraint ensures that site is chosen.

[21]At the port (the first decision point), the fisher chooses m sites and port so in total $m+1$ sites. However, at Site n_1^t other than the port (the tth decision point, $t \geq 2$), the fisher chooses $m+2$ sites. The extra 2 sites include the current site and the port.

51

2.4. Setting

The model and analysis in the chapter are motivated and parameterized to the extent possible by the Gulf of Mexico grouper-tilefish demersal longline fishery (Figure 2.2). OFarrell et al. (2019b) integrated three datasets (Vessel Monitoring System (VMS) data, observer data, logbook data) to capture the fine spatial behavior of the fleet. The dataset consists of more than one million hourly GPS positions (VMS pings) from the bottom longline fishery tracking 5508 trips made by 133 vessels from 2007 to 2014. Figure 2.1b is the fishing heat map plotted using 587,204 VMS pins from 106 vessels from 2007 to 2009.
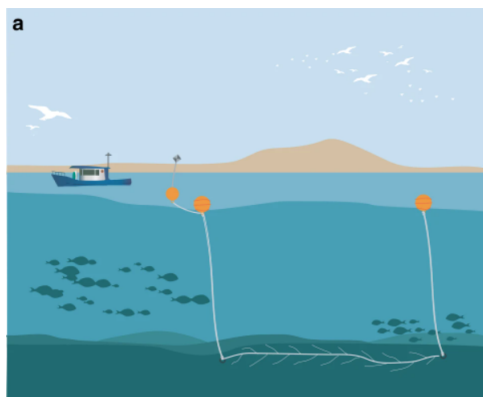
FIGURE 2.2. Bottom longlines fishing in Gulf of Mexico (OFarrell et al., 2019b)

At present, the chapter demonstrates the model on a 15-node problem (See Figure 2.3), where the port (Node 1) is set at Tampa, FL. The simulated vessel path in Figure 2.1c forms the basis for modeling a vessel leaving and returning to the same port.

The fishing ground modeled in the chapter is based on the eastern Gulf of Mexico and is created as a convex hull of the VMS pings classified as fishing using a supervised learning algorithm trained by the observer data (OFarrell et al., 2019b)[22]. The fourteen nodes representing fourteen fishing sites are randomly generated within the polygon. The inter-site distances are calculated in nautical miles as the great-circle distance based on the fishing site coordinates using Haversine formula. The fish stocks are random draws following a spatial pattern that stock is higher for inshore sites[23]. Fishing effort is defined as fishing hour (longline set, soak and retrieve time) times the number of hooks. The number of hooks is set to be 1000 to simplify the analysis[24]. In the harvest function, we use the output elasticity of

---

[22]VMS records east to the 87th meridian west are used in this chapter. The convex hull is created using `chull` function in R.

[23]At a close-to-shore site, stock (lbs) is a random draw from the uniform distribution [20000, 30000]. Stock at an offshore site is a random number that is uniformly distributed in [15000, 20000]. A site is considered as close-to-shore if the point-to-polygon (site-to-shore) distance is below a threshold. The Euclidean distance of 1 is used as the threshold.

[24]The observer data includes 8252 longline sets from 314 fishing trips by 83 vessels from 08/08/2006 to 04/24/2014. The hook number ranges from 150 to 3000 with a median of 1000 and a mean of 1019.

fishing effort $\gamma = 0.7$ and the catch stock elasticity $\beta = 1$ as Zhang and Smith (2011) estimate the output elasticity of fishing effort γ to be less than 1 (diminishing harvests in fishing effort) regardless of whether the catch stock elasticity β is restricted to 1 for all gears in the reef-fish fishery in the Gulf of Mexico[25].

(a) Map

(b) Simulated Fish Stock
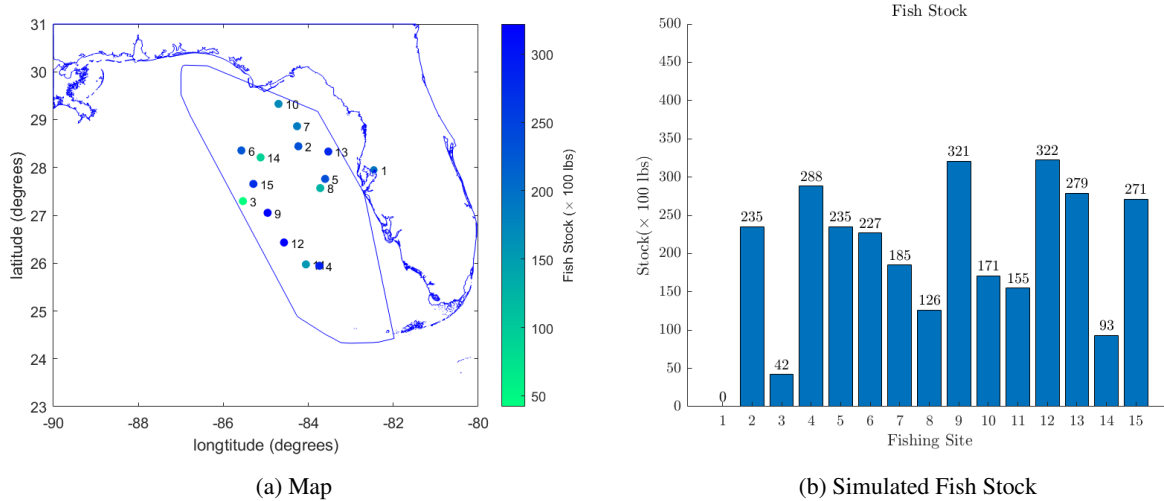
FIGURE 2.3. Spatial distribution and fish stock of the port (Node 1) and 14 fishing sites in the Gulf of Mexico

We consider the trips of a dynamic fisher, a myopic fisher, and a partially myopic fisher in the presence of three sets of technology constraints: no binding technology constraints (sufficiently large fuel capacity $F_{max} = 20000$ gallons and hold capacity $C_{max} = 200 \times 100$ lbs), a binding fuel capacity constraint {fuel capacity $F_{max} = 3000$ gallons, hold capacity $C_{max} = 200 \times 100$ lbs}, and a binding hold capacity constraint { fuel capacity $F_{max} = 20000$ gallons, hold capacity $C_{max} = 30 \times 100$ lbs}[26]. The problems are formulated as mixed-integer programming (MIP) problems and solved by the Gurobi solver.

The implicit temporal dimension can be constructed by the fishing and travelling times. Fishing effort reflects the fishing hours (longline set, soak, and retrieve time) spent at a fishing site. Travelling time can be calculated from the travel distance of the chosen edge with a given travel speed. Suppose the traveling speed is 5 knots (nautical mile per hour), traveling fuel consumption rate is 5 gallon per hour while fishing fuel consumption rate is 10 gallon per hour[27].

---

[25]The estimated catch effort elasticity for bottom longline is 0.3325 with standard error 0.0093 in Zhang and Smith (2011). However, the effort in Zhang and Smith (2011) is defined as number of crew times trip days while the effort in this chapter is defined as number of hooks times fishing hour (longline set, soak and retrieve time).

[26]The logbook data includes hold capacity and fuel capacity for 145 vessels. The hold capacity in pounds ranges from 1000 to 200,000 with mean of 15787 and median 12000. The fuel capacity in gallons ranges from 200 to 6000 with mean of 1319 and median of 1000.

[27]Fuel consumption rate for fishing is assumed to be twice as large as steaming. Accurate information on fuel consumption rates for steaming and fishing were not available yet. We are exploring ways to improve this parameterization by developing methods more appropriate for longline fishing in the Gulf of Mexico.

2.5. Results

Generally, we expect that the technology constraints affect the short-run decisions over fishing location, path, and fishing effort by imposing a trip level shadow price. Before reporting the simulation results that demonstrate those findings, we can analytically show the role that technology constraints play in determining the effort allocation at each site. Specifically, the trip level shadow price that holds across fishing sites either affects the marginal revenue $(p - \lambda_{hold})$ or the marginal cost $(c_{fuel} + \lambda_{fuel})$ depending on the constraint that is binding. Equation 2.19 shows the optimal effort allocation at site i.

$$
\begin{aligned}
\frac{\partial \mathscr{L}}{\partial A_i} = \ & pq\text{Stock}_i y_i \gamma A_i^{\gamma-1} - afc_{fuel} - \lambda_{fuel}af - \lambda_{hold}q\text{Stock}_i y_i \gamma A_i^{\gamma-1} \\
= \ & (p - \lambda_{hold})q\text{Stock}_i y_i \gamma A_i^{\gamma-1} - (c_{fuel} + \lambda_{fuel})af \\
= \ & 0
\end{aligned}
$$

(2.18)

$$
(2.19) \qquad \Rightarrow A_i^* = [\frac{(p - \lambda_{hold})q\text{Stock}_i y_i \gamma}{(c_{fuel} + \lambda_{fuel})af}]^{\frac{1}{1-\gamma}}
$$

Regardless of the binding constraint, the shadow price reduces the effort allocation at each site relative to the case where the constraints are not binding. The latter is representative of the myopic fisher at sites that are not their last fishing sites. Having said that, eventually the constraints will bind even in the myopic case and at the last decision point where they bind, there is a revealed shadow price. For example, if the myopic fisher is making their 5th decision of where to go on a trip and how much effort to exert and they calculate that they can't go to another site as they will run out fuel, then that decision's optimal calculus includes the shadow price attached to the binding fuel constraint. But for all decisions before their 5th, the constraint did not bind and therefore their decision calculus was independent of the shadow price.

The presence of the shadow price impacts directly the effort exerted in each patch which also determines the fuel used for fishing in each patch and the catch. As such, it influences the path taken on the trip (and the fuel expended steaming to and from the fishing sites).

2.5.1. Dynamic fisher vs myopic fisher. Figure 2.4 shows the location choice,travel path and fishing effort of the dynamic fisher and the myopic fisher under three sets of technology constraints. Table 2.3 highlights the differences in key variables across the cases including the trip profit, fuel use, harvest, shadow price, and endogenous trip length.

54

Variable	Unconstrained $F_{max} = 20,000, C_{max} = 200$		Fuel $F_{max} = 3,000, C_{max} = 200$		Hold $F_{max} = 20,000, C_{max} = 30$	
Fisher Type	Dynamic	Myopic	Dynamic	Myopic	Dynamic	Myopic
Profit		$0.94\pi_{\text{dynamic}}$		$0.44\pi_{\text{dynamic}}$		$0.61\pi_{\text{dynamic}}$
Fuel Usage	17518.03	17916.41	3000	3000	2138.7	3064
Harvest	160.88	160.88	40.74	29.16	30	30
Shadow price		-	$\lambda_{\text{fuel}} = 1.6031$		$\lambda_{hold} = 142.3355$	
Travel%	6.9%	10.8%	34.5%	10%	36.9%	9.8%
Fishing%	93.1%	89.2%	65.5%	90%	63.1%	90.2%
Trip Length (day)	75	79	15	13	11	13

(1) Travel% denotes percentage of travel time of the total trip length. Same for Fishing%.

TABLE 2.3. Fuel and hold Usage, binding Constraints, shadow Price, travel Route and time

2.5.1.1. *Nonbinding constraints.* With sufficient fuel and hold capacity[28], the dynamic fisher and myopic fisher visit and harvest at all fishing sites and exert fishing effort at each site until the marginal profit equals 0 ($\frac{\partial \pi}{\partial \text{effort}_i} = 0$). While the two are identical in terms of sites visited, harvest, and effort exerted, the trip profits differ because the dynamic fisher optimizes their route while the myopic does not[29]. Figure 2.4a and 2.4b show the route planning by the dynamic fisher while the myopic fisher only considers the next best choice (mainly following the order of fish stock).

2.5.1.2. *Binding fuel constraint.* While the unconstrained case is valuable for highlighting the role and value of route planning, vessels are constrained in their fuel and hold capacity, especially when considering the large choice set of fishing sites. To investigate the role of these technological constraints, we reduce the fuel capacity to ensure that it is binding. Specifically, when we set the fuel constraint to 3,000 gallons with the same hold capacity constraint of 200×100 lbs, we find that both fishers face a binding fuel constraint though it only appears in the last decision of the myopic fishers trip calculus[30].

In Figure 2.4d, we see that the dynamic fisher goes to the same location choices, as the unconstrained case, but reduces the effort at every visited site. In the presence of the constraint and with diminishing marginal harvest to effort, we find that it is optimal to spread fishing effort across fishing sites instead of concentrating effort on one or two sites with the largest fish stock. The effort is reallocated such that marginal profit of effort equals to the the shadow cost of fuel times the fuel consumption per unit of effort ($\frac{\partial \pi}{\partial \text{effort}_i} = af\lambda_{\text{fuel}}$).

The myopic fisher on the other hand concentrates effort at Site 13 with the highest fish stock (Figure 2.4e). When the fisher makes the choice to visit Site 13, the fuel constraint is not binding, and as such the fishing effort at Site 13 is the unconstrained optimal effort. The fuel constraint, however, is binding and hence reduces the effort spent at

[28]We set fuel capacity $F_{max} = 20,000$ gallons and hold capacity $C_{max} = 200 \times 100$ lbs so that neither constraints bind (Table 2.3).

[29]The bidirectional route for the dynamic fisher:1-5-8-4-11-12-9-15-14-6-10-7-2-13-1. The directional route for the myopic fisher:1-13-5-7-10-8-9-12-4-11-15-6-2-14-3-1.

[30]The bidirectional route for the dynamic fisher:1-5-8-4-11-12-9-15-14-6-10-7-2-13-1. The directional route for the myopic fisher:1-13-5-1.
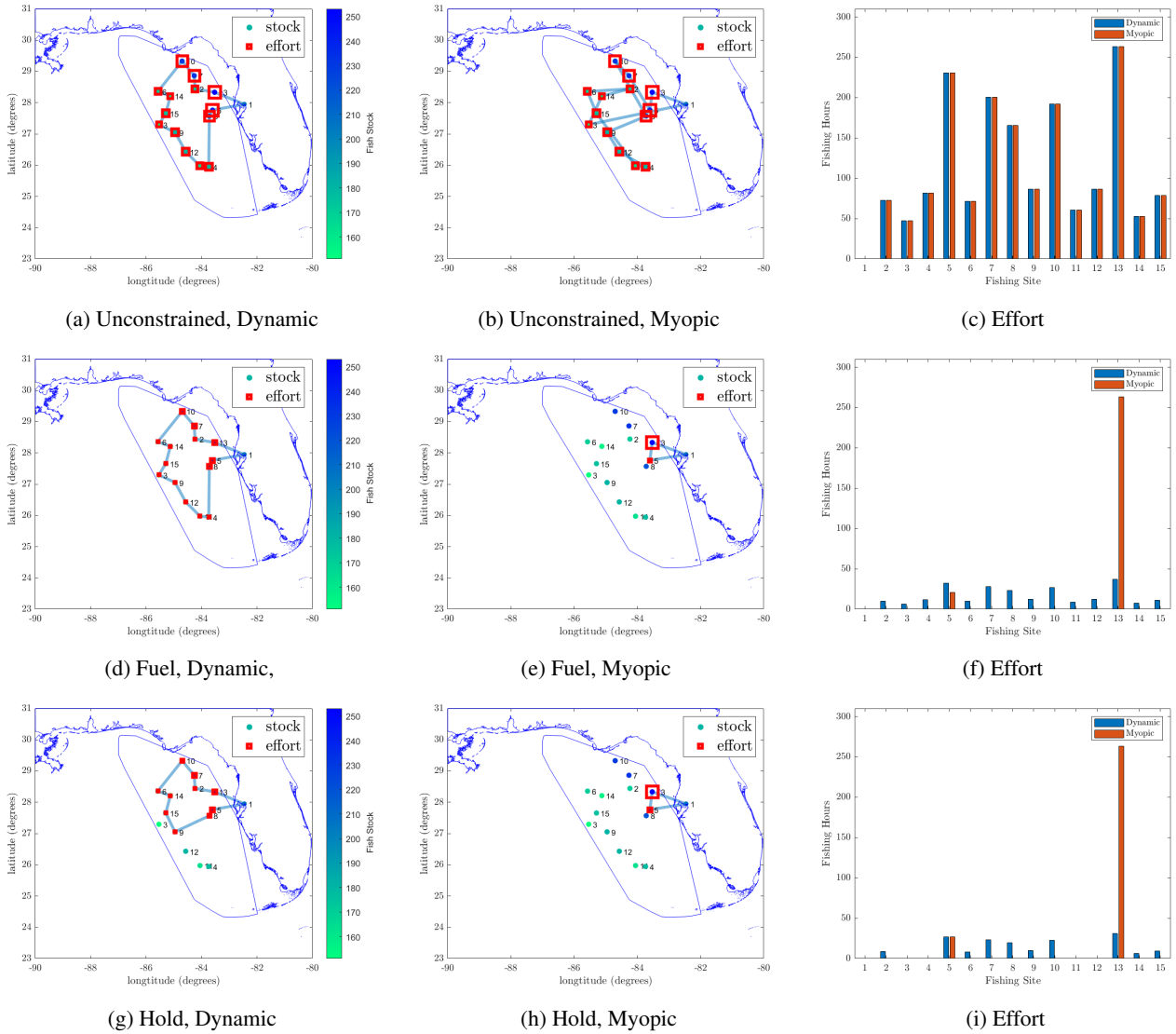
FIGURE 2.4. Travel path and fishing effort, dynamic fisher vs myopic fisher

Site 5, the last fishing site before the port. Since fishing and travelling consume fuel, we find that the relative shadow price of fuel for the myopic at site 5 is greater than the optimal shadow price ($\lambda_{fuel,5}^{myopic} = 2.1230 > \lambda_{fuel}^{dynamic} = 1.6031$). This results in the effort at Site 5 being smaller than the dynamic optimal level. The inefficient use of fuel[31] and concentrated levels of effort across fishing sites, limits the number of visited sites and leads to a much lower profit for the myopic fisher ($\pi_{\text{myopic}} \approx 0.44\pi_{\text{dynamic}}$).

---

[31]Because the myopic fisher visits the fishing sites following the order of fish stock, the first few visited fishing sites have the largest fish stock and therefore requires a lot of fishing effort/fuel to drive down the marginal profit of effort to zero.

2.5.1.3. *Binding hold constraint.* We now consider the case of reducing the hold capacity from 200×100 lbs to 30×100 lbs while using the unconstrained amount of fuel. Both fishers have a binding hold constraint but just as in the case with the binding fuel constraint, the dynamic fisher considers the constraint when deciding the trip and myopic only in their final decision point[32].

In Figure 2.4g, we see that the dynamic fisher no longer visits the relatively distant Sites 3, 4, 11 and 12 (a smaller circle), and reduces the effort at every visited site. The effort is reallocated such that marginal profit of harvest equals to the shadow cost of hold capacity ($\frac{\partial \pi}{\partial \text{harvest}_i} = \lambda_{\text{hold}}$). On the contrary, the myopic fisher concentrates effort at Site 13 with the highest fish stock (Figure 2.4h). The hold capacity constraint for the myopic fisher is binding at Site 5, the last decision point before returning to the port ($\lambda_{hold,5}^{myopic} = 154.47 > \lambda_{hold}^{dynamic} = 142.33$). Given the relative size of the shadow prices, we find that the effort at Site 5 is smaller in the myopic than the dynamic optimal level. The myopic fisher again has a much lower trip level profit ($\pi_{\text{myopic}} \approx 0.61 \pi_{\text{dynamic}}$), even though both fishers have the same harvest. We also find that the endogenous trip length is longer and that most of their fuel is spent fishing (they fish longer and harder at each patch before moving on as they are fishing until the marginal profit goes to zero).

2.5.2. M-site ahead partially myopic fisher. From the previous results, the dynamic fisher and the myopic (1-site ahead) fisher behave differently in route planning and incorporating shadow price of the technology constraints into fishing effort. In the unconstrained case, the myopic fisher makes less profit because of no route planning. In the fuel constrained case and hold constrained case, no route planning and ignoring the technology constraint before the last decision point lead to the smaller profit for the myopic fisher. This section decomposes the loss from route planing and the loss from ignoring the technology constraint shadow price in the fuel constrained case ($F_{max} = 3000$ gallons, $C_{max} = 200 \times 100$ lbs.).

The m-site ahead fisher is more forward looking with larger m, therefore the degree of route planning increases with m. To separate the impact of route planning from that of technology constraint shadow price, we consider an m-site ahead fisher who knows and incorporates the shadow price of the binding technology constraint. From Equation 2.19, the shadow price of fuel acts as extra fuel cost that affects the fishing effort at each fishing site when the fuel constraint is binding. Then the m-site ahead partially myopic fisher knowing λ_{fuel} faces the cost of $c_{fuel} + \lambda_{fuel}$ in the decision-making process. Figure 2.5 shows the location choice, travel path and fishing effort of the m-site ahead fisher and the m-site ahead fisher knowing λ_{fuel}. Table 2.4 summarizes the deviation of profit from the dynamic optimal profit, total catch, travel and fishing time.

---

[32]The bidirectional route for the dynamic fisher:1-5-8-9-15-14-6-10-7-2-13-1. The directional route for the myopic fisher:1-13-5-1.

For the myopic fisher who makes period-by-period/site-by-site decision, $\pi_{myopic} = 0.44\pi_{dynamic}$. With the shadow price of fuel embedded in the decision making, the profit almost doubled ($\pi_{myopic,\lambda_{fuel}} = 0.86\pi_{dynamic}$). The profit increases largely because the myopic fisher chooses the dynamic optimal level of effort, knowing the shadow price of fuel. The myopic fisher, however, visits fewer sites than the dynamic fisher because of the lack of route planning (Figure 2.5b). When m increases from 1 to 2, 3 and 6, the profit increases from better route planning that leads to less fuel wasted allowing visiting and fishing at more sites. However, the fuel is not used up with constrained route planning. We find that the magnitude of profit increase from route planning is lower compared to the magnitude of profit increase from embedding the shadow price of fuel. That is, the efficiency loss from overfishing at each site is much greater than the efficiency loss from poor route planning. Whether this holds in general is unclear and is something we plan to explore with further sensitivity analysis. For example, we are currently assuming that the travel fuel consumption rate is half of the fishing fuel consumption rate and as such, improving travel efficiency may not increase much profit.

In general, profit increases with increasing m due to both better route planning and accounting for the shadow price of the technology constraints. That is, greater forward-looking behavior results in spreading effort across fishing sites by considering the binding technology constraints. Although the shadow price of fuel is not equal across all visited fishing sites, the difference among the shadow price of fuel decreases with m[33]. From the third column of graphs in Figure 2.5, we can see that fishing efforts (red column by the m-site ahead partially myopic fisher) are more concentrated at early visited sites with smaller m ($m = 1, 2$ Figure 2.5c and 2.5f). Fishing efforts between the dynamic and partially myopic fisher are more equal across the fishing sites with larger m ($m = 3, 6$ Figure 2.5i and 2.5l).

Variable	Dynamic	1-site ahead		2-site ahead		3-site ahead		6-site ahead	
		Myopic	w/λ_{fuel}	Partially Myopic	w/λ_{fuel}	Partially Myopic	w/λ_{fuel}	Partially Myopic	w/λ_{fuel}
Profit[1]	6221.2	0.44	0.86	0.78	0.87	0.88	0.87	0.95	0.97
Fuel Usage	3000	3000	2994.5	3000	2771.43	3000	2887.08	3000	2914.54
Harvest	40.74	29.16	37.75	36.08	36.61	38.32	37.30	39.73	39.6
λ_{fuel}	1.6031		1.6031		1.6031		1.6031		1.6031
Travel%[2]	34.5%	10%	41.9%	17.2%	37.4%	21.2%	39.6%	26.3%	34.5%
Fishing%	65.5%	90%	58.1%	82.8%	62.6%	78.8%	60.4%	73.7%	65.5%
Trip Length (day)	15	13	16	13.7	14.2	14	15	14.4	14.7
# Sites	14	2	12	5	11	6	12	9	13

(1) Only the profit of the dynamic fisher is listed in the table. For the myopic and partially myopic fishers, the percentage of the dynamic profit $\frac{\pi}{\pi_{dynamic}}$ is listed.

(2) Travel% denotes percentage of travel time of the total trip length. Same for Fishing%.

TABLE 2.4. Fuel and hold usage by m-site ahead partially myopic fisher with binding fuel, $F_{max} = 3000$, $C_{max} = 200$

[33]Here are the revealed shadow price for partially myopic fishers.
2-site ahead: $\lambda_{fuel,5} = 0.3607$, $\lambda_{fuel,8} = 0.7460$, $\lambda_{fuel,7} = 1.3513$, $\lambda_{fuel,i} = 1.6359$, $i = 2, 13$.
3-site ahead: $\lambda_{fuel,8} = 0.5804$, $\lambda_{fuel,5} = 0.8955$, $\lambda_{fuel,10} = 1.2654$, $\lambda_{fuel,i} = 1.4262$, $i = 7, 2, 13$.
6-site ahead: $\lambda_{fuel,5} = 1.0821$, $\lambda_{fuel,8} = 1.1579$, $\lambda_{fuel,15} = 1.2996$, $\lambda_{fuel,i} = 1.3735$, $i = 14, 6, 10, 7, 2, 13$.

(a) Myopic 1 Site

(b) λ_{fuel} embedded

(c) Effort

(d) Partially Myopic 2-site

(e) λ_{fuel} embedded

(f) Efforts

(g) Partially Myopic 3-site

(h) λ_{fuel} embedded

(i) Efforts

(j) Partially Myopic 6-site

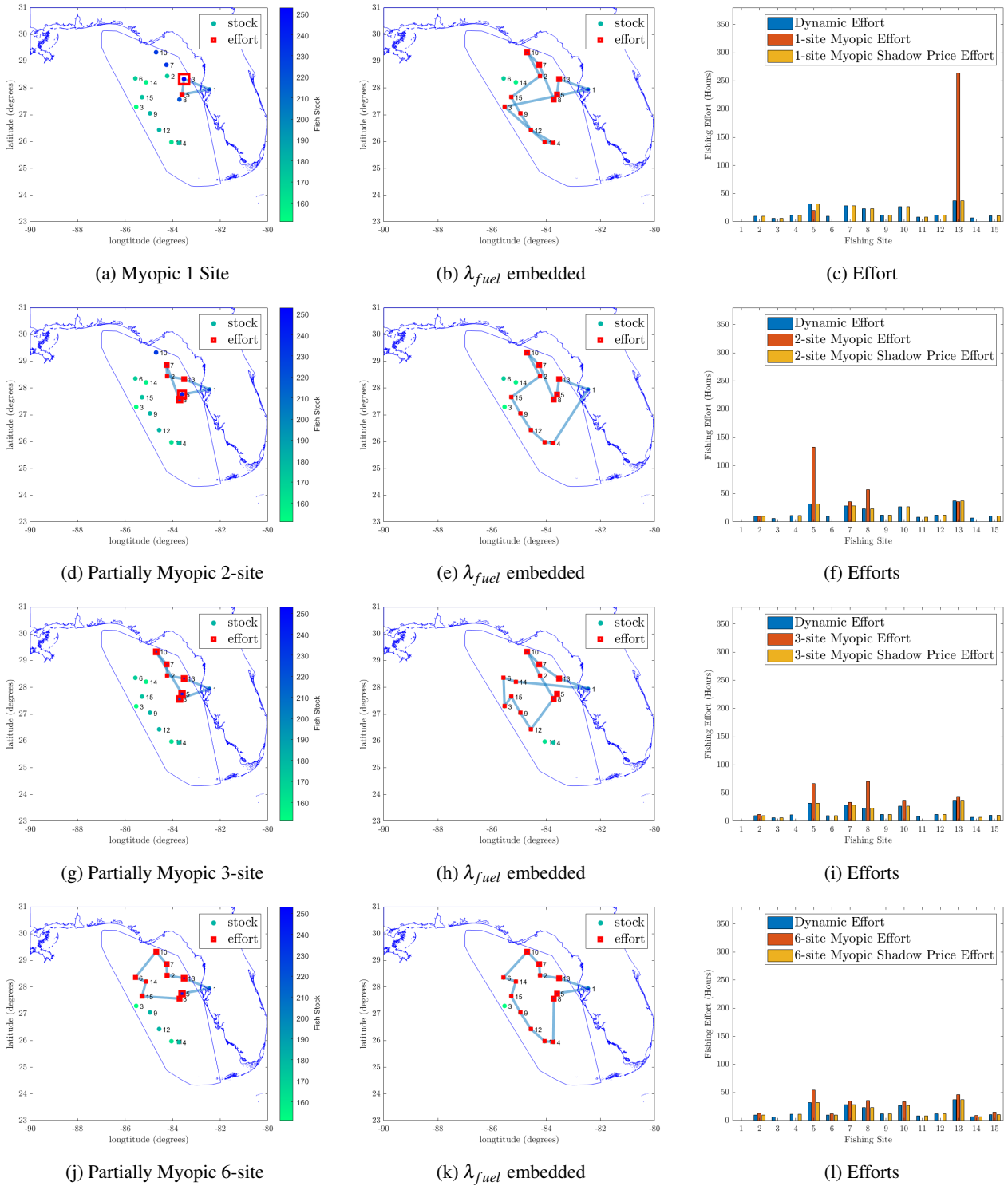(k) λ_{fuel} embedded

(l) Efforts

FIGURE 2.5. M-site ahead partially myopic fisher, binding fuel, $F_{max} = 3000$, $C_{max} = 200$

2.6. Conclusions

Fishing production function is uniquely shaped by space. This chapter constructs a spatial dynamic model of an individual fisher's decision on location choices, effort allocation, and a multi-day trip path with endogenous trip length. This structural behavioral model of ex-ante short run production decision-making is useful to fishery management and lays the foundation of a comprehensive model of the fishing production process. After estimation or calibration using the empirical data, the model can be used to predict fishers' responses to policies like area closure and access economic impacts for policy design or evaluation.

The individual fisher maximizes profit by choosing locations with high fish stock and low travel distance. Technology constraints such as fuel and hold capacity impose shadow prices affecting, from the outset of the trip, the interconnected decision on location choice, effort allocation, and travel path.

For this analysis we generate a random set of 14 fishing sites, each with a given fish stock following the spatial pattern that nearshore sites are higher in stock. We may have another set of stock or between-site distances with another draw of fishing sites distribution. Then the resulting chosen fishing sites, the fishing effort at each site, and the travel path for a specific type of fisher may change. However, the fisher has consistent behavior. The dynamic fisher always allocates effort at every visited site so that the marginal profit of harvest is equal to the shadow price of fuel or hold. The myopic fisher or the partially myopic tends to overfish at the early visited sites. With the current parameterization on consumption rate[34], fishing hours and fishing fuel consumption dominate travel hours and travel fuel consumption. This probably underlies the finding that the magnitude of profit increase from route planning is lower compared to the magnitude of profit increase from embedding the shadow price. However, since revenue comes only from fishing instead of traveling, a fisher may always tend to spend more time on fishing and fishing fuel consumption probably always dominates travel consumption. The qualitative result may still hold. We will leave this for a careful robustness check.

An implication of our findings is that in the traditional random utility model of fishing location (Equation 2.1) the coefficient of expected rewards is overestimated if the technology constraints are omitted. Route planning is also missing in the static RUM models. Considering one location choice at a time, the myopic fisher will not know all the chosen locations ahead and hence fail to find the shortest path. This will inversely restrict the fishing effort at each fishing site and the number of fishing sites that the fisher can visit. We conclude that the static RUM models are structurally misspecified but leave for future research an investigation into the empirical ramification of the incorrect specification.

---

[34]Fishing fuel consumption rate is 10 gallon per hour while the travel fuel consumption rate is 5 gallon per hour.

The current chapter accounts only for the deterministic case in which the fisher has perfect information on the fish stock at each fishing site. Under a stochastic setting, the individual fisher cannot observe the fish stock and has beliefs on the mean and variance of the stock at each site. Under uncertainty, the vessel hold capacity constraint also becomes a probabilistic constraint. Decision making with uncertainty also requires cognitive operations, including information acquisition and information processing. In future work, we plan to incorporate these features of fishery production into the structural model of trip level decision-making.
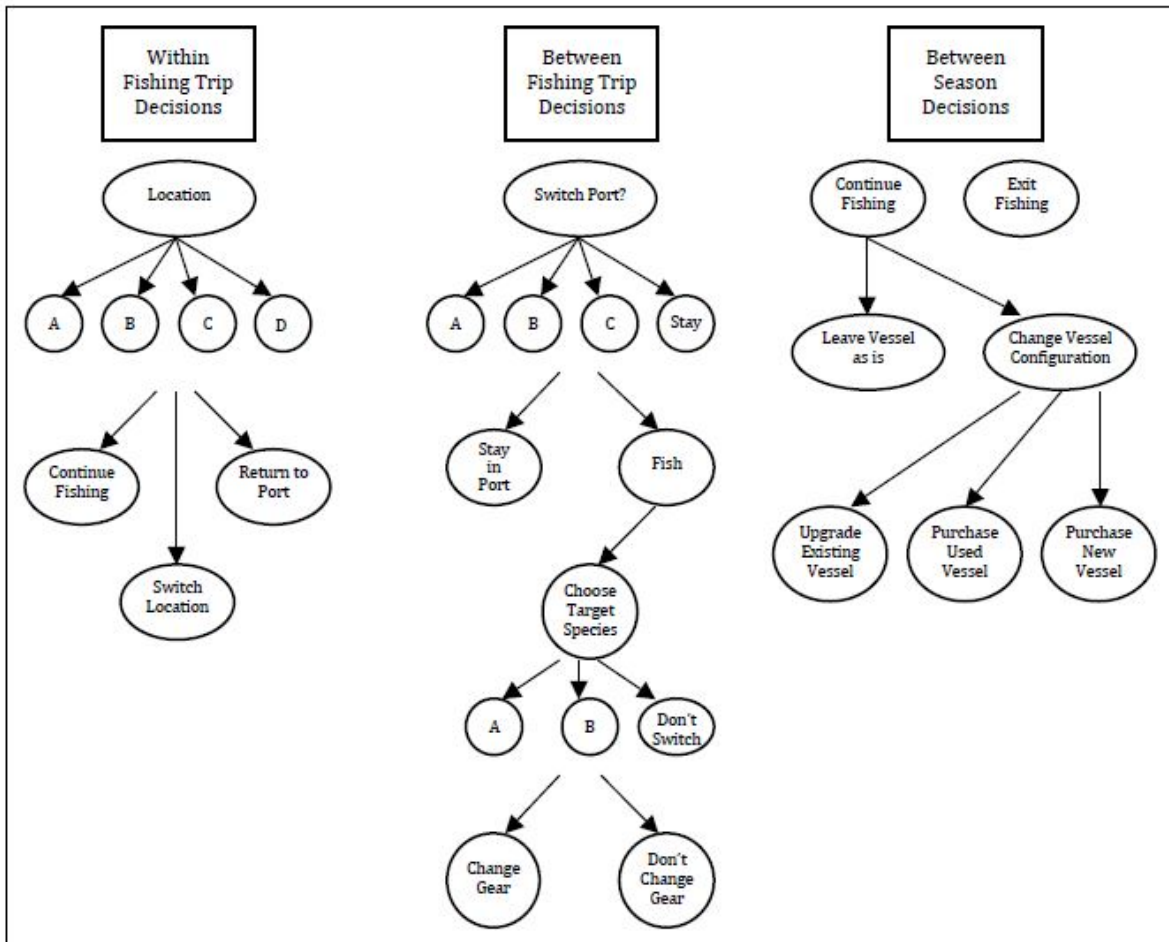
Fishing production process

Figure 1.1: The fishing production process -

FIGURE F.1. The fishing production process (Reimer, 2012)

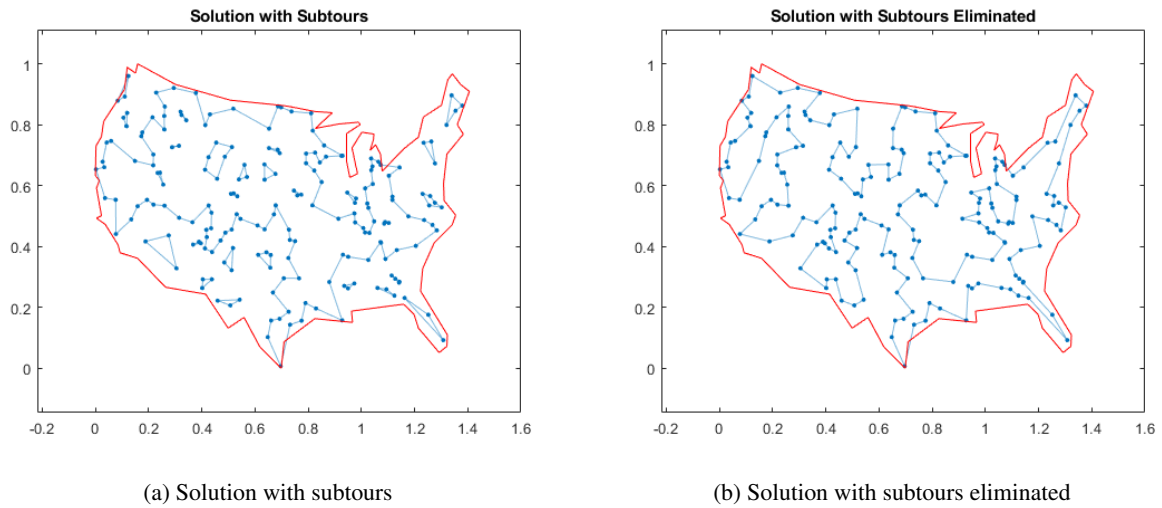APPENDIX G

Subtours in the traveling salesman problem

(a) Solution with subtours

(b) Solution with subtours eliminated

FIGURE G.1. Example of subtours from Traveling Salesman Problem: Problem-Based MathWorks (2021)

Derivations

H.1. Optimal unconstrained and constrained fishing effort

The Lagrange function of the dynamic fisher optimization problem (Problem 2.3) is

(H.1)
$$
\begin{aligned}
\mathscr{L}(x_{ij}, y_i, A_i, \lambda) = \quad & \textstyle\sum_{i \in N}(pqA_i^{\gamma}\text{Stock}_i y_i - afc_{fuel}A_i) - \sum_{(i,j)\in E} d_{ij}x_{ij}bfc_{fuel} \\
& -\lambda_{fuel}(\textstyle\sum_{(i,j)\in E} d_{ij}x_{ij}bf + \sum_{(i)\in N} A_i af - F_{max}) \\
& -\lambda_{hold}(\textstyle\sum_{i \in N} qA_i^{\gamma}\text{Stock}_i y_i - C_{max})
\end{aligned}
$$

The first order condition of fishing effort at each site is

(H.2)
$$
\begin{aligned}
\tfrac{\partial \mathscr{L}}{\partial A_i} = \quad & pq\text{Stock}_i y_i \gamma A_i^{\gamma-1} - afc_{fuel} - \lambda_{fuel}af - \lambda_{hold}q\text{Stock}_i y_i \gamma A_i^{\gamma-1} \\
= \quad & (p - \lambda_{hold})q\text{Stock}_i y_i \gamma A_i^{\gamma-1} - (c_{fuel} + \lambda_{fuel})af \\
\Rightarrow A_i^* = \quad & \left(\tfrac{(p-\lambda_{hold})q\text{Stock}_i y_i \gamma}{(c_{fuel}+\lambda_{fuel})af}\right)^{\frac{1}{1-\gamma}}
\end{aligned}
$$

(1) If neither of the fuel and hold constraint binds, $\lambda_{fuel} = 0, \lambda_{hold} = 0$. $A_i^* = \left(\tfrac{pq\text{Stock}_i y_i \gamma}{c_{fuel}af}\right)^{\frac{1}{1-\gamma}}$

(2) If the fuel constraint binds while hold constraint doesn't. $\lambda_{fuel} > 0, \lambda_{hold} = 0$. From the FOC, we can derive $A_i^*(\lambda_{fuel})$, the optimal fishing effort as a function of λ_{fuel}.

(H.3)
$$
\begin{aligned}
A_i^* = \quad & \left(\tfrac{(p-\lambda_{hold})q\text{Stock}_i y_i \gamma}{(c_{fuel}+\lambda_{fuel})af}\right)^{\frac{1}{1-\gamma}} \\
= \quad & \left(\tfrac{pq\text{Stock}_i y_i \gamma}{(c_{fuel}+\lambda_{fuel})af}\right)^{\frac{1}{1-\gamma}}
\end{aligned}
$$

Use the binding fuel constraint, we can solve λ_{fuel} and therefore A_i^*.

(H.4)
$$
\begin{aligned}
\textstyle\sum_{(i,j)\in E} d_{ij}x_{ij}bf + \sum_{(i)\in N} A_i af = \quad & F_{max} \\
\Rightarrow \textstyle\sum_{(i,j)\in E} d_{ij}x_{ij}bf + \sum_{(i)\in N}\left(\tfrac{pq\text{Stock}_i y_i \gamma}{(c_{fuel}+\lambda_{fuel})af}\right)^{\frac{1}{1-\gamma}}af = \quad & F_{max} \\
\Rightarrow \quad & \lambda_{fuel} \\
\Rightarrow A_i^* = \left(\tfrac{pq\text{Stock}_i y_i \gamma}{(c_{fuel}+\lambda_{fuel})af}\right)^{\frac{1}{1-\gamma}} \text{ using derived } \lambda_{fuel}
\end{aligned}
$$

(3) If the fuel constraint doesn't bind while the hold constraint binds, $\lambda_{fuel} = 0, \lambda_{hold} > 0$. Similarly, we can derive $A_i^*(\lambda_{hold})$ from the FOC, the optimal fishing effort as a function of λ_{hold}.

(H.5)
$$
\begin{aligned}
A_i^* &= \left(\frac{(p-\lambda_{hold})q\text{Stock}_i y_i \gamma}{(c_{fuel}+\lambda_{fuel})af}\right)^{\frac{1}{1-\gamma}} \\
&= \left(\frac{(p-\lambda_{hold})q\text{Stock}_i y_i \gamma}{c_{fuel}af}\right)^{\frac{1}{1-\gamma}}
\end{aligned}
$$

Using the binding hold constraint, we can solve λ_{hold} and therefore A_i^*.

(H.6)
$$
\begin{aligned}
\sum_{i\in N} qA_i^\gamma \text{Stock}_i y_i &= C_{max} \\
\Rightarrow \sum_{i\in N} q\left(\frac{(p-\lambda_{hold})q\text{Stock}_i y_i \gamma}{c_{fuel}af}\right)^{\frac{\gamma}{1-\gamma}}\text{Stock}_i y_i &= C_{max} \\
\Rightarrow \lambda_{hold} & \\
\Rightarrow A_i^* = \left(\frac{(p-\lambda_{hold})q\text{Stock}_i y_i \gamma}{c_{fuel}af}\right)^{\frac{1}{1-\gamma}} \text{ using derived } \lambda_{hold} &
\end{aligned}
$$

H.2. Derivation of catchability coefficient q

The catchability coefficient q is chosen so that the harvest from the unconstrained optimal effort at each site is interior $q(A_i^*)^\gamma \text{Stock}_i y_i < \text{Stock}_i$. With no constraint on fuel and hold, $\lambda_{fuel} = \lambda_{hold} = 0$,

(H.7)
$$
\begin{aligned}
A_i^* &= \left(\frac{(p-\lambda_{hold})q\text{Stock}_i y_i \gamma}{(c_{fuel}+\lambda_{fuel})af}\right)^{\frac{1}{1-\gamma}} \\
&= \left(\frac{pq\text{Stock}_i y_i \gamma}{c_{fuel}af}\right)^{\frac{1}{1-\gamma}}
\end{aligned}
$$

The optimal harvest at each site should not exceed the available stock.

(H.8)
$$
\begin{aligned}
q(A_i^*)^\gamma \text{Stock}_i y_i &< \text{Stock}_i \\
q(A_i^*)^\gamma y_i &< 1 \\
qy_i\left(\frac{pq\text{Stock}_i y_i \gamma}{c_{fuel}af}\right)^{\frac{\gamma}{1-\gamma}} &< 1 \\
q^{\frac{1}{1-\gamma}}y_i^{\frac{1}{1-\gamma}}\left(\frac{p\text{Stock}_i \gamma}{c_{fuel}af}\right)^{\frac{\gamma}{1-\gamma}} &< 1 \\
q^{\frac{1}{1-\gamma}}y_i^{\frac{1}{1-\gamma}} &< \left(\frac{p\text{Stock}_i \gamma}{c_{fuel}af}\right)^{\frac{-\gamma}{1-\gamma}} \\
qy_i &< \left(\frac{c_{fuel}af}{p\text{Stock}_i \gamma}\right)^{\gamma}
\end{aligned}
$$

Given parameter values of $\text{Stock}_i, a, p, c_{fuel}$, q is chosen so that works for all site, $qy_i = \frac{1}{2}min[(\frac{c_{fuel}af}{p\text{Stock}_i \gamma})^\gamma]$.

H.3. Scaling fishing effort

Fishing effort is defined as hook number $\times$ fishing hour. Replace effort A_i with $A_i\eta\kappa$ as $\eta = 1000$ is the number of hooks, κ is the scaling parameter, then A_i is just fishing hour.

Fishing fuel consumption is $af\eta\kappa A_i$ while the traveling fuel consumption is $bfd_{ij}x_{ij}$ is . Choose $a = 0.001$ so that $a \times \eta = 1$. A_i is the fishing hour, then $f \times \kappa$ is the fuel consumption per fishing hour. $d_{ij}x_{ij}$ is the traveling distance while b is $\frac{1}{\text{speed}}$, so $bd_{ij}x_{ij}$ is the travel hour. f is the fuel consumption per traveling hour. κ can be interpreted as scaling parameter for fuel consumption per fishing hour.

- $\kappa = 2$, fishing fuel consumption is twice of traveling fuel consumption per hour.
- $\kappa = 1$, fishing fuel consumption is the same as traveling fuel consumption per hour.
- $\kappa = 0.5$, fishing fuel consumption is half of traveling fuel consumption per hour.

So the Lagrange can be rewritten as

(H.9)
$$
\begin{aligned}
\mathcal{L}(x_{ij}, y_i, A_i, \lambda) = \quad & \sum_{i \in N}(pqA_i^\gamma \eta^\gamma \kappa^\gamma \text{Stock}_i y_i - afc_{fuel}A_i \eta \kappa) - \sum_{(i,j) \in E} d_{ij}x_{ij}bfc_{fuel} \\
& - \lambda_{fuel}(\sum_{(i,j) \in E} d_{ij}x_{ij}bf + \sum_{(i) \in N} A_i \eta \kappa af - F_{max}) \\
& - \lambda_{hold}(\sum_{i \in N} qA_i^\gamma \eta^\gamma \kappa^\gamma \text{Stock}_i y_i - C_{max})
\end{aligned}
$$

The first order condition of fishing effort at each site is

(H.10)
$$
\begin{aligned}
\frac{\partial \mathcal{L}}{\partial A_i} &= pq\text{Stock}_i y_i \gamma A_i^{\gamma-1} \eta^\gamma \kappa^\gamma - af\eta\kappa c_{fuel} - \lambda_{fuel}af\eta\kappa - \lambda_{hold}q\text{Stock}_i y_i \gamma A_i^{\gamma-1} \eta^\gamma \kappa^\gamma \\
&= (p - \lambda_{hold})q\text{Stock}_i y_i \gamma A_i^{\gamma-1} \eta^\gamma \kappa^\gamma - (c_{fuel} + \lambda_{fuel})af\eta\kappa \\
\Rightarrow A_i^* &= \left(\frac{(p-\lambda_{hold})q\text{Stock}_i y_i \gamma \eta^\gamma \kappa^\gamma}{(c_{fuel}+\lambda_{fuel})af\eta\kappa}\right)^{\frac{1}{1-\gamma}}
\end{aligned}
$$

The moment condition can be rewritten as

(H.11)
$$
\left(\frac{p-\lambda_{fuel}}{c_{fuel}+\lambda_{fuel}}\right)q_{vt}\text{Stock}_{ivt} y_{ivt} \gamma \text{Effort}_{ivt}^{\gamma-1} \eta^\gamma \kappa^\gamma = af\eta\kappa
$$

Timing of m-site ahead partially myopic fisher

Decision point t	Current Site	Choice set with order	Fuel Constraint	Capacity Constraint
t=1	$n_1^0 = 1$, port	$n_1^1, n_2^1, \cdots, n_m^1$, port	$F_{max}^1 = F_{max}$	$C_{max}^1 = C_{max}$
t=2	n_1^1	$n_1^2, n_2^2, \cdots, n_m^2$, port	$F_{max}^2 = F_{max}^1 - d_{1n_1^1}bf - A_{n_1^1}af$	$C_{max}^2 = C_{max}^1 - qStock_{n_1^1}A_{n_1^1}^\gamma$
t=3	n_1^2	$n_1^3, n_2^3, \cdots, n_m^3$, port	$F_{max}^3 = F_{max}^2 - d_{n_1^1 n_1^2}bf - A_{n_1^2}af$	$C_{max}^3 = C_{max}^2 - qStock_{n_1^2}A_{n_1^2}^\gamma$
t+1	n_1^t	$n_1^{t+1}, n_2^{t+1}, \cdots, n_m^{t+1} = $ port	$F_{max}^{t+1} = F_{max}^t - d_{n_1^{t-1}n_1^t}bf - A_{n_1^t}af$	$C_{max}^{t+1} = C_{max}^t - qStock_{n_1^t}A_{n_1^t}^\gamma$
t=T	n_1^{T-1}	$n_1^T = $ port	$F_{max}^T = F_{max}^{T-1} - d_{n_1^{T-2}n_1^{T-1}}bf - A_{n_1^{T-1}}af$	$C_{max}^T = C_{max}^{T-1} - qStock_{n_1^{T-1}}A_{n_1^{T-1}}^\gamma$

TABLE I.1. Timing of m-site ahead partially myopic fisher

Testing for point-identification in sign restricted SVARs

3.1. Introduction

We consider the problem of identification of impulse response functions in the prominent time series dynamic model, structural vector autoregressions (SVAR) using sign restrictions[1] . The model appears naturally in several areas of economics, but especially as linearized versions of dynamic stochastic general equilibrium models (DSGE) in macroeconomics and as models for asset prices in finance (Kilian (2013); Stock and Watson (2005)). In the SVAR framework, the object of interest for empirical macroeconomists is usually impulse response functions (IRF) of macroeconomic variables to structural shocks. For example, one can evaluate the impact of a shock in monetary policy on output using these models. Without any additional restrictions on the IRF it is impossible to decompose the estimated reduced form shocks into the set of the shocks implied by economic theory. The standard way to achieve this aim, *the recursive approach,* described in Kilian (2013), is to impose a finite number of zero restrictions on IRF motivated by underlying structural models. Zero restrictions do identify IRF in SVAR , but they are sometimes hard to justify from the viewpoint of economic theory. Sign restrictions, as proposed by Canova and De Nicolo (2002); Faust (1998); Uhlig (2005), are easier to justify using calibrated DSGE models (Canova and Paustian (2011); Paustian (2007)).

Generically, a finite number of sign restrictions provides only set identification of the IRF and requires special treatment (Fry and Pagan (2011); Gafarov et al. (2018a); Granziera et al. (2018)). These methods require the identified set to be non-singleton. According to practitioners (Canova (2011)), sign restrictions can produce a very narrow set of structural shocks. Paustian (2007) executes a Monte Carlo experiment with some popular DSGE models to show that the set of parameter values in SVAR models consistent with a sufficiently large number of sign restrictions motivated by these models is tight and can, effectively, be considered as a point. This result, however, lacks formal conditions for point identification in SVAR models with sign restrictions. We contribute to the literature in two ways.

First, we establish necessary and sufficient conditions for point identification using only sign restrictions. It turns out that a unique solution to the identification problem with sign restrictions will exist only if the set of the sign restrictions has a subset with a number of restrictions that are binding, i.e. the inequality restrictions become

---

[1]This chapter builds upon and extends Gafarov (2014).

equalities. The results complement results of Moon et al. (2011) by demonstrating that sign restrictions can uniquely identify SVARs and results of Rubio-Ramirez et al. (2010) on conditions for point identification in SVARs based on exclusion restrictions by considering conditions for point identification in case of sign restrictions.

Second, we provide a novel test of the positive linear dependence of the sign-restricted IRF coefficients, the main necessary condition of point identification. The test statistics resembles the J-statistics in generalized method of moments (GMM) in accounting for redundant sign restrictions. We also propose a consistent estimator of the optimal weighing matrix based on a regularization procedure to allow for the case when the linear dependence relationship between the gradients of the sign restrictions is not uniquely defined. The test uses critical values for the standard chi-squared distribution with one degree of freedom. We show using simulations that the test controls the size well and has high power against local alternative data generating processes with partial identification.

The structure of the rest of the chapter is as follows. Section 3.2 describes the framework and contains the main result about necessary and sufficient condition for point identification of the impulse response functions. Section 3.3 describes test conditions for point identification by sign restrictions, the Monte Carlo simulation designs and results. The last section concludes.

3.2. Model framework

Suppose that a stationary VAR $X_t \in \mathbb{R}^d$ can be represented as a *vector moving average* (VMA) process,

$$(3.1) \qquad X_t = \varepsilon_t + C_1\varepsilon_{t-1} + C_2\varepsilon_{t-2} + ... = C(L)\varepsilon_t,$$

where ε_t is a one-step ahead forecast error, i.e. $\varepsilon_t \overset{\Delta}{=} X_t - E(X_t|X_{t-1}, X_{t-2}, ...)$, with variance Σ_ε; The matrix lag polynomial $C(L)$ is called a matrix of *impulse response functions* (IRF), i.e . element (i, j) of a sequence of matrices $\{C_\ell\}_{\ell=1}^\infty$ corresponds to impulse response function of the time series x_{it} to the reduced form shock ε_{jt}. Representation (3.1) is valid, in particular, for *stationary vector autoregression* (VAR) models that are often used in empirical applications. It is commonly assumed that the forecast errors ε_t are linear transformations of so-called structural shock vector $\eta_t \in \mathbb{R}^d$,

$$(3.2) \qquad \varepsilon_t = B\eta_t.$$

It's further assumed that structural shocks are zero mean i.i.d. r.v and $\text{Cov}(\eta_t) = I_d$, where I_d is a $d \times d$ identity matrix. Following Faust (1998), we can represent B as

$$(3.3) \qquad B = \text{Chol}(\Sigma_\varepsilon)R,$$

where $\mathrm{Chol}(\Sigma_\varepsilon)$ is the Cholesky decomposition of Σ_ε and R is a $d \times d$ orthogonal matrix, i.e. $R'R = I_d$. A common practice is to impose zero and sign restrictions on components of $C(L)\mathrm{Chol}(\Sigma_\varepsilon)R$. The last column of R, θ, then has an interpretation of contemporaneous impact of $\eta_{t,d}$, the last component of the structural shock vector, on X_t. In other words,

$$(3.4) \qquad \theta \triangleq E(X_t | \eta_{t,d} = 1) - E(X_t | \eta_{t,d} = 0).$$

To interpret the structural shock $\eta_{t,d}$ as meaningful economic shock, like a demand or supply shock, we need to impose certain restrictions on components of impacts of $\eta_{t-j,d}$ on X_t for integer $j \geq 0$. Typically, we can assume that components of $A'\theta$, where A is a matrix containing finitely many linear combinations of rows from $C(L)\mathrm{Chol}(\Sigma_\varepsilon)$ multiplied by 1 or -1, are non-negative. In other words, θ satisfies system (3.5). If such θ is unique, we say that the impact of the structural shock $\eta_{t,d}$ is point-identified. Alternatively, it is possible that (3.5) has multiple solutions Θ (partially identified θ) or no solutions (a contradictory identifying assumptions or a misspecified model). $\qquad \square$

$$(3.5) \qquad A'\theta \geq 0$$

Although, methods for robust inference on solutions to a system of moment equalities and inequalities are available, it is conceptually important to distinguish between the three alternatives.

When the model is correctly specified, the existing partial identification methods like Gafarov et al. (2018b); Granziera et al. (2018) are only valid if the set of solutions to (3.5) is non-singleton. Thus it is important to test whether solution to (3.5) is not unique to guarantee validity of the existing methods. Moreover, either of the two procedures are not defined when an estimated version of (3.5) is empty. This situation can occur with positive probability even if θ is partially identified.

There are other more recent methods (Andrews and Kwon (2019)) that can perform valid inference on (pseudo-)parameters in a possibly point-identified or misspecified model. However, pseudo-parameters only have economic interpretation if the model is in fact correctly specified. So it is important to distinguish between misspecification and point identification. Finally, if θ is in fact point-identified, one does not need to perform a grid search and test inversion to obtain a consistent estimator of θ.

In the next section, we propose a criterion for point identification of θ.

3.2.1. Necessary and sufficient Conditions for Point Identification. In this section we are proposing conditions for unique solution of (3.5). It is illustrative to consider two dimensional example first.

EXAMPLE 1. *Suppose that $d = 2$ and $k = 3$. In this two-dimensional case, we can represent the set of possible values of θ on a unit circle. The inequalities in (3.5) correspond to half-planes with normal vectors $\{a_1, a_2, a_3\}$, the columns of A. The intersection of the half-spaces define the identified set Θ, which is shown as a red segment on the unit circle. It is instructive to study behavior of the identified set as we change one of the vectors, a_3. Figures below show three possible representative cases.*

$$A_{d \times k} = \begin{pmatrix} a_1 & a_2 & a_3 \end{pmatrix}, \text{ where } a_i = \begin{pmatrix} a_{i1} \\ a_{i2} \end{pmatrix}, \text{ the system is } A'\theta \geq 0, \ \theta_{d \times 1} = \begin{pmatrix} \theta_1 \\ \theta_2 \end{pmatrix}.$$

One can see, that the segment Θ collapses into a point when a_3 becomes collinear and directed in the opposite side with one of the other two vectors, i.e. $a_2'a_3 < 0$. Indeed, in that case $a_3 = -a_2$ so the last two inequalities of (3.5) represent an equality constraint $a_2'\theta = 0$ that defines two points on the unit circle. Only one of them satisfies $a_1'\theta \geq 0$, which makes Θ a singleton set. Thus a unique solution can only occur if there are at least three inequality constraints in (3.5).

An empty set Θ, Fig 3.2, occurs when the cone generated by vectors (a_1, a_2, a_3) is the whole plane. Indeed, in that case, $a_3 = -(\lambda_1 a_1 + \lambda_2 a_2)$ for some $\lambda_i > 0$, $i = 1, 2$. So the first two inequalities imply

(3.6)
$$\begin{aligned} a_1'\theta \geq \quad 0 \\ a_2'\theta \geq \quad 0 \end{aligned} \quad \Rightarrow \quad (\lambda_1 a_1 + \lambda_2 a_2)'\theta \geq 0$$
$$\Rightarrow a_3'\theta = \quad -(\lambda_1 a_1 + \lambda_2 a_2)'\theta \leq 0$$

which together with the last inequality $a_3'\theta \geq 0$ results in a restriction $a_3'\theta = 0$.

Both solutions to $a_3'\theta = 0$ violate at least one of the first two inequalities from (3.5). For example, suppose that $(a_{11}a_{22} - a_{12}a_{21}) > 0$, then a solution $\theta^* = (-a_{32}, a_{31})'^2$, would violate $a_2'\theta \geq 0$. See details in Appendix J.1. Indeed,

(3.7)
$$a_2'\theta^* = a_{21}(\lambda_1 a_{12} + \lambda_2 a_{22}) - a_{22}(\lambda_1 a_{11} + \lambda_2 a_{21}) = -\lambda_1(a_{11}a_{22} - a_{12}a_{21}) < 0.$$

The other solution, $\theta^* = (a_{32}, -a_{31})$ would in turn violate $a_1'\theta \geq 0$, as can be checked by direct computation. Thus an empty set Θ also can only occur if there are at least three inequality constraints in (3.5).

When (3.5) is neither point identified nor misspecified, Θ represents a non-degenerate segment of the unit circle as shown on Fig. 3.3.

□

---

[2]Because $a_3 = -(\lambda_1 a_1 + \lambda_2 a_2) = -\begin{pmatrix} \lambda_1 a_{11} + \lambda_2 a_{21} \\ \lambda_1 a_{12} + \lambda_2 a_{22} \end{pmatrix}$, $\theta^* = (-a_{32}, a_{31})' = \begin{pmatrix} \lambda_1 a_{12} + \lambda_2 a_{22} \\ -(\lambda_1 a_{11} + \lambda_2 a_{21}) \end{pmatrix}$.
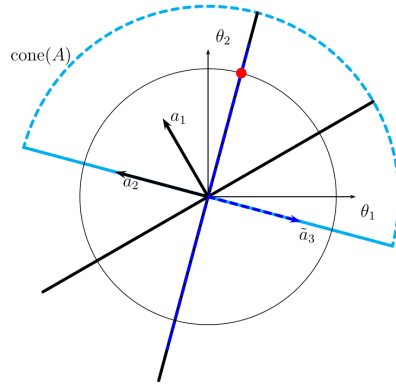
FIGURE 3.1. The point-identified case. The red dot represents the signleton Θ. Note that $a_3 = -a_2$.
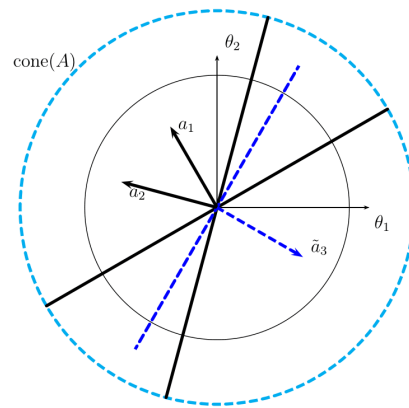

FIGURE 3.2. The misspecified model case. The set Θ is empty. Note that $cone(A) = \mathbb{R}^2$.
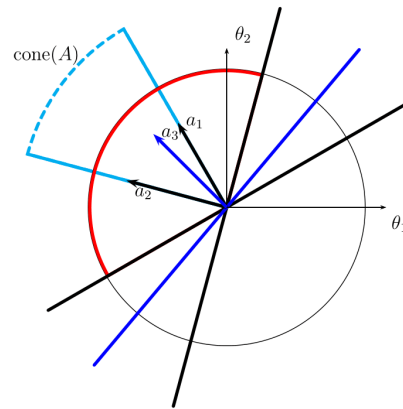

FIGURE 3.3. The set-identified case. The red arc corresponds to the set Θ.

Conditions for point identification in Example 1 can be generalized the case with arbitrary many inequalities for any finite dimensional θ, as the following theorem shows.

THEOREM 1. *System (3.5) has a unique solution with* $\|\theta\| = 1$ *iff the following conditions hold,*

(1) *There exist a vector* $\lambda \in \mathbb{R}_+^k$ *such* $A\lambda = 0$ *and columns of A, corresponding to positive components of* λ, *have rank* $d - 1$.

(2) *System (3.5) has a non-zero solution.*

(3) *Matrix A has full rank.*

PROOF. See Appendix. □

The proof of this theorem is an application of the convex cones theory which connects solutions of system (3.5) with the properties of its coefficients. In particular, the solutions constitute a convex cone which is dual to the cone generated by the coefficients of the system. Conditions 1-3 holds iff the cone of the coefficients, *cone*(A), is an entire half-space, an thus its dual defines a unique solution of (3.5) up to scale normalization (see Lemma 3 in Appendix J.2 for details).

All three conditions of the theorem can be tested using existing statistical tests. At the same time, a joint test of too many conditions may have low power against some generic alternatives. Namely, it is reasonable to expect that matrix A will typically have full rank if the number of inequalities is at least $d + 1$.

3.2.2. Testable condition. The first part of Condition 1 in Theorem 1 states that columns of A are positively linearly dependent (PLD), i.e. there exists a non-zero vector $\lambda \in \mathbb{R}_+^k$ such that $A\lambda = 0$. We can represent this condition in a optimization form that is convenient for testing.

Let $\iota \triangleq (1, ..., 1)$ and let W be a positive definite $d \times d$ matrix.

LEMMA 1. *PLD condition equivalent to* $\mathscr{J} > 0$, *where*

$$\mathscr{J} \triangleq \min_{\lambda \in \mathbb{R}_+^k} \quad \lambda' A' W A \lambda$$

(3.8)

$$s.t. \quad \iota\lambda = 1.$$

PROOF. The result then follows immediately from $\mathscr{J} = \|W^{\frac{1}{2}} A \lambda\|_2$ and the properties of the norm. □

Note that without the normalization $\iota\lambda = 1$, the minimum is always zero. This particular choice makes the optimisation problem quadratic.

In the next section we provide a statistical test of point-identification that is based on a subset of these three conditions.

3.3. Simple test for positive linear dependence

As shown in the previous section, one can test point identification of solutions to linear inequalities using the PLD condition. However, the matrix A, which enters the PLD condition, is unknown in practice. Instead, it can be estimated consistently using a sample analog. The estimator then would enable a statistical test of the hypothesis in Lemma 1 based on a statistic:

$$\hat{\mathscr{J}}_n \triangleq \min_{\lambda \in \mathbb{R}^k} \quad n(\lambda' \hat{A}'_n) W(\hat{A}_n \lambda)$$
(3.9)
$$\text{s.t.} \quad \lambda \geq \quad 0,$$
$$\iota \lambda = \quad 1.$$

Despite the fact that test statistics of similar structure have been extensively studied in the literature, to our knowledge, $\hat{J}_n$ does not fit the existing frameworks. In this section, we provide a novel testing framework that accommodates tests based on $\hat{J}_n$ as well as a number of other tests.

3.3.1. The hypothesis, the corresponding statistic and examples. Consider the following hypothesis of positive linear dependence,

(3.10)
$$H_0 : \exists \lambda \text{ s.t. } A\lambda = 0 \text{ and } C\lambda \leq d.$$

The PLD condition corresponds to the case $C = (-I_k, \iota, -\iota)$, $d = (0_k, 1, -1)$. Suppose that matrix (A) is unknown but admits of an asymptotically normal estimator $\hat{A}_n$ [3]. Then hypothesis of PLD in (3.10) can be tested using a statistic

(3.11)
$$\hat{\mathscr{J}}_n \triangleq \min_{\lambda \in \mathbb{R}^k} \quad n(\lambda' \hat{A}'_n) \hat{W}(\hat{A}_n \lambda)$$
$$\text{s.t.} \quad C\lambda \leq d.$$

This statistic can be used for consistent testing of H_0. Under H_0, $\hat{\mathscr{J}}_n$ is be bounded in probability. If H_0 is violated, $\hat{\mathscr{J}}_n$ would diverge to infinity as the sample size n grows.

ASSUMPTION 1. *The estimator $\hat{A}_n$ satisfies*

(3.12)
$$\sqrt{n}(\hat{A}_n - A) \xrightarrow{d} N(0, \Omega),$$

---

[3]One can allow for inequalities with unknown coefficients by introducing slack variables; equalities with known coefficients correspond to a pair of inequalities.

where Ω is a covariance matrix and (A) denotes the vectorization operator.

This assumption is trivially satisfied for an linear moment inequality model under conditions of some central limit theorem. In the SVAR application, one can obtain such estimator $\hat{A}_n$ using local projection of Jordà (2005) or VAR-IRF estimators. Matrix Ω can be consistently estimated using HAC estimators or block bootstrap. To simplify exposition, we will assume that Ω is know in the rest of the chapter.

Testing algorithm

Step 1. Compute $\hat{\lambda}^\mu$ as a solution to

$$\hat{\lambda}^\mu = \arg\min_{\lambda} \quad n(\hat{A}_n\lambda)'(\hat{A}_n\lambda) + \mu \|\lambda\|_2^2$$
$$\text{s.t.} \quad \lambda \geq 0$$
(3.13)
$$\iota'\lambda = 1$$
$$\mu = \frac{logn}{\sqrt{n}}$$
$$\hat{A}_n = A + \frac{\Sigma_n z_i}{n}, z_i \sim N(0,\sigma^2 I).$$

Step 2. Estimate $\hat{W}$ using $\hat{\lambda}^\mu$.

$$\hat{W} = c\hat{o}v(\hat{A}_n\hat{\lambda}^\mu)^{-1}.$$

Step 3. Compute the test statistic $\hat{\mathscr{J}}_n$.

$$\hat{\mathscr{J}}_n \triangleq \min_{\lambda \in \mathbb{R}^k} \quad n(\lambda'\hat{A}_n')\hat{W}(\hat{A}_n\lambda)$$
$$\text{s.t.} \quad \lambda_i \geq 0$$
(3.14)
$$\iota\lambda = 1$$
$$\hat{A}_n = A + \frac{\Sigma_n z_i}{n}, z_i \sim N(0,\sigma^2 I).$$

Step 4. Compare $\hat{\mathscr{J}}_n$ to critical values of $\chi^2(1)$ distribution. Reject H_0 (PLD) if $\hat{\mathscr{J}}_n > \chi^2_\alpha(1)$

Next, we use the 2-d example to illustrate the test.

EXAMPLE 2 (2 inequality restricitons). *Consider*

(3.15)
$$A = \begin{pmatrix} a_1 & a_2 \end{pmatrix} = \begin{pmatrix} a_{11} & a_{21} \\ a_{12} & a_{22} \end{pmatrix} = \begin{pmatrix} 1 & -1 \\ 0 & \varepsilon_p \end{pmatrix}$$

75

$H_0 : A\lambda = 0$ corresponds to the case $\varepsilon_p = 0$. We have the following moment conditions:

$$(3.16) \qquad\qquad E(\hat{a}_1 \lambda_1 + (1 - \lambda_1)\hat{a}_2) = 0$$

Because $\lambda_1 + \lambda_2 = 1$, $\lambda_2 = 1 - \lambda_1$. So we have two moment conditions $(dim(a_i) = 2)$. Then the test statistics takes form

$$(3.17) \qquad\qquad \hat{\mathscr{J}}_n = (\hat{a}_1 \hat{\lambda}_1 + (1 - \hat{\lambda}_1)\hat{a}_2)' \hat{W} (\hat{a}_1 \hat{\lambda}_1 + (1 - \hat{\lambda}_1)\hat{a}_2) \sim \chi^2(1),$$

where the limiting distribution follows from the standard asymptotics of GMM estimator of λ_1 corresponding to moment conditions (3.16). $\square$

The following theorem proves consistency of the proposed test in the general case .

THEOREM 2. *Suppose $\mu_n \to 0$, Assumption 1 holds, then*

$$(3.18) \qquad\qquad \lim_{n \to \infty} P\{\hat{\mathscr{J}}_n \leq \chi^2_\alpha(1)|H_0\} \geq 1 - \alpha$$

PROOF. See Appendix. $\qquad\qquad\qquad\qquad\qquad\qquad\qquad\qquad\qquad\qquad\qquad\qquad\qquad\square$

3.3.2. Monte Carlo designs. We next show the performance of the PLD test in a Monte Carlo study. Now consider the design

$$(3.19) \qquad A = \begin{pmatrix} a_1 & a_2 & a_3 & a_4 \end{pmatrix} = \begin{pmatrix} a_{11} & a_{21} & a_{31} & a_{41} \\ a_{12} & a_{22} & a_{32} & a_{42} \end{pmatrix} = \begin{pmatrix} 1 & -1 & 0 & 1 \\ 0 & \varepsilon_p & 1 & \varepsilon_s \end{pmatrix}.$$

ε_p distinguishes H_0 and H_a, while ε_s determines whether the positive linear dependence relationship, ie λ, is unique or not. If $\varepsilon_p > 0$, Θ is not point identified, $H_0 : A\lambda = 0$ does not hold. If $\varepsilon_s > 0$, there is unique solution for $\hat{\lambda}$. With $\varepsilon_s = 0$, there exists multiple solutions for $\hat{\lambda}$. When $\varepsilon_s < 0$, the model is misspecified.

We consider the following three cases:

(1) $A = \begin{pmatrix} a_1 & a_2 \end{pmatrix}$. If $\varepsilon_p = 0$, $A\lambda = 0$ suggests that $\lambda = \begin{pmatrix} 0.5 & 0.5 \end{pmatrix}'$. If $\varepsilon_p > 0$, H_0 no longer holds.

(2) $A = \begin{pmatrix} a_1 & a_2 & a_3 \end{pmatrix}$. If $\varepsilon_p = 0$, $A\lambda = 0$ suggests that $\lambda = \begin{pmatrix} 0.5 & 0.5 & 0 \end{pmatrix}'$. If $\varepsilon_p > 0$, H_0 no longer holds.

(3) $A = \begin{pmatrix} a_1 & a_2 & a_3 & a_4 \end{pmatrix}$. If $\varepsilon_p = 0$ and $\varepsilon_s = 0$, $A\lambda = 0$ holds and $\lambda = \begin{pmatrix} \alpha\frac{1}{\sqrt{2}} & \frac{1}{\sqrt{2}} & 0 & (1-\alpha)\frac{1}{\sqrt{2}} \end{pmatrix}', \forall \alpha$.
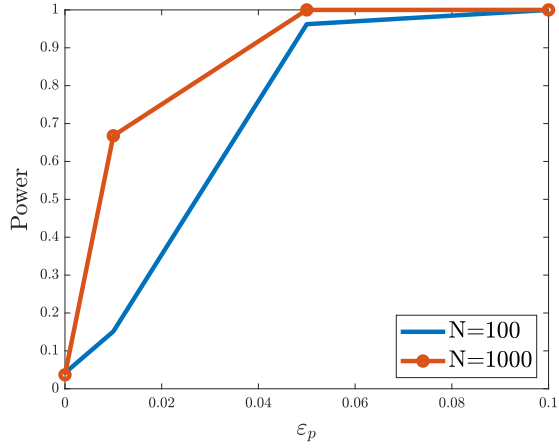
There are multiple solutions of $\hat{\lambda}$. If $\varepsilon_s > 0$, there is a unique λ. If $\varepsilon_p > 0$, H_0 no longer holds.

76

We consider $\varepsilon_p = \varepsilon_s = [0.01, 0.05, 0.1, 0.2, 0.3, 0.4, 0.5, 1]$. We generate 10,000 draws of $\hat{A}_n = A_{d \times k} + \frac{\sum_n z_i}{n}$, $z_i \sim N(\mathbf{0}_{d \times k}, \sigma^2 \mathbf{I}_{k \times k})$ for sample size of $n \in \{100, 1000\}$, and $\sigma = 0.1$. For each draw of $\hat{A}_n$, we compute $\hat{\lambda}^\mu$ by (3.13), and weighting matrix $\hat{W} = cov((A + z_i)\hat{\lambda}^\mu)$, $i = 1, \ldots, n$. Finally we compute the test statistics $\hat{\mathscr{J}}_n$ by (3.14). We compare the test statistics $\hat{\mathscr{J}}_n$ with $\chi^2(1)$. Then we count the rejection rate for the M=10000 Monte Carlo simulations. We compute power curves along the value of ε_p. The normal size of the test is $\alpha = 0.05$.

3.3.2.1. *Results.* Results are displayed in Figure 3.4 with the case of regularization $\mu = \frac{logN}{\sqrt{N}}$ (left column) and non-regularization $\mu = 0$ (right column)[4]. Full plot (Figure K.1) and detailed rejection rate tables (Table K.1 and K.2) are in Appendix K. The simulations indicate good size control and high power against alternative data generating process with partial identification of the test. For Case 1 and Case 2, we see the power goes to 1 when ε_p deviates from zero. Power improves with sample size (compare the $N = 100$ line and $N = 1000$ line) and regularization using $\mu = \frac{logN}{\sqrt{N}}$ (compare the left column figures and the right column figures).

For Case 3 (Figure 3.4e), given ε_s, power goes to one when ε_p deviates from zero. We can see from the figure that power improves with sample size : $N = 1000$ surface is more close to 0 compared to the $N = 100$ surface. Appendix Table K.2 shows that given $\varepsilon_p = 0$, if $\varepsilon_s = 0$, we can see a low rejection rate (size). But once $\varepsilon_s > 0$, we see the rejection rate (size) is around 5%.

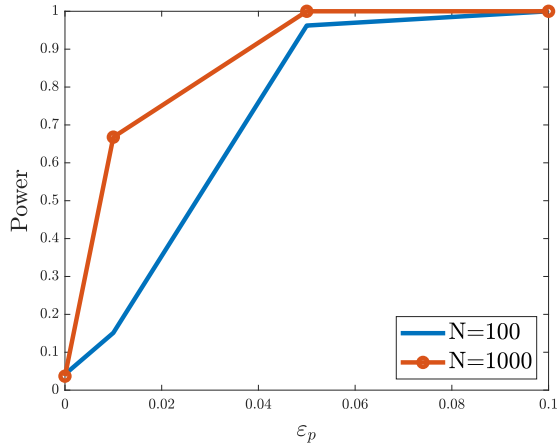[4]Figure 3.4 include results with $\varepsilon_p \leq 0.1$ to show power improvement because the rejection rate with $\varepsilon_p \geq 0.1$ equals to 1.
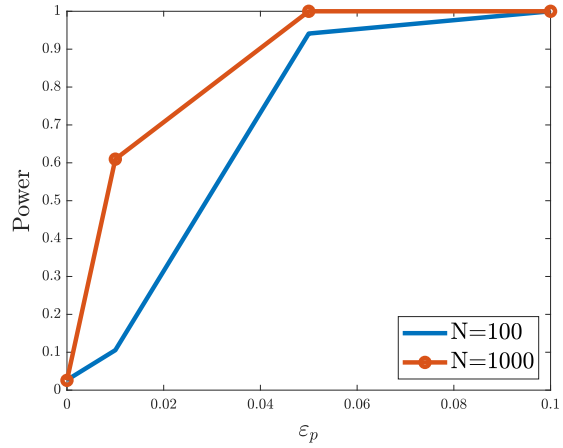
(a) $A = (a_1, a_2)$, $\mu = \frac{logN}{\sqrt{N}}$

(b) $\mu = 0$

(c) $A = (a_1, a_2, a_3)$, $\mu = \frac{logN}{\sqrt{N}}$

(d) $\mu = 0$
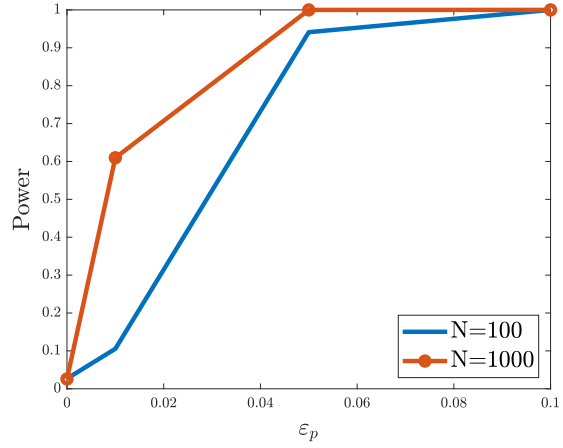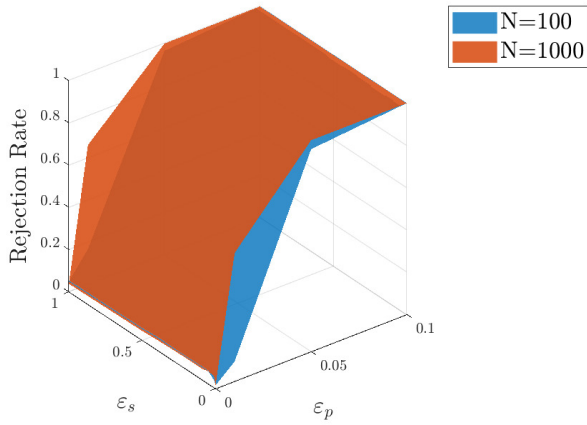
(e) $A = (a_1, a_2, a_3, a_4)$, $\mu = \frac{logN}{\sqrt{N}}$
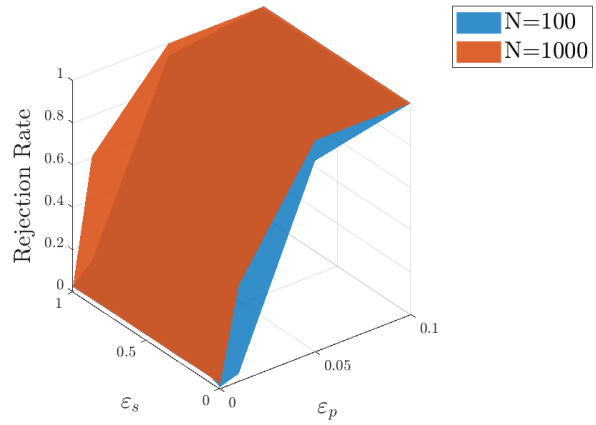
(f) $\mu = 0$

FIGURE 3.4. Rejection rate plot with $\varepsilon_p \leq 0.1$

3.4. Conclusion

In this chapter we provide the necessary and sufficient conditions for point identification of impulse response functions in the SVAR using sign restrictions. One might use this approach in cases when a justifiable set exclusion restrictions cannot be proposed based on theory while a large set of sign restrictions can be justified. We provide a novel test for the positive linear dependence of the vectors of sign-restricted IRF coefficients with standard chi-squared critical values. Simulation results shows that the proposed test has high power against the alternative data generating process with partial identification.

Proofs

J.1. Proof of Example 2

$$a_3 = \begin{pmatrix} a_{31} \\ a_{32} \end{pmatrix} = -(\lambda_1 a_1 + \lambda_2 a_2)$$

(J.1)

$$a_{31} = -(\lambda_1 a_{11} + \lambda_2 a_{21})$$

$$a_{32} = -(\lambda_1 a_{12} + \lambda_2 a_{22})$$

Solution to $a_3' \theta = 0$ is $\theta^* = \begin{pmatrix} -a_{32} \\ a_{31} \end{pmatrix}$ or $\theta^* = \begin{pmatrix} a_{32} \\ -a_{31} \end{pmatrix}$.

Suppose $a_{11}a_{22} - a_{12}a_{21} > 0$, when $\theta^* = \begin{pmatrix} -a_{32} \\ a_{31} \end{pmatrix}$, $a_2'\theta \geq 0$ is violated.

$$a_2'\theta^* = \begin{pmatrix} a_{21} & a_{22} \end{pmatrix} \begin{pmatrix} -a_{32} \\ a_{31} \end{pmatrix}$$

$$= -a_{21}a_{32} + a_{22}a_{31}$$

(J.2)

$$= a_{21}(\lambda_1 a_{12} + \lambda_2 a_{22}) - a_{22}(\lambda_1 a_{11} + \lambda_2 a_{21})$$

$$= \lambda_1 a_{12}a_{21} + \lambda_2 a_{22}a_{21} - \lambda_1 a_{11}a_{22} - \lambda_2 a_{21}a_{22}$$

$$= \lambda_1 a_{12}a_{21} - \lambda_1 a_{11}a_{22}$$

$$= -\lambda_1(a_{11}a_{22} - a_{12}a_{21}) < 0$$

Similarly, when when $\theta^* = \begin{pmatrix} a_{32} \\ -a_{31} \end{pmatrix}$, $a_1'\theta \geq 0$ is violated.

$$
\begin{aligned}
a_1'\theta^* &= \begin{pmatrix} a_{11} & a_{12} \end{pmatrix} \begin{pmatrix} a_{32} \\ -a_{31} \end{pmatrix} \\
&= a_{11}a_{32} - a_{12}a_{31} \\
&= -a_{11}(\lambda_1 a_{12} + \lambda_2 a_{22}) + a_{12}(\lambda_1 a_{11} + \lambda_2 a_{21}) \\
&= -\lambda_1 a_{12}a_{11} - \lambda_2 a_{22}a_{11} + \lambda_1 a_{11}a_{12} + \lambda_2 a_{21}a_{12} \\
&= -\lambda_2 a_{11}a_{22} + \lambda_2 a_{12}a_{21} \\
&= -\lambda_2(a_{11}a_{22} - a_{12}a_{21}) < 0
\end{aligned}
$$

(J.3)

J.2. Proofs for the condition for the point identification

The existence of non-zero solutions to (3.5) is characterized by Gordan's theorem (see Theorem 5 in Ben-Israel (2002)). For our purposes, we would like to restate this theorem in a geometric terms. First, introduce a conic hull of A is as

$$
\text{cone}(A) \triangleq \left\{ \sum_{i=1}^{k} \lambda_i a_i \,\middle|\, \lambda \in \mathbb{R}_+^k \right\}
$$

The following lemma is a geometric version of the Gordan's theorem.

LEMMA 2. *System (3.5) does not have a non-zero solution iff $\text{cone}(A) = \mathbb{R}^d$.*

PROOF. Solutions to (3.5) constitute a cone K. The corresponding dual cone $K^* = \text{cone}(A)$. For a d-dimensional cone $K = \{0_d\}$ iff the dual cone is the full space, $K^* = R^d$ (see sections 2.13.1.1 and E.9.2.1 in Dattorro (2019)). So the result follows immediately from this property of the dual cones. □

The following lemma provides a criterion for point-identification of θ in geometric terms.

LEMMA 3. Θ *is a singleton iff $\text{cone}(A)$ is a half-space.*

PROOF. First notice that Θ is a singleton iff the cone $K = \text{cone}(\Theta)$ is a half-line, $\{xb | x \in \mathbb{R}_+\}$ for some $b \in \mathbb{R}^d$. Dual to $\{xb | x \in \mathbb{R}_+\}$ is a half-space. Indeed, by definition of a dual cone

(J.4)
$$
\{xb | x \in \mathbb{R}_+\}^* = \{y \in \mathbb{R}^d | y'b \geq 0\}.
$$

So the statement of the lemma follows immediately, since $\text{cone}(A)$ is dual for $\text{cone}(\Theta)$. □

81

Now we can proceed to the proof of the main identification result.

PROOF OF THEOREM 1. We only need to verify that conditions 1-3 are equivalent to the criterion of Lemma 3.

Sufficiency.

Suppose that conditions 1 and 2 hold. Without loss of generality, assume that vectors a_i with $i = 1, \ldots, q$ satisfy condition 1. Since $(a_1, \ldots, a_q)$ has rank $d - 1$, their linear subspace $\text{lin}\{a_1, \ldots, a_q\} = \mathbb{R}^{d-1}$. Take any vector b from $\text{lin}\{a_1, \ldots, a_q\}$, i.e.

$$(J.5) \qquad b = \sum_{j=1}^{q} \mu_j a_j,$$

for some $\mu \in \mathbb{R}^q$. Let J^- the set of all $j = 1, \ldots, q$ such that $\mu_j < 0$, and J^+ being it's complement, $J^+ = \{1, \ldots, q\} \setminus J^-$. Suppose that set J^- is non-empty and $\mu_j < 0$ for some j. By condition 1, for any $j = 1, \ldots, q$

$$(J.6) \qquad a_j = -\frac{1}{\lambda_j} \left(\sum_{i=1, i \neq j}^{q} \lambda_i a_i \right).$$

Then $b \in \text{cone}\{a_1, \ldots, a_q\}$ since b can be represented as a positive linear combination of $\{a_1, \ldots, a_q\}$.

$$(J.7) \qquad b = \sum_{j \in J^-} \mu_j a_j + \sum_{j \in J^+} \mu_j a_j = \sum_{j \in J^-} (-\mu_j) \frac{1}{\lambda_j} \left(\sum_{i \neq j} a_i \lambda_i \right) + \sum_{j \in J^+} \mu_j a_j.$$

Since by construction $b \in \text{lin}\{a_1, \ldots, a_q\}$, equation (J.7) implies

$$(J.8) \qquad \text{cone}\{a_1, \ldots, a_q\} = \text{lin}\{a_1, \ldots, a_q\} = \mathbb{R}^{d-1}.$$

By conditions 1 and 3 there exist at least one additional row a_{q+1} in A such that $a_{q+1} \notin \text{cone}\{a_1, \ldots, a_q\}$. Then $\text{cone}(A)$, which contains $\text{cone}\{a_1, \ldots, a_q\}$, is either a half-space or $\mathbb{R}^d$. By Condition 2 and Lemma 2, $\text{cone}(A)$ is not a $\mathbb{R}^d$. So $\text{cone}(A)$ has to be a half-space, i.e. the sufficient criterion for point-identification from Lemma 3 holds.

Necessity.

Suppose $\text{cone}(A)$ is a half-space. Take any q vectors from A that generate the surface of $\text{cone}(A)$. To construct such q-vectors take any point a on the surface of $\text{cone}(A)$ which is hyperplane $\mathbb{R}^{d-1}$. By the Caratheodory theorem, such point b can be represented as a positive linear combination of d vectors $\mathscr{A}(b) \subset \{a_1, \ldots, a_k\}$. The desired q vectors are the union $\mathscr{A} \cup_{b \in \mathbb{R}^{d-1}} \mathscr{A}(b)$. By construction, $q = |\mathscr{A}| \leq k$ since $\mathscr{A} \subset \{a_1, \ldots, a_k\}$. Since those q vectors generate the surface of a half-space, which is $\mathbb{R}^{d-1}$, the rank of the matrix that corresponds to $\mathscr{A}$ is $d - 1$. So such set of vectors $\mathscr{A}$ would satisfy condition 1.

By Lemma 2, condition 2 is satisfied.

Now suppose that matrix A has a reduced rank r, i.e. $lin(A) = \mathbb{R}^r$ with $r < d$. Then $cone(A) \subset lin(A) = \mathbb{R}^r$, which is not a $d-$dimensional half-space. By contradiction, A is a full rank matrix and condition 3 holds. $\square$

J.3. Proofs of Theorem 2

LEMMA 4. *Suppose Assumption 1 holds, then $\hat{\lambda}^\mu \xrightarrow{P} \lambda^*$. λ^* is solution to*

(J.9)
$$
\begin{aligned}
\min_{\lambda} \quad & \|A\lambda\|^2 \\
s.t. \quad \lambda_i \geq \quad & 0 \\
\iota\lambda = \quad & 1.
\end{aligned}
$$

PROOF. Consistency of $\hat{\lambda}^\mu$ follows the Theorem of the Maximum (Berge, 1997; Mas-Colell et al., 1995)

Consider the program, parameterized by A and μ. Constraints are fixed and continuous in A and μ.

(J.10)
$$
\begin{aligned}
\min_{\lambda} \quad & (A\lambda)'(A\lambda) + \mu\|\lambda\|^2 \\
s.t. \quad \lambda_i \geq \quad & 0 \\
\iota\lambda = \quad & 1.
\end{aligned}
$$

Under $H_0 : A\lambda = 0$, the program is

(J.11)
$$
\begin{aligned}
\min_{\lambda} \quad & \|\lambda\|^2 \\
s.t. \quad \lambda_i \geq \quad & 0 \\
\iota\lambda = \quad & 1 \\
A\lambda = \quad & 0.
\end{aligned}
$$

$\hat{\lambda}^\mu = \arg\min \|\lambda\|^2$ satisfying all the constraints.

Under H_a, $A\lambda = 0$ no longer holds. The program is

(J.12)
$$
\begin{aligned}
\min_{\lambda} \quad & \|A\lambda\|^2 \\
s.t. \quad \lambda_i \geq \quad & 0 \\
\iota\lambda = \quad & 1.
\end{aligned}
$$

λ^* is the solution satisfying all the constraints.

By Assumption 1, $\hat{A} \xrightarrow{P} A$, so Theorem of the Maximum implies that $\hat{\lambda}^\mu \xrightarrow{P} \lambda^*$, given $\hat{\lambda}^\mu = f(\hat{A}, \mu) \to f(A, 0) = \lambda^*$ and f is continous. $\square$

PROOF OF THEOREM 2. Case 1. λ is unique. Then we will have $\lambda^* = \lambda$. The result follows from 4 and GMM theory.

Case 2, λ is not unique under H_0. Let $\hat{\mathscr{J}}_n$ denotes $\hat{\mathscr{J}}_n(\lambda^*)$ and $\hat{\mathscr{J}}_n^\mu$ denotes $\hat{\mathscr{J}}_n(\hat{\lambda}^\mu)$.

$$\hat{\mathscr{J}}_n = \min_\lambda \quad n(\hat{A}_n\lambda)'W(\lambda^*)(\hat{A}_n\lambda)$$

(J.13)
$$s.t. \quad \lambda_i \geq \quad 0$$
$$\iota\lambda = \quad 1.$$

We use regularization to find the λ with the minimized the norm.

$$\hat{\mathscr{J}}_n^\mu = \min_\lambda \quad n(\hat{A}\lambda)'W(\lambda^*)(\hat{A}\lambda) + \mu\,\|\lambda\|_2^2$$

(J.14)
$$s.t. \quad \lambda_i \geq \quad 0$$
$$\iota\lambda = \quad 1.$$

$\hat{\lambda}^\mu = \arg\min n(\hat{A}\lambda)'W(\lambda^*)(\hat{A}\lambda) + \mu\,\|\lambda\|_2^2$, subjecting to the constraints.

With extra constraints, $\hat{\mathscr{J}}_n^\mu$ is larger than $\hat{\mathscr{J}}_n$.

(J.15)
$$\hat{\mathscr{J}}_n^\mu - \mu\left\|\hat{\lambda}^\mu\right\|_2^2 = n(\hat{A}\hat{\lambda}^\mu)'W(\lambda^*)(\hat{A}\hat{\lambda}^\mu) \geq \hat{\mathscr{J}}_n.$$

(J.16)
$$\hat{\mathscr{J}}_n^\mu \to \chi^2(1) + \mu\left\|\hat{\lambda}^\mu\right\|_2^2 - \mu\left\|\hat{\lambda}^\mu\right\|_2^2 = \chi^2(1).$$

Therefore,

(J.17)
$$\lim_{n\to\infty} P\{\hat{\mathscr{J}}_n \leq \chi_\alpha^2(1)|H_0\} \geq \lim_{n\to\infty} P\{\hat{\mathscr{J}}_n^\mu \leq \chi_\alpha^2(1)|H_0\} = 1 - \alpha.$$

We have $\hat{\lambda}^\mu \xrightarrow{P} \lambda^*$, so we have $\hat{W}(\hat{\lambda}^\mu) \xrightarrow{P} W(\lambda^*)$ and $\hat{\mathscr{J}}_n^\mu \xrightarrow{d} \hat{\mathscr{J}}_n$ by Slutsky's Theorem.

$\square$

Monte Carlo results

The full plot of rejection rate of each case is in Figure K.1. The rejection rates under each case are shown in Table K.1, K.2 and K.3.

| ε_p | $Pr(\hat{\mathscr{J}}_n^{\mu} > \chi^2(1) = 3.8415)$ | | | |
| | $\mu = \frac{logN}{\sqrt{N}}$ | | $\mu = 0$ | |
	N=100	N=1000	N=100	N=1000
0	0.055	0.0486	0.0514	0.0535
0.01	0.1104	0.6093	0.114	0.6039
0.05	0.9388	1.0	0.9399	1.0
0.1	1.0	1.0	1.0	1.0
0.2	1.0	1.0	1.0	1.0
0.3	1.0	1.0	1.0	1.0
0.4	1.0	1.0	1.0	1.0
0.5	1.0	1.0	1.0	1.0
1.0	1.0	1.0	1.0	1.0

TABLE K.1. Power of PLD Test, with $A = (a_1, a_2)$

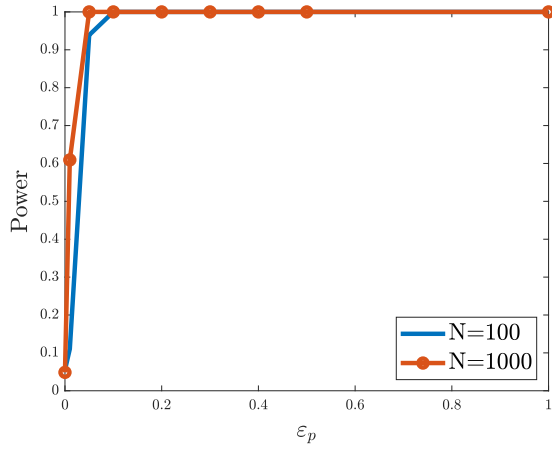| ε_p | $Pr(\hat{\mathscr{J}}_n^{\mu} > \chi^2(1) = 3.8415)$ | | | |
| | $\mu = \frac{logN}{\sqrt{N}}$ | | $\mu = 0$ | |
	N=100	N=1000	N=100	N=1000
0	0.0418	0.0369	0.0267	0.0258
0.01	0.1512	0.6678	0.1055	0.6097
0.05	0.9623	1.0	0.9412	1.0
0.1	1.0	1.0	1.0	1.0
0.2	1.0	1.0	1.0	1.0
0.3	1.0	1.0	1.0	1.0
0.4	1.0	1.0	1.0	1.0
0.5	1.0	1.0	1.0	1.0
1.0	1.0	1.0	1.0	1.0

TABLE K.2. Power of PLD Test, with $A = (a_1, a_2, a_3)$

|		$Pr(\hat{\mathscr{J}}_n^{\mu} > \chi^2(1) = 3.8415)$			
ε_s	ε_p	$\mu = \frac{logN}{\sqrt{N}}$		$\mu = 0$	
		N=100	N=1000	N=100	N=1000
0	0	0.0154	0.0132	0.0057	0.0049
0	0.01	0.0931	0.607	0.0347	0.4528
0	0.05	0.958	1.0	0.9034	1.0
0	0.1	1.0	1.0	1.0	1.0
0	0.2	1.0	1.0	1.0	1.0
0	0.3	1.0	1.0	1.0	1.0
0	0.4	1.0	1.0	1.0	1.0
0	0.5	1.0	1.0	1.0	1.0
0	1.0	1.0	1.0	1.0	1.0
0.01	0	0.0348	0.0554	0.0125	0.0251
0.01	0.01	0.1602	0.7348	0.0717	0.608
0.01	0.05	0.9767	1.0	0.9344	1.0
0.01	0.1	1.0	1.0	1.0	1.0
0.01	0.2	1.0	1.0	1.0	1.0
0.01	0.3	1.0	1.0	1.0	1.0
0.01	0.4	1.0	1.0	1.0	1.0
0.01	0.5	1.0	1.0	1.0	1.0
0.01	1.0	1.0	1.0	1.0	1.0
0.05	0	0.0601	0.058	0.0245	0.0256
0.05	0.01	0.2155	0.7295	0.1119	0.6097
0.05	0.05	0.9782	1.0	0.9383	1.0
0.05	0.1	1.0	1.0	1.0	1.0
0.05	0.2	1.0	1.0	1.0	1.0
0.05	0.3	1.0	1.0	1.0	1.0
0.05	0.4	1.0	1.0	1.0	1.0
0.05	0.5	1.0	1.0	1.0	1.0

0.05	1.0	1.0	1.0	1.0	1.0
0.1	0	0.0582	0.0511	0.0283	0.0261
0.1	0.01	0.1993	0.7334	0.1109	0.6082
0.1	0.05	0.9751	1.0	0.9363	1.0
0.1	0.1	1.0	1.0	1.0	1.0
0.1	0.2	1.0	1.0	1.0	1.0
0.1	0.3	1.0	1.0	1.0	1.0
0.1	0.4	1.0	1.0	1.0	1.0
0.1	0.5	1.0	1.0	1.0	1.0
0.1	1.0	1.0	1.0	1.0	1.0
0.2	0	0.0578	0.052	0.0265	0.0254
0.2	0.01	0.1955	0.7277	0.107	0.607
0.2	0.05	0.9786	1.0	0.9413	1.0
0.2	0.1	1.0	1.0	1.0	1.0
0.2	0.2	1.0	1.0	1.0	1.0
0.2	0.3	1.0	1.0	1.0	1.0
0.2	0.4	1.0	1.0	1.0	1.0
0.2	0.5	1.0	1.0	1.0	1.0
0.2	1.0	1.0	1.0	1.0	1.0
0.3	0	0.0574	0.0505	0.0272	0.0231
0.3	0.01	0.1969	0.714	0.1116	0.6161
0.3	0.05	0.9735	1.0	0.9374	1.0
0.3	0.1	1.0	1.0	1.0	1.0
0.3	0.2	1.0	1.0	1.0	1.0
0.3	0.3	1.0	1.0	1.0	1.0
0.3	0.4	1.0	1.0	1.0	1.0
0.3	0.5	1.0	1.0	1.0	1.0
0.3	1.0	1.0	1.0	1.0	1.0
0.4	0	0.0579	0.0481	0.0265	0.0252
0.4	0.01	0.1914	0.7151	0.1068	0.6145

|					
0.4	0.05	0.9698	1.0	0.9381	1.0
0.4	0.1	1.0	1.0	1.0	1.0
0.4	0.2	1.0	1.0	1.0	1.0
0.4	0.3	1.0	1.0	1.0	1.0
0.4	0.4	1.0	1.0	1.0	1.0
0.4	0.5	1.0	1.0	1.0	1.0
0.4	1.0	1.0	1.0	1.0	1.0
0.5	0	0.0528	0.0436	0.0246	0.0262
0.5	0.01	0.1798	0.6953	0.1101	0.6052
0.5	0.05	0.9737	1.0	0.9385	1.0
0.5	0.1	1.0	1.0	1.0	1.0
0.5	0.2	1.0	1.0	1.0	1.0
0.5	0.3	1.0	1.0	1.0	1.0
0.5	0.4	1.0	1.0	1.0	1.0
0.5	0.5	1.0	1.0	1.0	1.0
0.5	1.0	1.0	1.0	1.0	1.0
1.0	0	0.0486	0.0381	0.0274	0.0229
1.0	0.01	0.1675	0.6601	0.1109	0.606
1.0	0.05	0.9654	1.0	0.9422	1.0
1.0	0.1	1.0	1.0	1.0	1.0
1.0	0.2	1.0	1.0	1.0	1.0
1.0	0.3	1.0	1.0	1.0	1.0
1.0	0.4	1.0	1.0	1.0	1.0
1.0	0.5	1.0	1.0	1.0	1.0
1.0	1.0	1.0	1.0	1.0	1.0

TABLE K.3. Rejection rate of PLD Test, with $A = (a_1, a_2, a_3, a_4)$

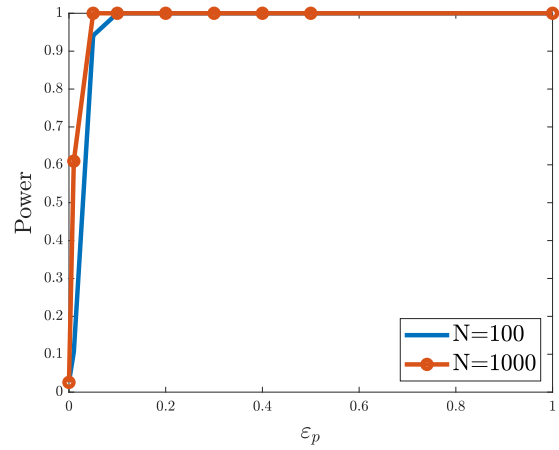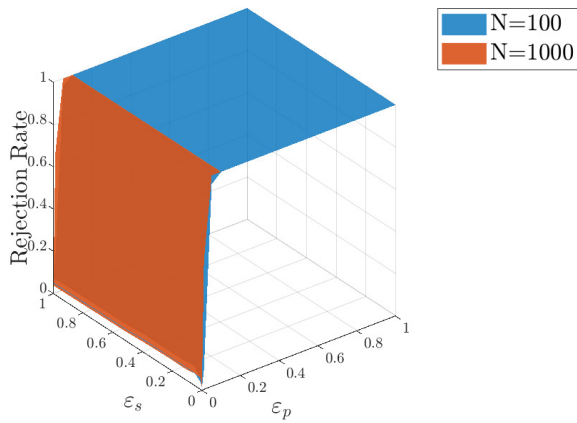(a) $A = (a_1, a_2)$, $\mu = \frac{logN}{\sqrt{N}}$
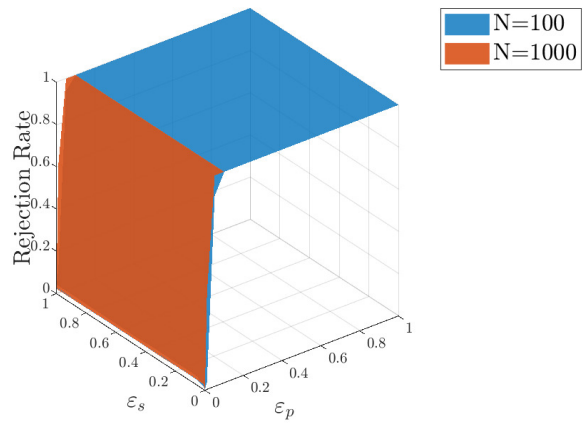
(b) $\mu = 0$

(c) $A = (a_1, a_2, a_3)$, $\mu = \frac{logN}{\sqrt{N}}$

(d) $\mu = 0$
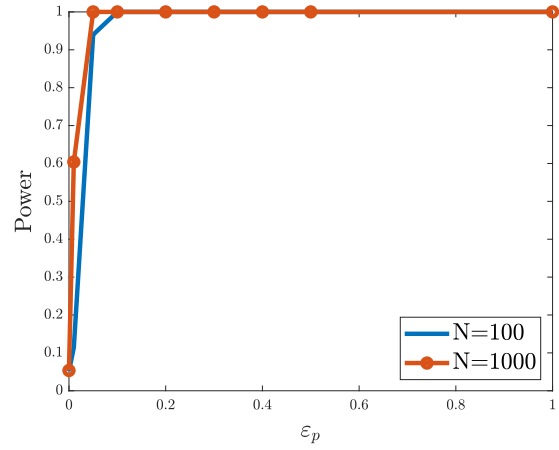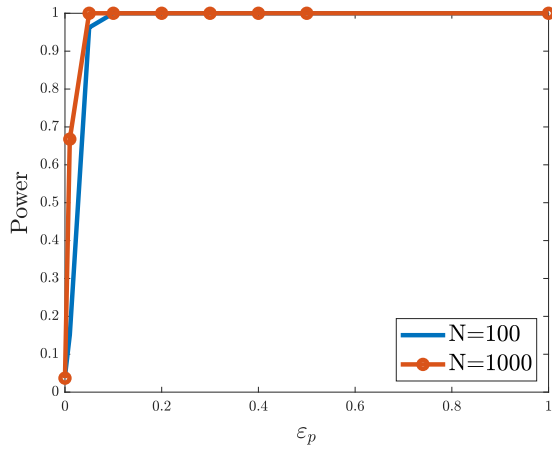
(e) $A = (a_1, a_2, a_3, a_4)$, $\mu = \frac{logN}{\sqrt{N}}$

(f) $\mu = 0$

FIGURE K.1. Rejection Rate Plot

Bibliography

ABBOTT, J. K. AND J. E. WILEN (2011): "Dissecting the tragedy: a spatial model of behavior in the commons," *Journal of Environmental Economics and Management*, 62, 386–401.

ABE, K. AND C. M. ANDERSON (2022): "A Dynamic Model of Endogenous Fishing Duration," *Journal of the Association of Environmental and Resource Economists*.

ANDREWS, D. W. AND S. KWON (2019): "Inference in moment inequality models that is robust to spurious precision under model misspecification," .

ATHEY, S., D. BLEI, R. DONNELLY, F. RUIZ, AND T. SCHMIDT (2018): "Estimating heterogeneous consumer preferences for restaurants and travel time using mobile location data," in *AEA Papers and Proceedings*, vol. 108, 64–67.

ATHEY, S., B. A. FERGUSON, M. GENTZKOW, AND T. SCHMIDT (2020): "Experienced segregation," Tech. rep., National Bureau of Economic Research.

BALAS, E. (1989): "The prize collecting traveling salesman problem," *Networks*, 19, 621–636.

BEN-ISRAEL, A. (2002): "Motzkin's transposition theorem, and the related theorems of Farkas, Gordan and Stiemke," *Encyclopaedia of Mathematics, Supplement III*.

BERGE, C. (1997): *Topological Spaces: including a treatment of multi-valued functions, vector spaces, and convexity*, Courier Corporation.

BIEBACH, H. (1996): "Energetics of winter and migratory fattening," in *Avian energetics and nutritional ecology*, Springer, 280–323.

BIRDLIFE INTERNATIONAL (2018): "*Leucogeranus leucogeranu*s. The IUCN Red List of Threatened Species 2018: e.T22692053A134180990," `http://dx.doi.org/10.2305/IUCN.UK.2018-2.RLTS.T22692053A134180990.en`, acessed on May 16, 2019.

BIRDORABLE BLOG (2019): "Crane extremes! More facts for crane week," `https://www.birdorable.com/blog/crane-extremes-more-facts-for-crane-week/`, acessed on May 16, 2019.

BJÖRKEGREN, D. (2019): "The adoption of network goods: Evidence from the spread of mobile phones in Rwanda," *The Review of Economic Studies*, 86, 1033–1060.

BLEM, C. R. (1980): "The energetics of migration," *Animal migration, orientation, and navigation*, 175–224.

BLUMENSTOCK, J., G. CADAMURO, AND R. ON (2015): "Predicting poverty and wealth from mobile phone metadata," *Science*, 350, 1073–1076.

BOCKSTAEL, N. E. AND J. J. OPALUCH (1983): "Discrete modelling of supply response under uncertainty: the case of the fishery," *Journal of Environmental Economics and Management*, 10, 125–137.

BOVE, J. (2019): "Siberian White Crane Facts," `https://www.thoughtco.com/profile-of-endangered-siberian-white-crane-1181995`, acessed on May 13, 2019.

BROWN, C., R. MEEKS, K. HUNU, AND W. YU (2011): "Hydroclimate risk to economic growth in sub-Saharan Africa," *Climatic Change*, 106, 621–647.

BÜCHEL, K., M. V. EHRLICH, D. PUGA, AND E. VILADECANS-MARSAL (2020): "Calling from the outside: The role of networks in residential mobility," *Journal of urban economics*, 119, 103277.

BULL, C. D., N. B. METCALFE, AND M. MANGEL (1996): "Seasonal matching of foraging to anticipated energy requirements in anorexic juvenile salmon," *Proceedings of the Royal Society of London. Series B: Biological Sciences*, 263, 13–18.

BURNHAM, J., J. BARZEN, A. M. PIDGEON, B. SUN, J. WU, G. LIU, AND H. JIANG (2017): "Novel foraging by wintering Siberian Cranes *Leucogeranus leucogeranus* at China's Poyang Lake indicates broader changes in the ecosystem and raises new challenges for a critically endangered species," *Bird Conservation International*, 27, 204–223.

CANOVA, F. (2011): *Methods for applied macroeconomic research*, vol. 13, Princeton university press.

CANOVA, F. AND G. DE NICOLO (2002): "Monetary disturbances matter for business fluctuations in the G-7," *Journal of Monetary Economics*, 49, 1131–1159.

CANOVA, F. AND M. PAUSTIAN (2011): "Business cycle measurement with some theory," *Journal of Monetary Economics*, 58, 345–361.

CELLINI, R. AND L. LAMBERTINI (2004): "Dynamic oligopoly with sticky prices: closed-loop, feedback, and open-loop solutions," *Journal of Dynamical and Control Systems*, 10, 303–314.

CHIBA, A. (2018): "Wintering behavior of a Siberian Crane Grus leucogeranus in Niigata, Japan, with special regard to food, foraging and vocal habits," *Ornithological Science*, 17, 187–194.

CLARK, C. W. AND M. MANGEL (2000): *Dynamic state variable models in ecology: methods and applications*, Oxford University Press on Demand.

COUTURE, V., J. I. DINGEL, A. GREEN, J. HANDBURY, AND K. R. WILLIAMS (2021): "JUE Insight: Measuring movement and social contact with smartphone data: a real-time application to COVID-19," *Journal of Urban*

Economics, 103328.

CUI, X., Y. ZHONG, L. WEI, AND J. CHEN (2000): "The effect of catastrophic flood on biomass and density of three dominant aquatic plant species in the Poyang Lake," *Acta hydrobiologica sinica*, 24, 322–325.

CURTIS, R. AND R. L. HICKS (2000): "The cost of sea turtle preservation: The case of Hawaii's pelagic longliners," *American Journal of Agricultural Economics*, 82, 1191–1197.

CURTIS, R. E. AND K. E. MCCONNELL (2004): "Incorporating information and expectations in fishermen's spatial decisions," *Marine Resource Economics*, 19, 131–143.

DANTZIG, G., R. FULKERSON, AND S. JOHNSON (1954): "Solution of a large-scale traveling-salesman problem," *Journal of the operations research society of America*, 2, 393–410.

DATTORRO, J. (2019): *Convex optimization & Euclidean distance geometry*, Lulu. com.

DEL HOYO, J. (1997): *Handbook of the birds of the world. Vol. 4, Sandgrouse to Cuckoos*, Lynx edicions.

DELL'AMICO, M., F. MAFFIOLI, AND P. VÄRBRAND (1995): "On prize-collecting tours and the asymmetric travelling salesman problem," *International Transactions in Operational Research*, 2, 297–308.

DÉPALLE, M., J. N. SANCHIRICO, O. THÉBAUD, S. O'FARRELL, A. C. HAYNIE, AND L. PERRUSO (2021): "Scale-dependency in discrete choice models: a fishery application," *Journal of Environmental Economics and Management*, 105, 102388.

DONOVAN, P., L. S. BAIR, C. B. YACKULIC, AND M. R. SPRINGBORN (2019): "Safety in numbers: cost-effective endangered species management for viable populations," *Land Economics*, 95, 435–453.

DUPONT, D. P. (1993): "Price uncertainty, expectations formation and fishers' location choices," *Marine Resource Economics*, 8, 219–247.

DUPONT, D. P., R. Q. GRAFTON, J. KIRKLEY, AND D. SQUIRES (2002): "Capacity utilization measures and excess capacity in multi-product privatized fisheries," *Resource and Energy Economics*, 24, 193–210.

EALES, J. AND J. E. WILEN (1986): "An examination of fishing location choice in the pink shrimp fishery," *Marine Resource Economics*, 2, 331–351.

EDELSTEIN-KESHET, L. (2005): *Mathematical models in biology*, SIAM.

EIDE, J. D., W. W. HAGER, AND A. V. RAO (2021): "Modified Legendre–Gauss–Radau Collocation Method for Optimal Control Problems with Nonsmooth Solutions," *Journal of Optimization Theory and Applications*, 1–34.

ENGLANDER, G. (2019): "Property rights and the protection of global marine resources," *Nature Sustainability*, 2, 981–987.

FAUST, J. (1998): "The robustness of identified VAR conclusions about money," in *Carnegie-Rochester Conference Series on Public Policy*, Elsevier, vol. 49, 207–244.

FEILLET, D., P. DEJAX, AND M. GENDREAU (2005): "Traveling salesman problems with profits," *Transportation science*, 39, 188–205.

FELTHOVEN, R. G. AND C. J. MORRISON PAUL (2004): "Multi-output, nonfrontier primal measures of capacity and capacity utilization," *American Journal of Agricultural Economics*, 86, 619–633.

FLOWER, M. (1938): "The duration of life in animals-IV. Birds: special notes by orders and families," in *Proceedings of the Zoological Society of London*, 195–235.

FRIEDMAN, J. (1992): *Operation Siberian Crane: The Story Behind the International Effort to Save an Amazing Bird*, Dillon Press.

FRY, R. AND A. PAGAN (2011): "Sign restrictions in structural vector autoregressions: A critical review," *Journal of Economic Literature*, 49, 938–60.

GAFAROV, B. (2014): "Identification in Dynamic Models Using Sign Restrictions," *Available at SSRN 2384811*.

GAFAROV, B., M. MEIER, AND J. L. MONTIEL OLEA (2018a): "Delta-method inference for a class of set-identified SVARs," *Journal of Econometrics*, 203, 316–327.

GAFAROV, B., M. MEIER, AND J. L. M. OLEA (2018b): "Delta-Method inference for a class of set-identified SVARs," *Journal of Econometrics*, 203, 316–327.

GARG, D., M. A. PATTERSON, C. FRANCOLIN, C. L. DARBY, G. T. HUNTINGTON, W. W. HAGER, AND A. V. RAO (2011): "Direct trajectory optimization and costate estimation of finite-horizon and infinite-horizon optimal control problems using a Radau pseudospectral method," *Computational Optimization and Applications*, 49, 335–358.

GERMOGENOV, N., N. SOLOMONOV, A. PSHENNIKOV, A. DEGTYAREV, S. SLEPTSOV, N. EGOROV, I. BYSYKATOVA, M. VLADIMIRTSEVA, AND V. OKONESHNIKOV (2013): "The ecology of the habitats, nesting, and migration of the eastern population of the Siberian crane (*Grus leucogeranus Pallas*, 1773)," *Contemporary Problems of Ecology*, 6, 65–76.

GOLDEN, B. L., L. LEVY, AND R. VOHRA (1987): "The orienteering problem," *Naval Research Logistics (NRL)*, 34, 307–318.

GRANZIERA, E., H. R. MOON, AND F. SCHORFHEIDE (2018): "Inference for VARs identified with sign restrictions," *Quantitative Economics*, 9, 1087–1121.

GRÉBOVAL, D. (1999): "Managing fishing capacity: selected papers on underlying concepts and issues," *FAO Fish. Tech. Pap.*, 386, 1–206.

——— (2003): "The measurement and monitoring of fishing capacity: introduction and major considerations," *Measuring Capacity in Fisheries*.

GULLAND, J. A. (1983): *Fish stock assessmenta manual of basic methods*, 639.2021 G8.

GUNAWAN, A., H. C. LAU, AND P. VANSTEENWEGEN (2016): "Orienteering problem: A survey of recent variants, solution approaches and applications," *European Journal of Operational Research*, 255, 315–332.

GUPTA, A., S. VAN NIEUWERBURGH, AND C. KONTOKOSTA (2020): "Take the Q train: Value capture of public infrastructure projects," Tech. rep., National Bureau of Economic Research.

HARRIS, J. (2016): "Poyang Lake, Yangtze River Basin, China," in *The Wetland Book*, Springer, 1–9.

HASTINGS, A. AND L. GROSS (2012): *Encyclopedia of theoretical ecology*, 4, Univ of California Press.

HAYNIE, A. C., R. L. HICKS, AND K. E. SCHNIER (2009): "Common property, information, and cooperation: commercial fishing in the Bering Sea," *Ecological Economics*, 69, 406–413.

HAYNIE, A. C. AND D. F. LAYTON (2010): "An expected profit model for monetizing fishing location choices," *Journal of Environmental Economics and Management*, 59, 165–176.

HICKS, R. L., J. KIRKLEY, AND I. E. STRAND JR (2004): "Short-run welfare losses from essential fish habitat designations for the surfclam and ocean quahog fisheries," *Marine Resource Economics*, 19, 113–129.

HICKS, R. L. AND K. E. SCHNIER (2006): "Dynamic random utility modeling: a Monte Carlo analysis," *American Journal of Agricultural Economics*, 88, 816–835.

——— (2008): "Eco-labeling and dolphin avoidance: A dynamic model of tuna fishing in the Eastern Tropical Pacific," *Journal of Environmental Economics and Management*, 56, 103–116.

HOLLAND, D. S. AND J. G. SUTINEN (2000): "Location choice in New England trawl fisheries: old habits die hard," *Land Economics*, 133–149.

HU, Z. (2020): *Ecohydrological charateristics and evolution of Lake Poyang*, China Science Publishing Media.

HURD, B., J. M. CALLAWAY, J. B. SMITH, AND P. KIRSHEN (2002): "Economic effects of climate change on US water resources," in *Water resources and climate change*, Edward Elgar Publishing.

HUTNICZAK, B. AND A. MÜNCH (2018): "Fishermen's location choice under spatio-temporal update of expectations," *Journal of choice modelling*, 28, 124–136.

INTERNATIONAL CRANE FOUNDATION (2019): "Siberian White Crane Facts," `https://www.savingcranes.org/species-field-guide/siberian-crane/`, acessed on May 16, 2019.

JIA, Y., S. JIAO, Y. ZHANG, Y. ZHOU, G. LEI, AND G. LIU (2013): "Diet shift and its impact on foraging behavior of Siberian crane (*Grus leucogeranus*) in Poyang Lake," *PLoS One*, 8, e65843.

JOHNSGARD, P. A. (1983): "Cranes of the World: Demoiselle Crane (Anthropoides virgo)," .

JORDÀ, Ò. (2005): "Estimation and inference of impulse responses by local projections," *American economic review*, 95, 161–182.

KANG, W., I. M. ROSS, AND Q. GONG (2008): "Pseudospectral optimal control and its convergence theorems," in *Analysis and design of nonlinear control systems*, Springer, 109–124.

KILIAN, L. (2013): "Structural vector autoregressions," in *Handbook of research methods and applications in empirical macroeconomics*, Edward Elgar Publishing.

KIRKLEY, J., C. J. M. PAUL, AND D. SQUIRES (2002): "Capacity and capacity utilization in common-pool resource industries," *Environmental and Resource Economics*, 22, 71–97.

KRAEMER, M. U., A. SADILEK, Q. ZHANG, N. A. MARCHAL, G. TULI, E. L. COHN, Y. HSWEN, T. A. PERKINS, D. L. SMITH, R. C. REINER, ET AL. (2020): "Mapping global variation in human mobility," *Nature Human Behaviour*, 4, 800–810.

KREINDLER, G. E. AND Y. MIYAUCHI (2021): "Measuring Commuting and Economic Activity Inside Cities with Cell Phone Records," *The Review of Economics and Statistics*, 1–48.

KROODSMA, D. A., J. MAYORGA, T. HOCHBERG, N. A. MILLER, K. BOERDER, F. FERRETTI, A. WILSON, B. BERGMAN, T. D. WHITE, B. A. BLOCK, P. WOODS, B. SULLIVAN, C. COSTELLO, AND B. WORM (2018): "Tracking the global footprint of fisheries," *Science*, 359, 904–908.

LI, L., X. ZHANG, H. QIN, X. HU, AND J. CHEN (2015): "Effects of tuber-feeding waterbird guild and water level fluctuation on tuber distribution of submerged macrophytes in Shahu Lake," *Chinese Journal of Ecology*, 34, 661–669.

LI, S., L. TONG, J. XING, AND Y. ZHOU (2017): "The market for electric vehicles: indirect network effects and policy design," *Journal of the Association of Environmental and Resource Economists*, 4, 89–133.

LIMA, S. L. (1986): "Predation risk and unpredictable feeding conditions: determinants of body mass in birds," *Ecology*, 67, 377–385.

MAI, H. (2018): *Record of the Listener: Selected Stories from Hong Mai's Yijian Zhi*, Hackett Publishing.

MARCOUL, P. AND Q. WENINGER (2008): "Search and active learning with correlated information: Empirical evidence from mid-Atlantic clam fishermen," *Journal of Economic Dynamics and Control*, 32, 1921–1948.

MARGOLIS, M. AND E. NÆVDAL (2008): "Safe minimum standards in dynamic resource problems: conditions for living on the edge of risk," *Environmental and Resource Economics*, 40, 401–423.

MAS-COLELL, A., M. D. WHINSTON, J. R. GREEN, ET AL. (1995): *Microeconomic theory*, vol. 1, Oxford university press New York.

MATHWORKS (2021): "Traveling Salesman Problem: Problem-Based," [Online; accessed April 2021].

MEINE, C. AND G. ARCHIBALD (1996): *The cranes: status survey and conservation action plan*, IUCN.

MISTIAEN, J. A. AND I. E. STRAND (2000): "Location choice of commercial fishermen with heterogeneous risk preferences," *American Journal of Agricultural Economics*, 82, 1184–1190.

MIYAUCHI, Y., K. NAKAJIMA, AND S. J. REDDING (2021): "Consumption Access and the Spatial Concentration of Economic Activity: Evidence from Smartphone Data," .

MOON, H. R., F. SCHORFHEIDE, E. GRANZIERA, AND M. LEE (2011): "Inference for VARs identified with sign restrictions," Tech. rep., National Bureau of Economic Research.

MURDOCH, W. W., C. J. BRIGGS, AND R. M. NISBET (2003): *Consumer-resource dynamics*, vol. 36, Princeton University Press.

OFARRELL, S., I. CHOLLETT, J. N. SANCHIRICO, AND L. PERRUSO (2019a): "Classifying fishing behavioral diversity using high-frequency movement data," *Proceedings of the National Academy of Sciences*, 116, 16811–16816.

OFARRELL, S., J. N. SANCHIRICO, O. SPIEGEL, M. DEPALLE, A. C. HAYNIE, S. A. MURAWSKI, L. PERRUSO, AND A. STRELCHECK (2019b): "Disturbance modifies payoffs in the explore-exploit trade-off," *Nature communications*, 10, 1–9.

PACHAURI, R. K., M. R. ALLEN, V. R. BARROS, J. BROOME, W. CRAMER, R. CHRIST, J. A. CHURCH, L. CLARKE, Q. DAHE, P. DASGUPTA, ET AL. (2014): *Climate change 2014: synthesis report. Contribution of Working Groups I, II and III to the fifth assessment report of the Intergovernmental Panel on Climate Change*, Ipcc.

PALOMO-MARTÍNEZ, P. J., M. A. SALAZAR-AGUILAR, AND V. M. ALBORNOZ (2017): "Formulations for the orienteering problem with additional constraints," *Annals of Operations Research*, 258, 503–545.

PATTERSON, M. A. AND A. V. RAO (2014): "GPOPS-II: A MATLAB software for solving multiple-phase optimal control problems using hp-adaptive Gaussian quadrature collocation methods and sparse nonlinear programming," *ACM Transactions on Mathematical Software (TOMS)*, 41, 1–37.

PAUSTIAN, M. (2007): "Assessing sign restrictions," *The BE Journal of Macroeconomics*, 7.

REED, W. J. (1984): "The effects of the risk of fire on the optimal rotation of a forest," *Journal of environmental economics and management*, 11, 180–190.

REIMER, M. N. (2012): *Revisiting the Fishery Production Function: Space, Time, and Policy Invariant Relationships*, University of California, Davis.

ROSS, I. M. AND C. N. D'SOUZA (2005): "Hybrid optimal control framework for mission planning," *Journal of Guidance, Control, and Dynamics*, 28, 686–697.

ROSS, I. M. AND F. FAHROO (2004): "Pseudospectral knotting methods for solving nonsmooth optimal control problems," *Journal of Guidance, Control, and Dynamics*, 27, 397–405.

RUBIO-RAMIREZ, J. F., D. F. WAGGONER, AND T. ZHA (2010): "Structural vector autoregressions: Theory of identification and algorithms for inference," *The Review of Economic Studies*, 77, 665–696.

SANCHIRICO, J. N. AND J. E. WILEN (1999): "Bioeconomics of spatial exploitation in a patchy environment," *Journal of Environmental Economics and Management*, 37, 129–150.

SCHAEFER, M. B. (1954): "Some aspects of the dynamics of populations important to the management of the commercial marine fisheries," *Inter-American Tropical Tuna Commission Bulletin*, 1, 23–56.

SCHEFFER, M. (1997): *Ecology of shallow lakes*, vol. 22, Springer Science & Business Media.

SHANKMAN, D., B. D. KEIM, AND J. SONG (2006): "Flood frequency in China's Poyang Lake region: trends and teleconnections," *International Journal of Climatology*, 26, 1255–1266.

SHEFFIELD, J. AND E. F. WOOD (2008): "Projected changes in drought occurrence under future global warming from multi-model, multi-scenario, IPCC AR4 simulations," *Climate dynamics*, 31, 79–105.

SINGH, A. AND R. M. NISBET (2007): "Semi-discrete host–parasitoid models," *Journal of theoretical biology*, 247, 733–742.

SMITH, C. L. AND S. S. HANNA (1990): "Measuring fleet capacity and capacity utilization," *Canadian Journal of Fisheries and Aquatic Sciences*, 47, 2085–2091.

SMITH, M. D. (2002): "Two econometric approaches for predicting the spatial behavior of renewable resource harvesters," *Land Economics*, 78, 522–538.

——— (2005): "State dependence and heterogeneity in fishing location choice," *Journal of Environmental Economics and Management*, 50, 319–340.

SPONBERG, A. F. AND D. M. LODGE (2005): "Seasonal belowground herbivory and a density refuge from waterfowl herbivory for Vallisneria americana," *Ecology*, 86, 2127–2134.

STEELE, J. E., P. R. SUNDSØY, C. PEZZULO, V. A. ALEGANA, T. J. BIRD, J. BLUMENSTOCK, J. BJELLAND, K. ENGØ-MONSEN, Y.-A. DE MONTJOYE, A. M. IQBAL, ET AL. (2017): "Mapping poverty using mobile phone and satellite data," *Journal of The Royal Society Interface*, 14, 20160690.

STOCK, J. H. AND M. W. WATSON (2005): "Implications of dynamic factor models for VAR analysis," Tech. rep., National Bureau of Economic Research.

SUN, J., M. G. HINTON, AND D. WEBSTER (2016): "Modeling the spatial dynamics of international tuna fleets," *PloS one*, 11, e0159626.

TSILIGIRIDES, T. (1984): "Heuristic methods applied to orienteering," *Journal of the Operational Research Society*, 35, 797–809.

UHLIG, H. (2005): "What are the effects of monetary policy on output? Results from an agnostic identification procedure," *Journal of Monetary Economics*, 52, 381–419.

VANSTEENWEGEN, P. AND A. GUNAWAN (2019): *Orienteering problems: Models and algorithms for vehicle routing problems with profits*, Springer Nature.

WANG, M.-H., S. D. SCHROCK, N. VANDER BROEK, AND T. MULINAZZI (2013): "Estimating dynamic origin-destination data and travel demand using cell phone network data," *International Journal of Intelligent Transportation Systems Research*, 11, 76–86.

WATSON, J. T., A. C. HAYNIE, P. J. SULLIVAN, L. PERRUSO, S. O'FARRELL, J. N. SANCHIRICO, AND F. J. MUETER (2018): "Vessel monitoring systems (VMS) reveal an increase in fishing efficiency following regulatory changes in a demersal longline fishery," *Fisheries Research*, 207, 85–94.

WEILL, J. A., M. STIGLER, O. DESCHENES, AND M. R. SPRINGBORN (2020): "Social distancing responses to COVID-19 emergency declarations strongly differentiated by income," *Proceedings of the National Academy of Sciences*, 117, 19658–19660.

WETLANDS INTERNATIONAL, WAGENINGEN, T. N. (2012): "Waterbird Population Estimates, Fifth Edition. Summary Report," *Wetlands International*.

WIKIPEDIA (2019): "Siberian crane," `https://en.wikipedia.org/wiki/Siberian_crane`, acessed on May 16, 2019.

WITTER, M. S. AND I. C. CUTHILL (1993): "The ecological costs of avian fat storage," *Philosophical Transactions of the Royal Society of London. Series B: Biological Sciences*, 340, 73–92.

WU, G., J. DE LEEUW, A. K. SKIDMORE, H. H. PRINS, E. P. BEST, AND Y. LIU (2009): "Will the Three Gorges Dam affect the underwater light climate of *Vallisneria spiralis L.* and food habitat of Siberian crane in Poyang Lake?" *Hydrobiologia*, 623, 213–222.

WU, Y. AND W. JI (2002): *Study on Jiangxi Poyang Lake National Nature Reserve (in Chinese)*, China Forestry Publishing House.

YUAN, L.-Y., W. LI, G.-H. A. LIU, G. DENG, ET AL. (2012): "Effects of different shaded conditions and water depths on the growth and reproductive strategy of Vallisneria spinulosa," *Pakistan Journal of Botany*, 44, 911–918.

ZENG, Z. (2014): "Studies on Diversity, Age and Growth of Fishes in Sublakes of Poyang Lake National Nature Reserve, Jiangxi China (in Chinese)," Master's thesis, Nanchang University, China.

ZHANG, J. AND M. D. SMITH (2011): "Estimation of a generalized fishery model: A two-stage approach," *Review of Economics and Statistics*, 93, 690–699.

ZHAO, J. AND J. WU (1999): "Effects of the 98 Flood of the Yangtze River on Wintering Waterfowl at Poyang Hu Reserve," *Conservation and Managment (in Chinese)*.